



UNIVERSITY
OF
JOHANNESBURG

COPYRIGHT AND CITATION CONSIDERATIONS FOR THIS THESIS/ DISSERTATION

 creative
commons



- Attribution — You must give appropriate credit, provide a link to the license, and indicate if changes were made. You may do so in any reasonable manner, but not in any way that suggests the licensor endorses you or your use.
- NonCommercial — You may not use the material for commercial purposes.
- ShareAlike — If you remix, transform, or build upon the material, you must distribute your contributions under the same license as the original.

How to cite this thesis

Surname, Initial(s). (2012) Title of the thesis or dissertation. PhD. (Chemistry)/ M.Sc. (Physics)/ M.A. (Philosophy)/M.Com. (Finance) etc. [Unpublished]: [University of Johannesburg](https://ujcontent.uj.ac.za/vital/access/manager/Index?site_name=Research%20Output). Retrieved from: https://ujcontent.uj.ac.za/vital/access/manager/Index?site_name=Research%20Output (Accessed: Date).



**APPLICATION OF NEURAL NETWORK TECHNIQUES TO THE ION-EXCHANGE
PROCESS AND PREDICTION OF ABRASIVENESS CHARACTERISTICS OF
THERMAL COAL**

by

JOHN TSHILENGE KABUBA



submitted in partial fulfilment of the requirements for the degree of

DOCTOR OF TECHNOLOGY

in the

Faculty of Engineering and the Built Environment

at the

University of Johannesburg

Supervisor: PROF AF MULABA-BAFUBIANDI

JUNE 2016

DECLARATION

I hereby declare that this submission is my own work and that, to the best of my knowledge and belief, it contains no material previously published or written by another person nor material which to a substantial extent has been accepted for the award of any other degree or diploma of the university or other institute of higher learning, except where due acknowledgment has been made in the text.

.....

.....

John Tshilenge Kabuba

Prof A.F. Mulaba-Bafubiandi

.....day of.....

.....day of.....



UNIVERSITY
OF
JOHANNESBURG

ABSTRACT

The construction of a model for the prediction of process outputs is a valuable tool in the field of engineering. The models play an important role in the simulation and optimization of systems leading to the design of efficient and economical processes. Since 1943 neural network (NN) techniques have been considered as promising tools for use in simulation, prediction and modelling because of their simplicity.

In this thesis a feed-forward neural network (FFNN) with back-propagation (BP) is used to test its effectiveness in modelling the ion-exchange process.

The ion-exchange process has been widely employed in the removal of heavy metals from industrial wastewater. This process is a complex non-linear process involving many factors influencing the chemical process which is not well understood (the ions uptake mechanisms from the pregnant solution, the subsequent step being the elution). In order to improve the performance of the ion-exchange process, optimization and analysis of the process should be accomplished. Modelling and simulation are tools which can be used to achieve the objectives.

The experimental design using analysis of variance (ANOVA) was chosen to compare to the NN techniques and for optimizing the effective input parameters (pH, temperature and initial concentration). The FFNN successfully tracked the non-linear behaviour of the ion-exchange process versus the input parameters with a mean square error (MSE), correlation coefficient (R) and mean square relative error (MSRE) of 0.102, 0.998 and 0.004, respectively. The results showed that the FFNN modelling techniques could effectively predict and simulate the highly complex system and non-linear process such as the ion exchange using activated zeolite.

After this validation, the ability of a different type of NN as assessed to predict the abrasiveness index (AI) of coal. In this application a generalized regression neural network (GRNN) approach was used. Coal characterization techniques allow for the mineral inclusions in coal that are responsible for the abrasive nature of the coal to be accurately characterized. There is therefore scope to make an improved prediction of wear based on detailed knowledge of the mineral matter (MM) in a particular coal. It is important to understand the nature and properties of the MM in coal that would contribute to abrasive wear. Most of the empirical equations available in literature for the AI of coal are based on linear assumptions which may lead to erroneous estimations and do not simultaneously take into consideration most of the relevant factors. The GRNN technique was employed to assess the AI of coal. The sensitivity analysis was conducted to determine the influence of the input variables on the performance of the model. For this, four different models were trained and tested by applying GRNN techniques using the same training and testing data set. The result showed that quartz is the most influential component in coal responsible for wear and abrasion. The performance of the GRNN technique for the prediction of abrasiveness characteristics of thermal coal was found to be impressive.

DEDICATION

This work is dedicated to my wife Cathy Ntumba Makabu Tshilenge.



UNIVERSITY
OF
JOHANNESBURG

ACKNOWLEDGMENTS

I express my gratitude to my supervisor, Professor Antoine Floribert Mulaba-Bafubiandi, for his guidance and support during my research. I would also like to thank Doctor Kimberly Battle for assisting me with Neural Network tutorials.

To all the individuals who contributed to this work, I extend my thanks. Their fruitful contributions are highly appreciated, particularly the anonymous reviewers of several conference papers, journal articles and a book chapter. I am grateful to the Next Generation Scholarship, University of Johannesburg, Postgraduate Funding for the financial support.

I thank my colleagues from the Mineral Processing Research Centre for creating a suitable environment for research. My gratitude goes to Miss D. Nyembe and K. Oliviera for providing experimental data, and my work family, the Chemical Engineering and Metallurgical Department staff members, friends and community for their friendship.

I sincerely thank my parents for their unwavering support and encouragement throughout my studies.

Finally I would like to thank my powerful GOD.

TABLE OF CONTENTS

DECLARATION.....	i
ABSTRACT.....	ii
DEDICATION.....	vi
ACKNOWLEDGMENTS.....	ix
TABLE OF CONTENTS.....	x
LIST OF FIGURES.....	xvi
LIST OF TABLES.....	xxi
LIST OF ABBREVIATIONS AND SYMBOLS.....	xxii
RELATED PUBLICATIONS.....	xxiii
Chapter 1: Introduction.....	1
1.1 Introduction.....	1
1.2 Background and motivation.....	1
1.2.1 The ion-exchange process.....	1
1.2.2 The coal abrasiveness index (AI).....	1
1.3 Research problems/questions.....	1
1.4 Aim and objectives.....	4
1.4.1 Aim.....	4
1.4.2 Objectives.....	4
1.5 Scope and limitations of the study.....	4
1.6 Expected contribution to knowledge.....	5
1.7 Structure of the thesis.....	5
Chapter 2: Literature Review.....	6
2.1 Introduction.....	6
2.2 Zeolites as the ion-exchange material.....	6

2.2.1 Clinoptilolite characterization.....	8
2.2.2 Treatment of Clinoptilolite for loading.....	9
2.2.3 The Fourier transform infrared spectroscopy (FTIR) analysis.....	12
2.3 The ion-exchange process.....	14
2.3.1 Factors influencing the kinetics of the ion-exchange process.....	15
2.3.2 Rate controlling steps in the ion-exchange process.....	16
2.3.3 The ion-exchange isotherm.....	17
2.3.4 The Cation exchange capacity.....	20
2.4 Review of modelling the ion-exchange process.....	21
2.5 Review of the application of FFNN.....	26
2.5.1 Biological wastewater treatment.....	28
2.5.2 Physico-chemical wastewater treatment.....	29
2.6 Determination of the AI of coal.....	30
2.6.1 Introduction.....	30
2.6.2 Minerals in coals.....	33
2.6.3 Grindability.....	35
2.6.4 Grindability and abrasion.....	38
2.7 Generalized regression neural network (GRNN).....	42
2.8 Predicting abrasiveness.....	43
2.9 Review of the application of the GRNN.....	48
2.10 Conclusion.....	54
Chapter 3: Experimental Materials and Methods.....	55
3.1 Introduction.....	55
3.2 Chemical reagents and materials.....	55
3.3 Preparation of clinoptilolite and synthetic solutions.....	55

3.3.1 Preparation and treatment of clinoptilolite.....	56
3.3.2 Atomic adsorption spectroscopy analysis.....	57
3.3.3 Synthetic solution preparation.....	57
3.3.4 Adsorption studies.....	59
3.3.5 Verification of sorption mechanisms.....	59
3.4 Experimental procedure.....	60
3.5 Data processing.....	60
3.6 Conclusion.....	62
Chapter 4: Feed-forward Neural Network Analysis	63
4.1 Introduction.....	63
4.2 Application of the FFNN technique on loading.....	63
4.2.1 Selection of a back-propagation training algorithm.....	64
4.2.2 Data distribution.....	67
4.2.3 Selection of the NN structure.....	70
4.2.4 Selection of initial weight.....	73
4.2.5 Sensitivity analysis.....	75
4.2.6 Effect of pH on removal efficiency.....	77
4.2.7 Effect of temperature on removal efficiency.....	79
4.2.8 Effect of initial concentration of Cu (II) ions on the loading efficiency.....	82
4.2.9 Testing the NN generalization.....	84
4.2.10 Mathematical model (MaMo).....	89
4.2.11 Comparing MaMos and NNs.....	96
4.2.12 Confirmation experiments.....	99
4.2.13 Conclusion on the loading.....	99

4.3 Application of the FFNN technique on elution	100
4.3.1 Effect of H ₂ SO ₄ and HCl on the elution of Co (II) and Cu (II).....	104
4.3.2 NN model for elution.....	107
4.3.3 Conclusion on the elution.....	110
4.4 Conclusion	110
Chapter 5: Generalized Regression Neural Network Analysis.....	111
5.1 Application of the GRNN to the coal AI.....	111
5.1.1 Experimental data on the coal AI.....	111
5.1.2 Minerals influencing the abrasiveness quality of coal.....	111
5.1.3 Application of the NNs on the abrasiveness index of coal.....	116
5.1.4 Prediction results of abrasiveness based on GRNN.....	117
5.1.5 Estimation of abrasiveness characteristics of thermal coal on the AI using NNs.....	119
5.1.6 Comparing work on empirical equations.....	119
5.1.7 Sensitivity analysis.....	124
5.2 Conclusion.....	125
Chapter 6: Conclusions and Recommendations.....	127
6.1 Introduction.....	127
6.2 Conclusions.....	127
6.2.1 The ion-exchange process.....	127
6.2.2 The coal AI.....	128
6.3 Recommendations.....	129
APPENDICES.....	131
Appendix A: Physical Properties of Clinoptilolite	131

Appendix B: Atomic Absorption Spectroscopy: Results for Loading and Elution
..... **132**

Appendix C: Proximate Analysis of Coal **138**

REFERENCES..... **141**



LIST OF FIGURES

Figure 2.1: Model structure of clinoptilolite	7
Figure 2.2: Mineralogical diffraction pattern of the natural clinoptilolite.....	9
Figure 2.3: Scanning Electron Microscopy (SEM) image of original clinoptilolite.....	11
Figure 2.4: SEM image of HCl activated clinoptilolite.....	11
Figure 2.5: The FTIR-spectra for original and HCl-activated clinoptilolite	12
Figure 2.6: YGP abrasion index tester pot.....	32
Figure 4.1: Training, validation and test MSEs for the LMA.....	68
Figure 4.2: Regression analysis of the network response between NN output and the corresponding targets.....	70
Figure 4.3: Relationship between MSE and number of neurons at hidden layer for the LMA.....	72
Figure 4.4: Structure of the NN used in this study for the removal.....	73
Figure 4.5: Comparisons between NN outputs and experimental data for initial pH 2 and temperature 30°C	77
Figure 4.6: Comparisons between NN outputs and experimental data for initial pH 2.5 and temperature 30°C.....	78
Figure 4.7: Comparisons between NN outputs and experimental data for initial pH 3 and temperature 30°C	78
Figure 4.8: Comparisons between NN outputs and experimental data for initial pH 4 and temperature 45°C.....	79
Figure 4.9: Comparisons between NN outputs and experimental data for temperature 30°C and pH 4.....	80

Figure 4.10: Comparisons between NN outputs and experimental data for temperature 45°C and pH 4	80
Figure 4.11: Comparisons between NN outputs and experimental data for temperature 60°C and pH 4	81
Figure 4.12: Comparisons between NN outputs and experimental data for temperature 90°C and pH 4	81
Figure 4.13: Comparisons between NN outputs and experimental data for initial concentration of 0.361 mg/L.....	82
Figure 4.14: Comparisons between NN outputs and experimental data for initial concentration of 1.099 mg/L.....	83
Figure 4.15: Comparisons between NN outputs and experimental data for initial concentration of 1.969 mg/L.....	83
Figure 4.16: Comparisons between NN outputs and experimental data for initial concentration of 2.748 mg/L.....	84
Figure 4.17: Generalization performances of optimal NN: effect of temperature and pH.....	86
Figure 4.18: Generalization performances of optimal NN: effect of temperature and initial concentration.....	87
Figure 4.19: Generalization performances of optimal NN: effect of pH and concentration.....	88
Figure 4.20: MaMo prediction values compared with experimental data: effect of pH on the percentage removal at the different temperatures.....	96
Figure 4.21: MaMo prediction values compared with experimental data: effect of pH on the percentage removal at the different concentrations.....	96

Figure 4.22: Comparisons between MaMo, NN and experimental data: effect of temperature on the removal.....	98
Figure 4.23: Comparisons between MaMo, NN and experimental data: effect of pH on the removal	98
Figure 4.24: Comparisons between MaMo, NN and experimental data: effect of the initial concentration on the removal.....	99
Figure 4.25: The optimized NN structure for elution	101
Figure 4.26: Learning curves for training, validation and testing.....	103
Figure 4.27: Effect of the H ₂ SO ₄ concentration on the elution of Co.....	105
Figure 4.28: Effect of the HCl concentration on the elution of Co.....	105
Figure 4.29: Effect of the H ₂ SO ₄ concentration on the elution of Cu.....	106
Figure 4.30: Effect of the HCl concentration on the elution of Cu	106
Figure 4.31: Comparison of experimental data and NN model for Co using H ₂ SO ₄	108
Figure 4.32: Comparison of experimental data and NN model for Co using HCl.....	109
Figure 4.33: Comparison of experimental data and NN model for Cu using H ₂ SO ₄	109
Figure 4.34: Comparison of experimental data and NN model for Cu using HCl	110
Figure 5.1: Effects of quartz on the AI of coal	112
Figure 5.2: Effects of pyrite on the AI of coal	113
Figure 5.3: Effects of ash on the AI of coal.....	114
Figure 5.4: Effects of CaCO ₃ on the AI of coal.....	114
Figure 5.5: Effects of mineral matter (MM) on the AI of coal	115

Figure 5.6: Effects of free H ₂ O on the AI of coal.....	115
Figure 5.7: AI target of the GRNN in the training process versus the output	118
Figure 5.8: AI predicted by GRNN in the testing process versus actual measured....	118
Figure 5.9: Prediction of the AI based on Equation (5.3).....	121
Figure 5.10: Target of the GRNN versus the output.....	121
Figure 5.11: Comparison of the training results with experimental values.....	122



LIST OF TABLES

Table 2.1: Results of pore volume measurements of clinoptilolite.....	10
Table 4.1: Comparison of 10 BP algorithms.....	64
Table 4.2: Statistical criteria for the evaluation of the NN model.....	66
Table 4.3: Relative importance of input variables.....	75
Table 4.4: Performance evaluation of combinations of input variables.....	76
Table 4.5: ANOVA for the regression model.....	85
Table 4.6: Comparison between the MaMo and the NN.....	97
Table 4.7: Effect of number of neurons on MSE, mean absolute error (MAE) and regression coefficient (R).....	103
Table 5.1: The performance of the model.....	117
Table 5.2: Comparison of performances of the prediction model and Raask equation.....	120
Table 5.3: Comparison of performances of GRNN models.....	125

LIST OF ABBREVIATIONS AND SYMBOLS

AAS	Atomic Absorption Spectroscopy
AI	Abrasiveness Index
ANN	Artificial Neural Network
ANOVA	Analysis of Variance
ASTM	American Society for Testing and Materials
BET	Brunauer–Emmett–Teller
BLE	Best Linear Equation
BP	Back-propagation
CEC	Cation Exchange Capacity
D-R	Dubini-Radushkevish
EDS	Energy Dispersive Spectroscopy
FLN	Functional Link Network
FTIR	Fourier Transform Infrared Spectroscopy
FFNN	Feed-forward Neural Network
GRNN	Generalized Regression Neural Network
HGI	Hardgrove Grindability Index
IN	Iteration Number
LDF	Linear Driving Force
LMA	Levenberg-Marquardt back-propagation algorithm
MAE	Mean Absolute Error
MLP	Multiple-layered Perceptron
MaMo	Mathematical Model
MM	Mineral Matter

MSE	Mean Square Error
MSRE	Mean Square Relative Error
NN	Neural Network
RMSE	Root Mean Square Error
RSM	Response Surface Methodology
SEM	Scanning Electron Microscopy
SE	Standard Error
WI	Work Index
XRD	X-ray Diffractometry
XRF	X-ray Fluorescence
YGP	Yancey, Geer and Price



RELATED PUBLICATIONS

Book chapter

1. **J. Kabuba**, E. Muzenda, F. Ntuli and A.F. Mulaba-Bafubiandi
“Investigation of Cu (II) removal from synthetic solution by ion exchange using South African clinoptilolite”
IAENG Transactions on Engineering Technologies, Lecture notes in Electrical Engineering, 2013, vol. 170, pp. 249-261, ISBN 978-94-007-4786-9.

Peer reviewed journal publications

1. **J. Kabuba** , A.F. Mulaba-Bafubiandi and K. Battle
“Neural network technique for modelling of Cu (II) removal from aqueous solution by clinoptilolite”
Arabian Journal for Science and Engineering, October 2014, vol. 39, Issue10, pp. 6793-6803.
2. **J. Kabuba**, A.F. Mulaba-Bafubiandi and K. Battle
“Prediction of abrasiveness characteristics of thermal coal on abrasive index using Neural Networks”
Manuscript, SAIMM Journal paper 13/160 assigning for review in The Journal of the Southern African Institute of Mining and Metallurgy.

Peer reviewed conference proceedings

1. **J. Kabuba** and A.F. Mulaba-Bafubiandi

“The use of neural networks for modelling of copper removal from aqueous solution by the ion-exchange process”

International Conference Proceedings of (Planetary Scientific Research Centre) PSRC, 2013, International Conference on Chemical, Industrial, Environment, Mining and Metallurgical Engineering (ICCIEMME 2013) & International Conference on Energy, Nanotechnology and Environmental Sciences (ICENES 2013), Johannesburg, South Africa, April 15-16, 2013. pp. 131-135. ISBN: 978-93-82242-26-0.

2. **J. Kabuba** and A.F. Mulaba-Bafubiandi

“Comparing empirical models and neural networks for the determination of the coal abrasiveness index”

International Conference Proceedings of (Planetary Scientific Research Centre) PSRC, 2013, International Conference on Chemical, Industrial, Environment, Mining and Metallurgical Engineering (ICCIEMME 2013) & International Conference on Energy, Nanotechnology and Environmental Sciences (ICENES' 2013), Johannesburg, South Africa, April 15-16, 2013. pp. 136-140. ISBN: 978-93-82242-26-0.

3. **J. Kabuba** and A.F. Mulaba-Bafubiandi

“Comparison of equilibrium study of binary system Co-Cu ions using adsorption isotherm models and neural networks”

International Conference Proceedings of (Planetary Scientific Research Centre) PSRC, 2013, International Conference on Chemical, Industrial, Environment, Mining and Metallurgical Engineering (ICCIEMME 2013) & International Conference on Energy, Nanotechnology and Environmental Sciences (ICENES 2013), Johannesburg, South Africa, April 15-16, 2013. pp. 126-130. ISBN: 978-93-82242-26-0.

4. **J. Kabuba** and A.F. Mulaba-Bafubiandi

“Modeling of Co-Cu elution from clinoptilolite using neural networks”

Proceedings of the World Academy of Science, Engineering and Technology, WASET 68, 2012, Paris, France, August 22-23, 2012. pp. 1222-1225. ISSN 2010-376X.

5. **J. Kabuba**, A.F. Mulaba-Bafubiandi and Kim Battle

“Binary mixture of copper-cobalt ions uptake by zeolite using neural networks”

Proceedings of the World Academy of Science, Engineering and Technology, WASET 68, 2012, Paris, France, August 22-23, 2012. pp. 1216-1221. ISSN 2010-376X.

6. **J. Kabuba**, A.F. Mulaba-Bafubiandi and Kim Battle

“A critic’s study of neural networks applied to the ion-exchange process”

Proceedings of the World Academy of Science, Engineering and Technology, WASET 68, 2012, Paris, France, August 22-23, 2012. pp. 1226-1229. ISSN 2010-376X.

7. **J. Kabuba**, F. Ntuli, E. Muzenda and M. Mollagee

“Thermodynamics of Cu (II) adsorption onto South Africa clinoptilolite from synthetic solutions by the ion-exchange process”

Proceedings of the 2011 2nd International Conference on Chemistry and Chemical Engineering, IPCBEE, vol. 14, pp. 75-78, Chengdu, China, July 29-31, 2011. ISBN: 978-981-08-9082-7.

8. E. Muzenda, **J. Kabuba**, F. Ntuli, M Mollagee and A.F. Mulaba-Bafubiandi

“Cu (II) removal from synthetic waste water by the ion-exchange process”

Proceedings of the World Congress on Engineering and Computer Science 2011WCECS 2011, vol. II, pp. 685-689. October 19-21, 2011, San Francisco, USA. ISBN: 978-988-19251-7-6.

9. A. Amankwah, **J. Kabuba** and A.F. Mulaba-Bafubiandi

“Modeling of the ion-exchange processes using time delayed neural networks”

Proceedings of the 2011 3rd International Conference on Mechanical and Electrical Technology, ICMET, vol. I, pp. 447-451. Dalian, China. August 26-27, 2011. ISBN: 0-7918-5981-9.


CHAPTER 1: INTRODUCTION

1.1 Introduction

This chapter firstly presents the background and motivation to the application of neural networks (NN) to the ion-exchange process and to the Abrasiveness Index (AI) of coal, secondly the research problems, thirdly the aim and objectives, fourthly the scope and limitations of the study and fifthly the expected contribution to the present knowledge on the subject. The last part of this chapter provides the overview of the thesis.

1.2 Background and motivation

1.2.1 The ion-exchange process



The application of NN) and specifically feed-forward neural networks (FFNNs) with back-propagation (BP) has been considered a promising tool for the analysis of ion-exchange processes because of their simplicity with respect to simulation, prediction and modelling. The advantages of NNs are that they require less time for development than the traditional mathematical models. In addition, the need for extensive experimentation is avoided as limited numbers of experiments are sufficient to predict the degree of non-linearity and their ability to learn complex relationships without requiring the knowledge of model structure (Aber *et al.*, 2009; Daneshvar *et al.*, 2006; Fagundes-Klen *et al.*, 2007; Prakash *et al.*, 2008; Salari *et al.*, 2005; Yetilmezsay & Demired, 2008).

In recent years, the ion-exchange process has been widely employed for the removal of heavy metals from industrial wastewaters (Al-Enozi *et al.*, 2004; Dabrowski *et al.*, 2004; Thanasiadis & Helmreich, 2005; Kuronen *et al.*, 2006; Mamba *et al.*, 2009). This process is complex, non-linear and involves many factors influencing the ions' uptake mechanisms from the pregnant solution, the subsequent step being the elution. In order to improve the performance of the ion-exchange process, optimization and analysis of the process should be accomplished. Modelling and simulation are tools to achieve the objectives. However, the modelling of a process covers a broad spectrum. At one extreme lie theoretical models based on fundamental knowledge of the process. These models are also called knowledge based models. At the other end lie empirical models, which do not rely on the fundamental principles governing the process. The majority of models based on the ion-exchange process are theoretical. Most of these models are derived from physical descriptions and an understanding of the ion-exchange process under certain assumptions. These types of models are very useful for scale-up applications. However, as mentioned above, they are mathematically complex, computationally expensive and they ideally require a very detailed knowledge of the ion-exchange process itself. Therefore, there is a need to find an alternative means for predicting process performance which has led to the interest by researchers in applying neural network techniques.

1.2.2 The coal abrasiveness index (AI)

The importance and applications of NN techniques increased significantly leading to them being successfully used in research studies and in coal engineering applications (Raask, 1985; Spero, 1990; Li *et al.*, 2005). The generalized regression neural network

(GRNN) was used in this thesis to predict the AI of coal. The GRNN falls in the category of probabilistic NNs that can solve any function approximation problem if sufficient data are available. The additional knowledge needed to get a satisfactory fit is relatively limited and can be done without additional inputs from the user. This makes the GRNN a very useful tool to perform predictions of system performance in practice (Specht, 1991; Li *et al.*, 2005).

When coal is used for electricity generation it is usually pulverized (ground) to an efficient burnable size in a mill and then combusted (burned) in a furnace with a boiler. During grinding friction occurs which causes abrasive wear or erosion on the critical components and thereby affects the performance of the power plant. It is therefore important to assess the relative abrasion characteristics of thermal coal by selecting the right type of materials for crushing, grinding and burning of the coal.

Coal characterization techniques allow the mineral inclusions in coal that are responsible for the abrasive nature of the coal to be accurately characterized. This means there is scope to make improved predictions of wear based on a detailed knowledge of the mineral matter (MM) in a particular coal. It is important to understand the nature and properties of the MM in a coal that would contribute to abrasive wear. Although there are several linear formulas available for predicting the AI, most take into consideration only a limited number of the relevant factors, primarily related to coal rank, chemical composition and material content (Raask, 1985; Spero, 1990; Bandopadhyay, 2010b). These approaches mostly correlate the AI with some variables, possibly due to inherent restrictions in the mathematical expressions, although the effect of other variables, collectively and implicitly, in lumped empirical

factors is well known. Motivated by these considerations, a new approach such as the GRNN is suggested here for the prediction of the AI of coal.

1.3 Research problems/questions

Ion exchange is a non-linear process, which is difficult to model and simulate as there are many factors influencing the chemical process which are not well understood. In the past, empirical isotherm equations were used but there were definite shortcomings resulting in unreliable simulations. There is need to find a way to effectively predict and simulate the highly complex system and non-linear process of ion exchange.

Coal characterization techniques allow the mineral inclusions in a coal that are responsible for the abrasive nature of the coal to be accurately characterized. Hence, there is scope for improved prediction of wear based on a detailed knowledge of the MM in a particular coal. It is important, however, to understand the nature and properties of the MMs in a coal that would contribute to abrasive wear. Most of the empirical equations available in literature for the A of coal are based on linear assumptions which may lead to erroneous estimations and do not simultaneously take into consideration most of the relevant factors.

1.4 Aim and objectives

1.4.1 Aim

In this thesis, the development and implementation of the FFNNs with BP is investigated, in order to test the effectiveness in modelling the ion-exchange process

for the removal of heavy metals from industrial wastewaters. The GRNN approach is used to assess the AI of coal.

1.4.2 Objectives

The research objectives of this thesis are to:

- Examine the effectiveness in modelling the removal of dissolved copper and cobalt from an aqueous solution through an ion-exchange process using a FFNN approach.
- Investigate the possibility of the prediction of abrasiveness characteristics of the thermal coal by the AI using the GRNN.

1.5 Scope and limitations of the study

In this thesis the experimental design using analysis of variance (ANOVA) was chosen to compare to FFNN modelling techniques and for optimizing the effective input parameters.

The sensitivity analysis was conducted to determine the influence of the input variables on the performance of the model. For this four different models were trained and tested with GRNN techniques using the same training and testing data set.

1.6 Expected contribution to knowledge

The FFNN modelling techniques are expected to effectively predict and simulate the highly complex system and non-linear process such as the ion exchange using activated zeolite.

The GRNN technique is expected to provide results which would make it an effective tool to be employed to assess the AI of coal.

1.7 Structure of the thesis

This thesis is structured in five chapters.

Chapter 1 contains the introduction to the study, explains what has led to the study and what the study hopes to achieve.

Chapter 2 reviews the relevant research in a number of areas crucial to this research.

First of all the current status of prediction and modelling of the two metallurgical processes: The ion-exchange process and determination of coal abrasiveness is presented. Then the research literature specific to the application of various NN techniques is reviewed.

Chapter 3 presents the experimental methodology for the ion-exchange process.

Chapter 4 presents the findings and discussion in the light of the literature on the FFNN.

Chapter 5 presents the findings and discussion in the light of the literature on the GRNN.

Chapter 6 concludes the thesis and makes recommendations for further research.

CHAPTER 2: LITERATURE REVIEW

2.1 Introduction

This chapter will review the relevant research in a number of areas crucial to this study. First the current status of prediction and modelling of the two metallurgical processes will be covered and the ion exchange and determination of coal abrasiveness will be presented. Thereafter the research literature specific to the application of NN techniques will be reviewed.

2.2 Zeolites as the ion-exchange material

Natural zeolites were used as the ion-exchange material for the loading and elution of copper and cobalt respectively from an aqueous solution. These zeolites are crystalline alumina-silicate minerals with excellent cation exchange and high heavy metal selective properties (Dhermendra *et al.*, 2008). The mechanism of adsorption by zeolites was found to be via ion-exchange (Dhermendra *et al.*, 2008). In the three dimensional structure of the zeolites there are large channels containing negatively charged sites resulting from Al^{3+} replacement of Si^{4+} in the O_4 . These are tetrahedrally-linked by sharing oxygen atoms in rings and cage-cavities occupied by cations which are weakly held in the structure to compensate the charge imbalance (Chojnacki *et al.*, 2004). Zeolites contain various types of cationic sites (Abusafa & Yucel, 2002). The overall negative charge of the anions is balanced by cations that occupy the channels within the structure, and can be replaced with heavy metal ions (Chojnacki *et al.*, 2004). There are about forty natural zeolite structures that have been identified

during the past 200 years; the most common are analcime, chabazite, clinoptilolite, erionite, ferrierite, heulandite, laumontite, mordenite and phillipsite (Virta, 1998). As it is not the aim of this section to present an exhaustive description of all structures, only the clinoptilolite structure, which is the natural zeolite used in this thesis, will be described. The typical model structure of clinoptilolite is shown in Figure 2.1.

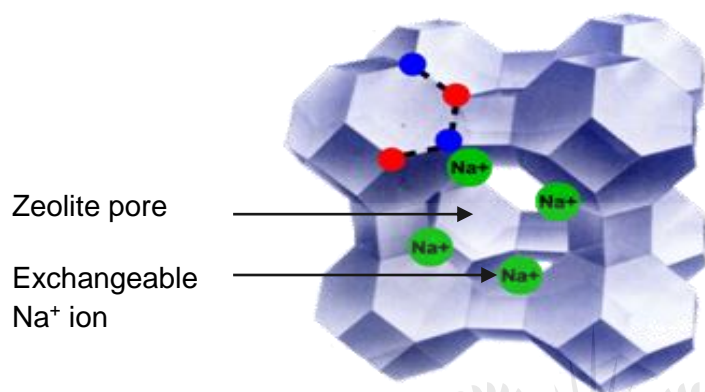


Figure 2.1: Model structure of clinoptilolite (Gilchrist, 1989)

Clinoptilolite is the most abundant and cosmopolitan natural zeolite and it has been widely exploited for its ion-exchange capabilities, since it can easily exchange its interstitial cations for external cations in solution (Gilchrist, 1989). Natural zeolites such as clinoptilolite are able to lose and gain water in a reversible manner and to exchange their extra framework cations, both without changing the crystal structure. The typical formula for natural clinoptilolite is $\text{Na}_6[(\text{AlO}_2)_6(\text{SiO}_2)_{30}]\cdot 24\text{H}_2\text{O}$ (Breck, 1974). The ion exchange is made possible by the presence of extra-framework cations which are located in the regular array of channels and cages that constitute the rigid anionic framework. Cations are bound to the lattice and to water molecules which normally fill the clinoptilolite micropores (Gilchrist, 1989). When the clinoptilolite comes into contact with an electrolytic solution, the exchangeable cations in the clinoptilolite can be removed from their sites and replaced by ions (cation) in the solution. The substitution

is stoichiometric and depends on the parameters provided during experimental procedures (Nyembe, 2010).

2.2.1 Clinoptilolite characterization

The X-ray fluorescence (XRF) and X-ray diffractometry (XRD) characterization done by Mamba *et al.* (2009) showed that clinoptilolite contained exchangeable ions of sodium, potassium, calcium and magnesium. This zeolite (clinoptilolite) has a Si/Al ratio of 5.96 (mol/mol) and the corresponding ratio of $\frac{(Na^+ + K^+)}{Ca^{2+}}$ was 3.4. XRF also confirmed that the zeolite was a high silica clinoptilolite enriched with Mg^{2+} , K^+ and Na^+ . Figure 2.2 shows a typical mineralogical diffraction pattern of a crystallite with a composition of 70% SiO_2 , 12% Al_2O_3 , 5% K_2O , 2.5% Fe_2O_3 , 2% Na_2O , 2% CaO and 0.2% traces of TiO_2 . In Figure 2.2, **C**, **D** and **Q** represent calcite, dolomite and quartz respectively. The XRF technique revealed the following composition for the original clinoptilolite: 74% SiO_2 , 12.4% Al_2O_3 , 3.8% KO , 1.5% Fe_2O_3 , 1.5% CaO , 1.3% Na_2O , 1.1% MgO and 0.2% TiO_2 . This composition suggested that the clinoptilolite was a silicon based zeolite, when taking into account that its major component was silicon dioxide (Mamba *et al.*, 2009). The XRF and XRD determinations to a very large extent were thus in agreement particularly with the dominance of the silicon species followed by aluminium. Traces of other elements not accounted for in the XRD determinations were probably the titanium and magnesium moieties which XRF analysis could not detect. Thus the percentage composition detected by XRF did not add up to 100% (Mamba *et al.*, 2009).

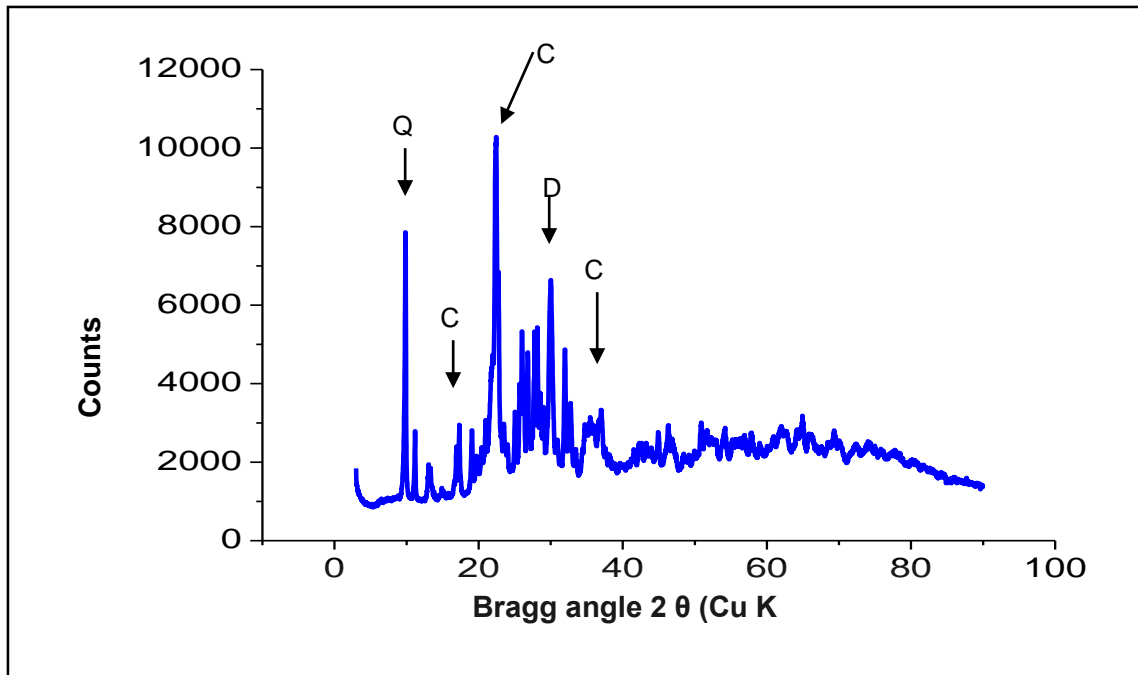


Figure 2.2: Mineralogical diffraction pattern of the natural clinoptilolite (Mamba *et al.*, 2009)

2.2.2 Treatment of clinoptilolite for loading

Clinoptilolite was treated with hydrochloric acid (HCl) at different concentrations with the aim of using it as an adsorbent for the removal of copper and cobalt from an aqueous solution. The Brunauer–Emmett–Teller (BET) analysis done by Mamba *et al.*, (2009) shows no significant changes in pore volume and surface area with an increase in the HCl activation concentration of the zeolites. The relationship between HCl concentrations used for the activation and both the surface area and pore volume of clinoptilolite are shown in Table 2.1.

Table 2.1: Results of pore volume measurements of clinoptilolite (Mamba *et al.*, 2009)

HCl Conc. (g/mol)	Pore volume (cm ³ /g)	Surface area (m ² /g)
Original clinoptilolite	0.068	20.88
0.02	0.068	19.80
0.04	0.064	18.73

Figures 2.3 and 2.4 illustrate the surface texture and porosity of clinoptilolite with holes and small openings on the surface which will increase the contact area of the adsorbent and consequently lead to the pores' diffusion during adsorption (Swayampakula, 2009). The surface morphology of treated clinoptilolite as shown in Figure 2.4 developed more pores and a more softened structure than the original clinoptilolite. The adsorption capacity of the treated clinoptilolite was found to be higher than the original clinoptilolite. This observation can be attributed to the fact that adsorption is a surface phenomenon, i.e. surface area is related to the adsorption capacity of the adsorbent. An increase in surface area provides more binding sites for the adsorbate to be adsorbed (Taty-costodes *et al.*, 2003).

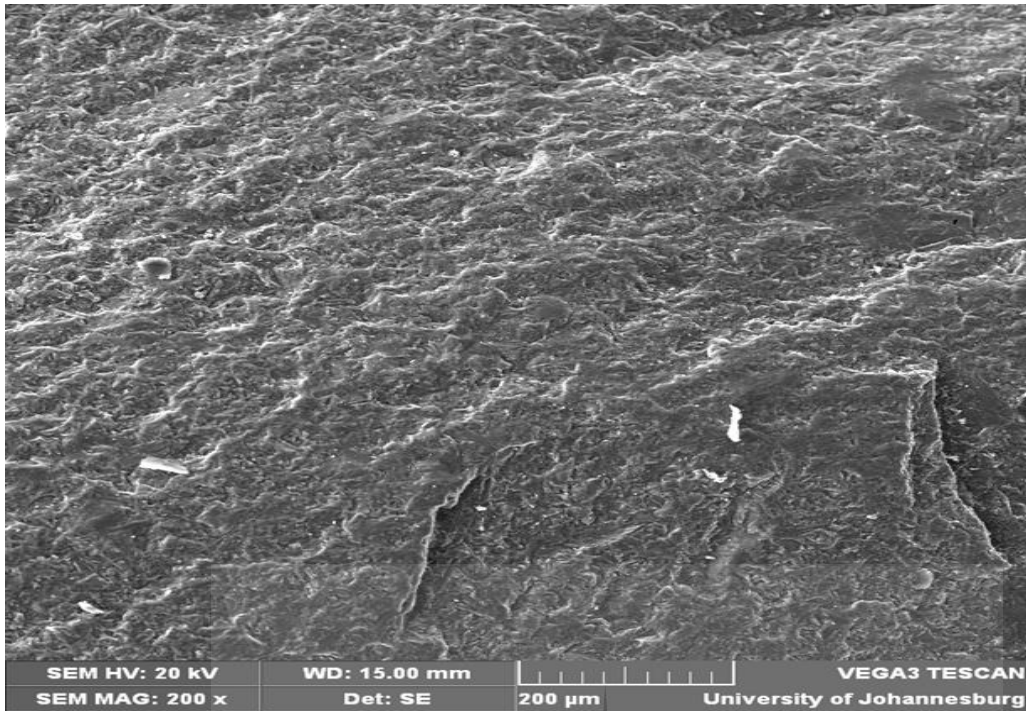


Figure 2.3: Scanning electron microscopy (SEM) image of original clinoptilolite (Abdulkareem *et al.*, 2012)

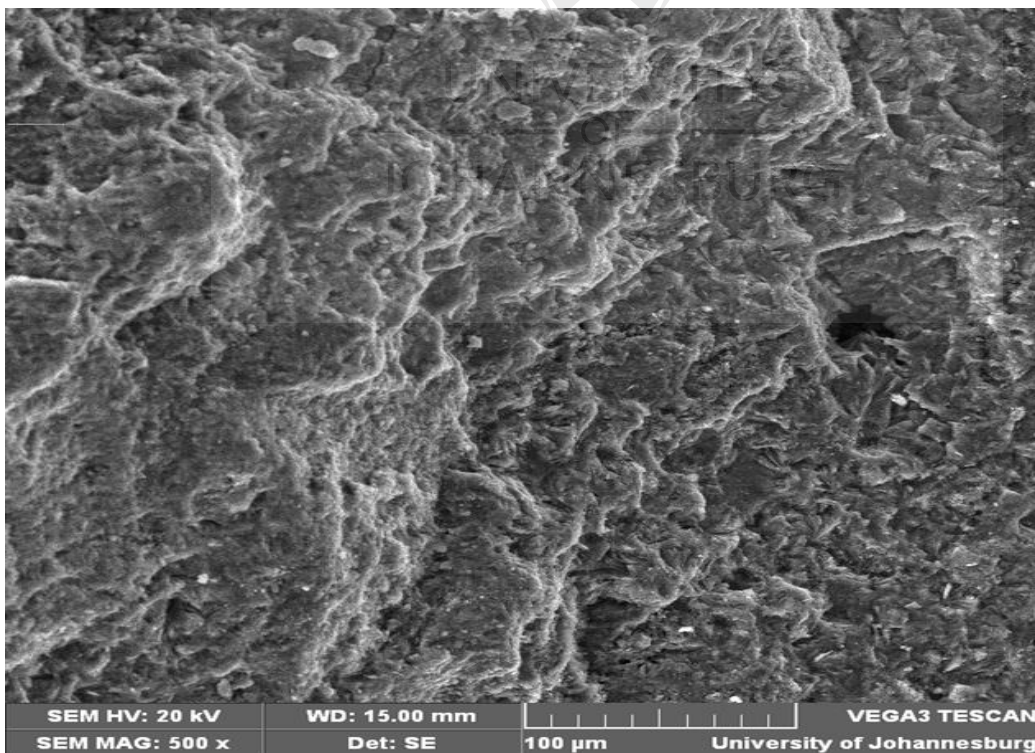


Figure 2.4: SEM image of HCl activated clinoptilolite (Abdulkareem *et al.*, 2012)

2.2.3 The Fourier transform infrared spectroscopy (FTIR) analysis

Figure 2.5 shows the FTIR spectra for the original and activated clinoptilolite. This figure gives a clear picture of the effect of the treatment of the clinoptilolite. HCl treatment is said to remove the non-zeolitic components thus increasing the concentration of zeolite minerals (Vanloon & Duffy, 2000).

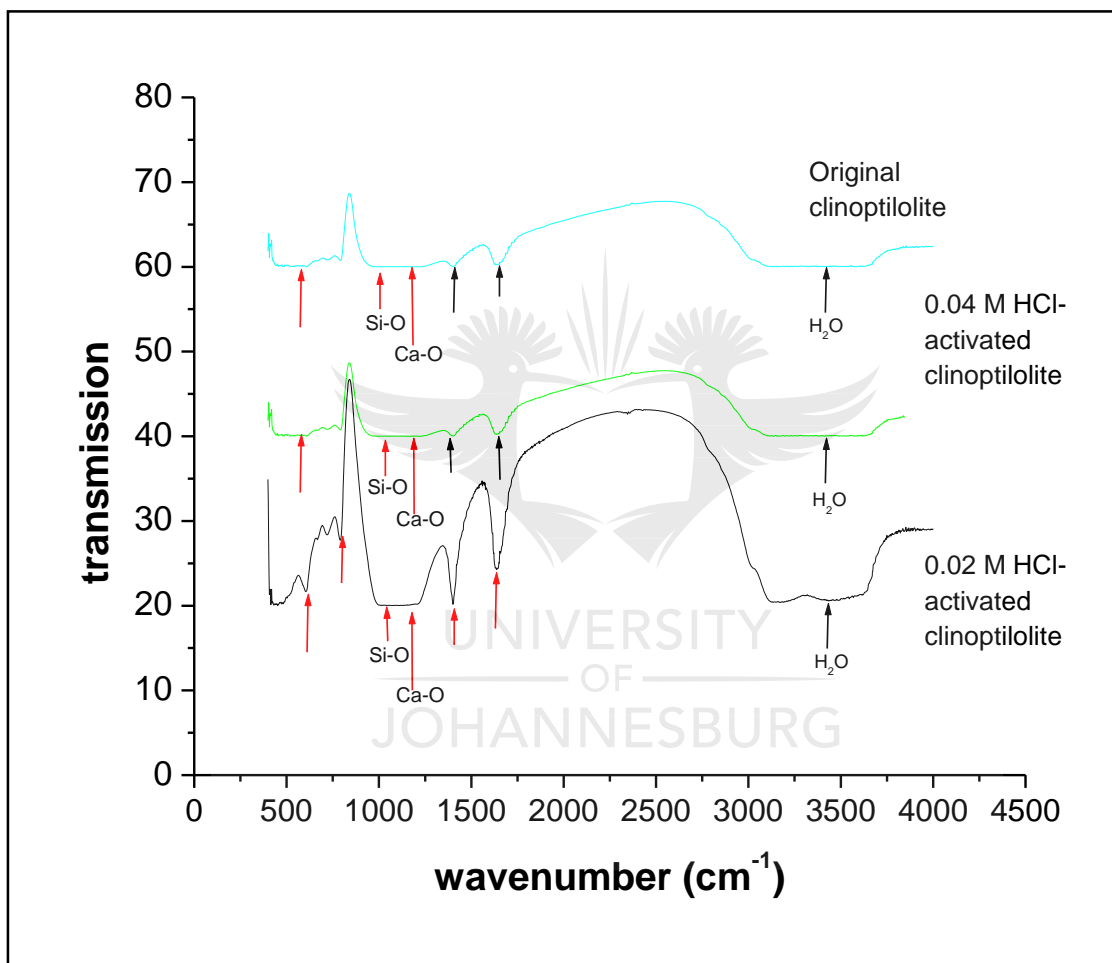


Figure 2.5: The FTIR spectra for original and HCl-activated clinoptilolite (Mamba *et al.*, 2009)

In Figure 2.5 at the range of 4000 and 3000 cm⁻¹, the original and HCl-activated clinoptilolite forms at a concentration of 0.04 M and the 0.02 M HCl-activated forms of

clinoptilolite showed distinct stretching at this range which is typical of water absorption (Madejova, 2003; Al-Degs *et al.*, 2003). This shows that water adsorption and retention by clinoptilolite is increased by HCl activation at 0.02 M concentration. At the range of 2000 and 1500 cm^{-1} , the 0.02 M HCl-activated clinoptilolite showed two intensive peaks, and yet again the original and the 0.04 M activated forms showed none. This could be as a result of 0.02 M activation washing out the non-zeolitic impurities present in the original clinoptilolite as confirmed by XRD, XRF and SEM. The disappearance of these peaks with the 0.04 M HCl-activated form could be due to the strength of the acid resulting in the destruction of the active sites observed with the 0.02 M HCl-activated clinoptilolite. There were peaks observed for all the clinoptilolite forms at 1558 cm^{-1} , which may be due to the bending vibrations of adsorbed water. This is expected, since given its porous structure, desiccation of the zeolite at the high temperature of 50°C will increase its hydrophilic (water absorption) properties (Ng & Mintova, 2008). Zeolites that have K^+ in high amounts have low water absorption capacity (Mamba *et al.*, 2009). This could probably explain why the original clinoptilolite does not show such peaks. It is also possible that the K^+ in the acid-activated zeolite was leached out by the acid. The intensity of the peak at this range is more pronounced with the 0.02 M HCl activation than it is with the 0.04 M HCl activation and the original forms. Since this is a water sorption peak, it could be possible that water sorption capacity is low with the original clinoptilolite and high with 0.02 M HCl-activated clinoptilolite. An increase in HCl activation to 0.04 M concentration diminishes the water sorption capacity of the zeolite.

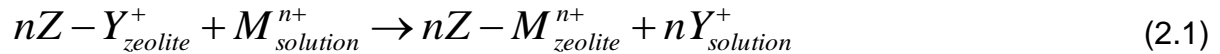
The stretching between 1500 and 1000 cm^{-1} observed in Figure 2.5 indicates the presence of a high content of calcite in the sample as confirmed by SEM-energy dispersive spectroscopy (EDS). The strong band at 1341 cm^{-1} (due to Si–O stretching)

is the main characteristic band for quartz (Al-Degs *et al.*, 2003). The peaks observed between 1000 and 600 cm^{-1} are present in all the forms of clinoptilolite. One characteristic band appears at 836 cm^{-1} for all the forms. This is the quartz band. Quartz is common in zeolites, especially those of the Heulandite family (Al-Degs *et al.*, 2003). The peak that appears at 753 cm^{-1} in the original clinoptilolite form appears at 759 cm^{-1} for the activated zeolite. There is a peak that appears at 686 cm^{-1} in the original form while in the acid-activated forms it appears at 635 cm^{-1} . This shift could be attributed to the action of the acid. It has been documented that acid treatment of natural clinoptilolite improves its sorption properties in ion-exchange applications which is due to decatenation, dealumination and the dissolution of amorphous silica fragments blocking the channels (Kuronen *et al.*, 2006; Inglezakis & Grigoropoulou, 2004). A study by Korkunen *et al.* (2006) also revealed that there is a change in the clinoptilolite structure after acid treatment, with dilute acid activations accounting for improved heavy metal removal capacity of the clinoptilolite (Kuronen *et al.*, 2006). Studies by Hernandez (2000) confirm findings in this study with respect to the effect of acid conditioning of natural clinoptilolite (Kuronen *et al.*, 2006; Hernandez, 2000).

2.3 The ion-exchange process

Ion exchange is a reversible chemical reaction in which ions are exchanged between a solution and an insoluble solid. The ion-exchange process refers to the interaction of ionic species in aqueous solutions with adsorbent solid materials. It is distinguished from conventional adsorption by the nature and morphology of the adsorbent material which in most cases is either a dynamic *polymer* matrix or an inorganic structure containing exchangeable functional groups (Slater, 1991). The physico-chemical

processes that occur during metal ion exchange can be expressed in the following reaction:



Where Z represents the zeolite, M represents the cationic group in the solution and n is the reaction component that depends on the oxidation state of the metal ions (Dabrowski *et al.*, 2004).

2.3.1 Factors influencing the kinetics of the ion-exchange process

There are various factors that may influence the kinetics of the ion-exchange process (Helfferich, 1962). Examples of these are the following:

- Movement of the metal ions from the solution;
- Diffusion of ions through the laminar film surrounding the material (the ion exchanger)
- Diffusion of ions through the pores of the ion-exchanger material;
- The physical process of ion exchange;
- Diffusion of counter-ions outwards through the material;
- Diffusion of counter-ions through the laminar layer;
- Movement of counter-ions into the aqueous solution.

Many researchers have indicated that film and pore diffusions are the two main factors that influence the rate of the ion-exchange process (Van Deventer, 1984).

2.3.2 Rate controlling steps in the ion-exchange process

An intraparticle diffusion model for metal uptake kinetics is conceptualized according to the “two-step mass transport mechanism” (Chen & Wang, 2007). It is assumed that the metal ions first transfer through the external liquid film from the aqueous solution, then diffuse inside the ion-exchange material before being taken up by the functional group. However, the driving force for each of these two steps is different. In the liquid, the concentration difference is found between the bulk solution and the liquid at the surface of the zeolite (the ion-exchange material), which can never be larger than the bulk concentration. In the zeolite, the concentration difference is found between the outer surface and the centre of the particle.

Although much has been documented regarding the sorption of metal ions, a comprehensive study on the rate-controlling steps has not yet been documented. However, the roles of several relevant factors have become clear. Studies have shown that control by liquid-phase mass transfer is favoured by the following:

- Low liquid-phase concentration (a small driving force in the liquid);
- High ion-exchange capacity (a large driving force in the exchanger);
- Small particle size (a short mass transfer distance in the zeolite);
- Open structure of the exchanger (little obstruction to diffusion in the exchanger);
- Ineffective agitation of the liquid (low contribution from convection to liquid-phase mass transfer).
- With regard to diffusion it can be imagined that the ion exchange depends on the wandering of ions within the solution, across the boundary film around the zeolite particle and within the zeolite bead to and from the exchange site. Some of these effects are probably the controlling factors of the process. However, it

has been found that the exchange rate may obey neither model equations for diffusion, whether it is film or particle, nor chemically controlled mechanisms (Van den Bosch, 2009).

2.3.3 The Ion-exchange isotherms

The ion-exchange isotherm studies are of fundamental importance in the design of ion-exchange systems since they indicate how the ions are partitioned between the adsorbent and liquid phases when in equilibrium as a function of increasing ion concentrations. When an adsorbent and an ion solution are placed in contact, the concentration of ions in the adsorbent will increase until a dynamic equilibrium is reached. At this point, there is a defined distribution of ions between the solid and liquid phases (Peric *et al.*, 2004). The equations which are often used to describe the experimental isotherms were developed by Langmuir, Freundlich and Dubini-Radushkevich (D-R).

2.3.3.1 Langmuir isotherm

The Langmuir isotherm is a commonly applied model for adsorption on a completely homogenous surface with negligible interaction between adsorbed molecules. The model assumes uniform adsorption energies onto the surface, and maximum adsorption depends on the saturation level of the monolayer. Traditionally, the Langmuir model is represented as (Santo *et al.*, 2011):

$$q_e = \frac{Q_{\max} K_L C_e}{1 + K_L C_e} \quad (2.2)$$

Where q_e is the number of ions exchanged per unit weight of clinoptilolite at equilibrium (mg/g), C_e (mg/L). The equilibrium concentration of ions in the solution, Q_{max} (mg/g) is the maximum adsorption capacity (mmg/g), and K_L (L/mg) is the Langmuir constant related to the ion-exchange capacity and energy of the ion exchange.

2.3.3.2 Freundlich isotherm

The Freundlich isotherm is known as the earliest empirical equation and is shown to be consistent with an exponential distribution of active centres, characteristic of heterogeneous surfaces (Castaldi *et al.*, 2008). This Freundlich isotherm is also a non-linear model that assumes a heterogeneous energetic distribution as well as interaction between the adsorbed molecules. The Freundlich model is expressed using the following equation (Demarchi *et al.*, 2013):

$$q_e = K_F C_e^{\frac{1}{n}} \quad (2.3)$$

Where K_F and n (dimensionless) are the Freundlich isotherm constants determined from the non-linear regression.

2.3.3.3 Dubini-Radushkevich (D-R) isotherm

The D-R model is based on the Polanyi adsorption potential theory which defines an adsorption potential, ε related to the energy freed from a substance when going from the liquid to the zeolite phase. In contrast to the Langmuir and Freundlich models, the D-R considers a micropore volume filling adsorption process and is temperature dependent. In order to understand the adsorption type and the mechanism, the equilibrium data was applied to the (D-R) isotherm model (Chatterjee *et al.*, 2009):

$$\ln Q = \ln Q_m - K_{D-R} \varepsilon^2 \quad (2.4)$$

$$\text{Where: } \varepsilon \text{ (Polanyi potential)} = RT \ln[1 + (1/C_e)] \quad (2.5)$$

Q is the amount of anion adsorbed per unit weight of adsorbent, Q_m is the adsorption capacity, C_e the equilibrium concentration of anion in the solution, K_{D-R} is the constant related to adsorption energy, R the universal gas constant and T is the temperature.

2.3.4 The cation exchange capacity

The evaluation of the equilibrium data obtained from equilibrium studies with a suitable mathematical description is of great importance not only for the design of the ion-exchange processes, but also for the investigation of the mechanisms involved in heavy metal-ion exchanger interactions (Bailey & Esterie, 1996). The ion-exchange capacity of zeolites is usually described in terms of equilibrium isotherms. It depends on the system's temperature, the total initial concentration of the solution in contact with the exchanger and on the characteristics of the ion-exchange system, such as solution composition, mineral type and pH. They are the most widely used methods for evaluating the capability of clinoptilolite (zeolite) for the loading of heavy metals.

The quantity of ions exchangeable by a solid exchanger, depending on its chemical and structural features, is called the ion-exchange capacity and is usually expressed in milli-equivalents per gram (m_{eq}/g) (Petrus & Warchol, 2003). During the ion-exchange process, two phases are involved and these compete in mutually sharing two ions. The ion transfer from one phase to the other is dependent upon electro neutrality and is regulated by the ion concentration in both phases as well as by selectivity. This parameter is a function of both the energy of ion-lattice interaction and

ion-hydration energy. Many researchers have carried out equilibrium studies with various clinoptilolite samples under different initial experimental conditions to determine the capabilities of their ion-exchange materials towards heavy metal cations. The ion-exchange capability of minerals influences their unique physical properties, such as the cation retention and diffusion processes of charged and neutral molecules. The numerical value of this property is described by the cation exchange capacity (CEC). Methods for determining CEC involve the complete exchange of the naturally occurring cations by a cationic species, such as ammonium, K, Na and Cu (Petrus & Warchol, 2003).

2.4 Review of modelling the ion-exchange process

The ion-exchange process, both on natural or synthetic materials, is usually carried out in a fixed bed apparatus in which the exchanging material is packed in the form of granules, and the stream to be purified is allowed to flow through the packing (Pepe *et al.*, 2013). Modelling of the ion-exchange process has been studied. Warchol & Petrus (2006) considered clinoptilolite-rich tuff from Ukraine, even though they used a rather simplified modelling approach named the “Lumped-Kinetic” model for the ion-exchange equilibrium and column dynamics. A different modelling approach, derived from Khosrow Nikkha (2002), used dynamic simulation in the design of ion-exchange systems, and the investigation of equipment based on the consideration of the effect of input criteria such as expected ion-loading and elution profiles. The methodology for dynamic modelling using IDEAS™ in the design of multicolumn ion-exchange trains operating in parallel was presented. The IDEAS simulation was best suited for modelling ion-exchange systems because it depicts the process material and energy

flows as a function of time. For hydrometallurgical plants, where sequential ion exchange systems and other continuous operations interact and are interdependent, it is necessary to perform dynamic computer modelling of the design process. Loading and elution reactions are also dependent on process stream concentrations, temperature and the way in which the solution makes contact with the resin. If enough information is available from test work, it can be incorporated in a dynamic ion-exchange model to provide some degree of predictive capability.

Another modelling approach derived from the work of Ogata and Banks (1961), has often been used. According to this approach, equilibrium conditions between solids and liquids are assumed, and an adjustable “hydrodynamic dispersion” is used to describe the effects of flow non-idealities, diffusional resistances to mass transfer and kinetic resistances (Appelo & Postma, 1999). Rahman *et al.* (2009) recently published a series of papers using this approach to describe ion-exchange processes involving synthetic zeolites (Rahman *et al.*, 2009). They illustrated the use of hydrodynamic dispersion in the forecast of long-term performance of active barriers against radionuclides. In contrast, Borba *et al.* (2011) investigated the ion exchange both on synthetic zeolites and synthetic resins using a more detailed model, taking great care of the form of the material balance equations. These authors also pointed out the crucial role played by an appropriate description of the thermodynamics of the ion exchange in modelling the overall process. Cobzaru (2005) used the Table Curve 3D programme in order to describe the behaviour of the ion-exchange processes of sodium modified clinoptilolite with heavy metal ions (Cr^{3+} , Fe^{3+} , Ni^{2+} , Cd^{2+} and Pd^{2+}) from residual waters. The resulting models showed common characteristics such as a very good arrangement of the experimental points on the response surfaces and similar correlation coefficients close to unity. Although these models exhibit

similarities, they differed with regard to the response surface shape and model equation. Despite the good results presented, the author did not compare their prediction to experimental data. The model was also unable to accurately predict the process as affected by operating parameters. Phongikaroon and Simpson (2006) extend the modelling approach originally proposed by Simpson and Gougar (2003) from a covalent species to include divalent and trivalent cations, using the same fundamental approach. The principal challenge was to derive a model that was sufficiently sophisticated to capture a realistic mechanism for ion exchange while still being simple enough to apply to available data without having to revert to complicated numerical solutions. Previous work on modelling equilibrium ion exchanges between zeolite-A and molten chloride salts involved two different types of models that fitted well with experimental data for monovalent species. The approach taken by Lexa and Johnson (2001) was strictly empirical and based on simple geometrical arguments, limited zeolite cage volume versus involved ionic radii. In contrast the approach taken by Simpson and Gougar (2003) was based on balancing the adsorption and desorption rates from two different types of sites in the zeolite. Neither approach was encumbered with the complexity of considering divalent and trivalent species. Each such species occupies two or three sites, respectively. Despite the complexity described above, Gougar (2004) has provided a model that accounts for divalent and trivalent cations while avoiding mathematical complexity. In this research of Gougar, cesium and neodymium were studied as surrogate fission species. The model was derived from an analogy of probability through reaction kinetics and expressed in a one-dimensional domain. The resulting model presented therein revealed a decent fit to experimental data.

Natural zeolites are often characterized by very complex structures as described in Section 2.2, which are not even fully characterized, making modelling of both the thermodynamics and kinetics of the ion-exchange process rather problematic. As concerns the first aspect, Brigatti *et al.* (1999) studied the selectivity of a phillipsite and chabazite rich tuff towards Co^{2+} , Cu^{2+} , Zn^{2+} , Cd^{2+} and Pb^{2+} , focusing on the fact that phillipsite and chabazite have a complex mixture of different solid phases, with different ion-exchange properties. With regard to the kinetics of the process, the use of a lumped parameter model such as the Linear Driving Force (LDF) model is in practice mandatory (Glueckauf, 1955). According to the LDF model, both liquid-solid and intra-particle mass transfer rates depend linearly on their respective driving forces, with equilibrium prevailing at the liquid-solid interface, despite the fact that the LDF model is rigorously valid only when a linear isotherm exists. Santacesaria *et al.* (1982) and Ruthven (1984) indicate that, even in the presence of non-linear isotherms, the LDF model continues to give good results when used to evaluate breakthrough curves. Following this suggestion, Pepe *et al.* (2013) satisfactorily applied the LDF model to ion exchange on natural zeolites, describing the kinetics of the $\text{Pb}^{2+}/\text{Na}^+$ exchange process on a phillipsite-rich tuff. Pepe *et al.* (2013) used the LDF model to interpret the experimental data. The model established that both the internal and the external mass transfer resistances play a significant role in the kinetics of the ion-exchange process. The estimated values of the internal and the external mass transfer coefficients did not depend on the composition of the liquid phase, thereby confirming the validity of the LDF model approximation.

Van den Bosch (2009) used the neuro-fuzzy computing technique to test the effectiveness in simulating the ion-exchange processes. The primary aim was to test neuro-fuzzy reasoning as a modelling technique for complex ion-exchange processes.

The obtained results were then compared with conventional ion-exchange techniques. The comparison was based on data sets obtained from laboratory scale ion-exchange batch experiments. Mass transfer parameters were determined for a film diffusion model, which were then used to simulate the ion-exchange profiles for copper and cobalt. Before commencing the design of the neuro-fuzzy system, the number rule, input and type of membership functions had to be decided upon. Sensible initial values for the neuro-fuzzy parameters were chosen and manipulated (or trained) using MS EXCEL SOLVER. The programme could model up to five inputs and one output. The results obtained from the film diffusion method did not result in the same accuracy as the neuro-fuzzy system, indicated by the lower percentage error obtained (4.15% by ANFIS 6). It was also noted that an increase in the number of inputs in the neuro-fuzzy system did not necessarily generate a better ion-exchange model. It was found that the combination of copper and cobalt solution concentrations, the copper and cobalt resin loading and the stirring speed resulted in the most accurate model. SOLVER, which is based on a Newtonian algorithm, is a relatively good tool to use for ion-exchange modelling as was shown in the results. There was no need to introduce any sophisticated algorithms. Although it is a very useful tool and can be applied in many different processes, developing neuro-fuzzy software is time consuming.

The correct modelling of the ion-exchange process requires all factors to be taken into account and combined into one model. The combination of these factors is obviously complex, hence the application of the NN.

2.5 Review of the application of the FFNN

Much effort has been devoted to develop and improve the environment. To achieve optimum control and management in environmental engineering problems, new concepts involving efficient operation and design should be developed and understood. A high quality representative model can provide a favourable solution in the process control. It helps to explain the real process performance and to develop a continuous control strategy for these types of technologies. Because of their reliable, robust and salient characteristics in capturing the non-linear relationships existing between variables in complex systems, it has become apparent that numerous applications of NN have been successfully applied (Yetilmezsay & Demired, 2008).

A NN is an information processing paradigm that is inspired by the way a biological nervous system, such as the brain, processes information and learns (Haykin, 1994). FFNNs are among the most important and widely used forms of NNs for time series modelling (Khashei & Bijari, 2012). FFNNs are flexible computing frameworks and universal approximators that can be applied to a wide range of wastewater treatment problems with a high degree of accuracy. Several distinguishing features of FFNNs make them valuable and attractive for wastewater treatment process tasks. Firstly, FFNNs are data-driven self-adaptive methods in that there are few *a priori* assumptions about the models for problems being studied. Secondly, it can generalize. Thirdly, FFNNs are universal functional approximators that can approximate a large class of functions with a high degree of accuracy. Finally, FFNNs are non-linear. Their power comes from the parallel processing of the information from the data. No prior assumption of the model form is required in the model building process (Khashei & Bijari, 2012). Instead, the network model is largely determined by the characteristics of the data. The model is characterized by a network of three layers of simple processing units connected by acyclic links (Khashei & Bijari, 2012). The

Equation 2.6 represents the relationship between the output (y_t) and the input (y_{t-1}, \dots, y_{t-p}).

$$y_t = w_o + \sum_{j=1}^Q w_j g \left(w_{oj} + \sum_{i=1}^P w_{ij} y_{t-i} \right) + e_t \quad (2.6)$$

Where, w_{ij} ($i = 0, 1, 2, \dots, P, j = 1, 2, \dots, Q$) and w_j ($j = 0, 1, 2, \dots, Q$) are model parameters often called connection weights; P is the number of input nodes; Q is the number of hidden nodes; e_t is the residual of model at time t , and g is the transfer function.

The FFNN model in Equation 2.6, in fact, performs non-linear functional mapping from the past observations to the future value (Khashei & Bijari, 2012).

2.5.1 Biological wastewater treatment

Cote *et al.* (1995) developed a procedure to improve the accuracy of an existing mechanistic model of the activated sludge process, previously described by Lessard and Beck (1993). As a first step, parameter optimization of the model was performed using a least square regression analysis. The optimization procedure did not succeed in improving the prediction of the four remaining key variables. In the second step, FFNNs were used to successfully simulate the prediction errors of the mechanistic model. If no significant improvement is observed, it may suggest that the data are not sufficiently rich in information or that important variables are not considered in the model. Gontarski *et al.* (2000) used NN for the simulation of an industrial wastewater treatment plant. Pai *et al.* (2007) in contrast used NN to predict the suspected solids and chemical oxygen demand in hospital wastewater treatment plant effluent. Luccarini *et al.* (2002) used NN for soft sensors for the control of nitrogen and

phosphorus removal from wastewaters. Hong *et al.* (2007) used NN for monitoring a sequencing batch reactor for nitrogen and phosphorus removal. Sinha *et al.* (1982) applied NN for the simulation of upflow of an anaerobic sludge blanket reactor performance and Zeng *et al.* (2003) used NN for a predictive control system for paper mill wastewater treatment.

Although a number of studies have been successfully conducted on engineering problems using back-propagation (BP) NNs for biological wastewater treatment, physico-chemical wastewater treatment was used due to their many favourable features such as efficiency, generalization and simplicity.

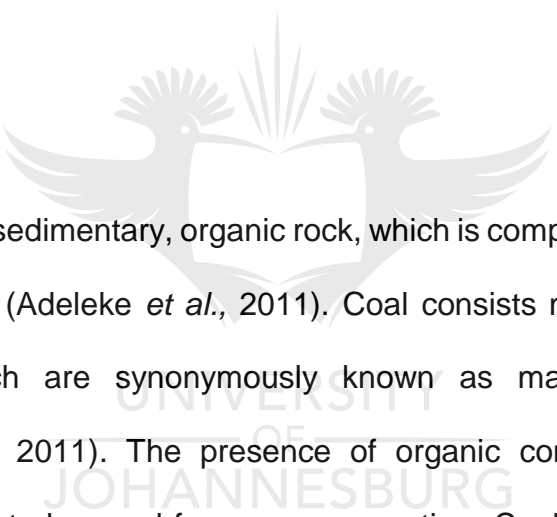
2.5.2 Physico-chemical wastewater treatment

Piron *et al.* (1997) applied NN for crossflow microfiltration modelling: “black-box” and semi-physical approaches. Hamachi *et al.* (1999) used dynamic modelling of cross-flow microfiltration of a bentonite suspension using recurrent NNs. Teodosiu *et al.* (2000) used NN models for ultrafiltration and backwashing. Bhattacharjee and Singh (2002) studied the applicability of artificial NNs in continuous stirred ultrafiltration. Shetty *et al.* (2003) used NNs for predicting contaminant removal during municipal drinking water nanofiltration. Wang *et al.* (2006) in turn applied radial basis function NNs based modelling of the membrane separation process for hydrogen recovery from refinery gases. Cinar *et al.* (2006) applied NNs for modelling the submerged membrane bioreactor treating cheese whey wastewater. Sadrzadeh *et al.* (2009) applied NN modelling of Pb^{2+} removal from wastewater using electro dialysis. NNs successfully tracked the non-linear behaviour of separation percentage and the current efficiency versus temperature, voltage, concentration and flow rate with a

standard deviation of not more than 1%. For almost all experiments, the NN was confirmed to be an adequate interpolation tool where good prediction was obtained. Numerous applications of NNs have been successfully conducted to solve environmental problems, since it is reliable and robust in capturing the non-linear relationships existing between variables (input/output) in complex systems (Turan *et al.* 2011). The ion-exchange process was used in this thesis due to its many advantages, such as high treatment capacity, high removal efficiency and fast kinetics.

2.6 Determination of the AI of coal

2.6.1 Introduction



Coal is a combustible, sedimentary, organic rock, which is composed mainly of carbon, hydrogen and oxygen (Adeleke *et al.*, 2011). Coal consists mainly of organics and organic matters which are synonymously known as macerals and minerals, respectively (Tlotleng, 2011). The presence of organic constituents in coal has rendered coal suitable to be used for power generation. Coal is primarily used as a solid fuel to produce electricity and heat through combustion. When coal is used for electricity generation, it is usually pulverized (ground) to an efficient burnable size in a mill and then combusted (burned) in a furnace with a boiler. During grinding, friction occurs, causing abrasive wear or erosion on the critical components and thereby affecting the performance of the power plant (Tlotleng, 2011).

Abrasion is a phenomenon that involves either erosion and/or material wear which occurs when a particle is trapped between the mill components and its walls during grinding. More precisely, abrasion has a tendency for coal to wear away mill

components (Falcon & Falcon, 1987). It is a physical property that is measured using the AI tester pot and is reported as the AI (mg/kg). Abrasion always manifests itself during the grinding of materials, particularly when hard minerals are ground (Hutchings, 1992).

It is understood that friction occurs during the grinding of hard minerals which causes abrasive wear or erosion of the critical components and thereby affects the performance of the power plant. The AI gives an indication of the abrasiveness of these components.

The abrasion of coals is studied using the AI tester pot following a method proposed by Yancey, Geer and Price (YGP) in 1951. The abrasive nature of coals is determined by calculating the AI of ground coals. The AI is a function of the total mass lost by the iron blades divided by the load mass of coal (Scieszka, 1985; 1996; Spero, 1990; Spero *et al.*, 1991). Raask (1985) has shown how to determine the AI of coals using an empirical formula, but recent developments which involve the use of mills and grinders for determining the AI of coals have seen the empirical formula being discontinued (Tlotleng, 2011).

The YGP AI tester mill used in testing coals for their AI is shown in Figure 2.6. This figure illustrates the impact forces that act on the coal particle during grinding. Centrifugal and radial forces lead to particle reduction. In this figure, \mathbf{n} represents the null vector, which in most cases is a unit vector of such force that the cosine force exists. The gyration radius \mathbf{R} shown in the Figure 2.6 is important because it is normally used to calculate the force and mass moment of inertia which is used to calculate the energy of the grinding mill. The square, top-open chamber is a coal container used to enclose coal particles during grinding (Spero *et al.*, 1991).

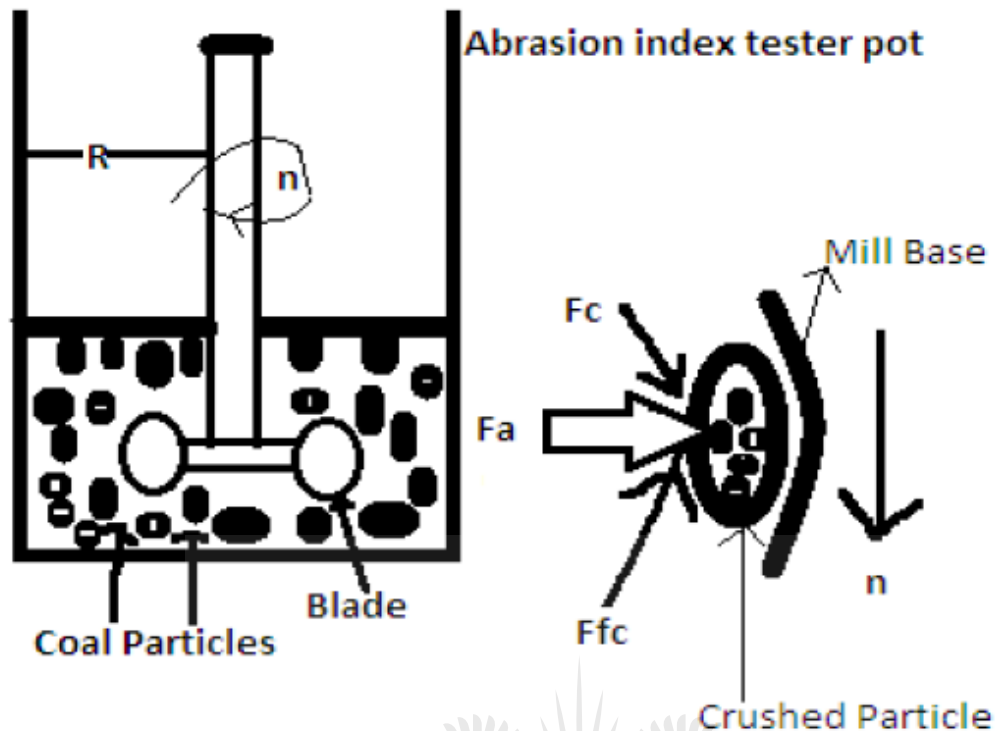


Figure 2.6: YGP AI tester pot (Spero *et al.*, 1991)

In general, the abrasiveness of coals is known to be influenced by different coal constituents (Spero, 1990; Spero *et al.*, 1991), which can be divided into chemical, physical and mechanical properties. The chemical properties that influence abrasiveness are moisture; ash content does not influence the AI of coals (Terchick *et al.*, 1963). Physical properties of coals that influence abrasion are minerals (excluded minerals, quartz, pyrite and clays), microlitho types (carbominerite) and macerals (inertinite rich). Abrasion intensity and abrasion factors are two mechanical properties on which abrasion is dependent (Spero, 1990). Hardness and grindability of coals may also influence abrasion (Scieszka, 1996; Spero *et al.*, 1991; Hutchings, 2002).

2.6.2 Minerals in coals

Mineral matter in coal is a very important aspect of coal technology, especially in processing and utilization. In coal studies, MM refers to the inorganic materials which are free and are disseminated within the coal's matrix and macerals (Gary *et al.*, 1972; Harvey & Ruch, 1986; Creelman & Ward, 1996). Their definitions embrace the following three different fundamental constituents of mineral occurrence in coals; (1) dissolved salts and other inorganic substances in the coal's pore water; (2) inorganic elements incorporated within the organic compounds of the coal macerals and discrete inorganic particles; (3) both crystalline and non-crystalline materials of true mineral components (Tlotleng, 2011).

The difference between these three constituents of minerals is that the first two are characterized as apparent in the MM of low rank coals. They are also described as non-mineral in organics, which contribute greatly to the formation of ash in the deposit of low rank coals (Given & Spackman, 1978; Benson & Holm, 1985). Discrete inorganic particles occur in both low rank and high rank coals. Dissolved salts and inorganic elements occur in small amounts in high rank coals. Their occurrence in small quantities is due to their removal by moisture and chemical structure changes of organic matter (Ward, 2002).

Excluded minerals are defined as discrete minerals or those minerals that are liberated from the carbon matrix during grinding, while included minerals are said to be those minerals that are associated with organic matter. These definitions are based on the computer controlled scanning electron microscope (CCSEM) which paved the way for coal particle classification of pulverized coals. South African coal seams are comprised mainly of clay, quartz and pyrite minerals (Falcon & Falcon, 1983). Abrasion and erosion are amongst many problems that can be related to coal comminution (Tlotleng, 2011). Abrasive wear is attributed by Wells *et al.* (2004) and Foster *et al.* (2004) to the

minerals present in the coals, especially those that are harder than steel. This is supported by Wigley and Williamson (2005) who say coals that are free of ash (or coals that have small amounts of minerals) would not cause significant abrasion or erosion in coal plants. However, the most mineral impurities present in coals are the main cause of the greatest of wear in the full scale power plants. Meintjes (1965) and Terchick *et al.* (1963) attribute abrasion wear to the ash content of coals, and moisture content playing a role in ash content as a contributor to coal's abrasiveness. Ash content in raw coals may be taken as the residue of self-heated or in situ oxidized minerals (Tlotleng, 2011).

During grinding or milling, inorganic minerals can be liberated from the coal's organic matrix. These are excluded and included minerals. Minerals such as quartz and pyrite are known to be very abrasive. Quartz in coals occurs as moderately large particles of free MM, whereas pyrite occurs as finely dispersed grains in coals and the clay sediments (Wigley & Williamson, 2005). It is well established that quartz is more abrasive than pyrite on volume percentage (Raask, 1985). This may be attributed to the fact that quartz, which is hard, will shatter when milled thereby producing sharp-edged fragments. The observation that quartz is more abrasive than pyrite was made with UK coals; this observation has not been reported on world trade coals (Wells *et al.*, 2004). However, Wells *et al.* (2004) found that angular quartz and pyrite on volume percentage are equally abrasive.

Other hard minerals capable of inducing abrasive wear are orthoclase, kyanite, topaz and alumina. This list of minerals may occur in coals in small amounts or may generally be present in trace quantities. This might be the reason why they sometimes have a minimal effect on the overall reported AI of coals (Wells *et al.*, 2004; Wigley & Williamson, 2005). Other mineral groupings such as the clays, carbonates, sulphates

and phosphate are relatively soft and do not cause any significant abrasive wear. In general, excluded minerals are most abrasive when compared to included minerals, but it is highlighted elsewhere in literature that a mineral associated with the organic matrix of coal can be abrasive if only a little of it is protruding (Tlotleng, 2011).

2.6.3 Grindability

The grindability of coal is defined as the property for coals to wear down (grind) the components of equipment, and the AI gives an indication of the wear of those components (Callcott, 1956). The grindability of coal is determined experimentally using a grinding machine, following particular standards, and it is reported as the Hardgrove grindability index (HGI). The HGI is indicative of the hardness of coals to grind (Bagherieh *et al.*, 2008).

The HGI is important for boiler designs (Tichanek, 2008) and commercial use where coals on trade are classed according to their hardness, realizing their HGI values (Tichanek, 2008; Chelgani *et al.*, 2008). HGI values are used by mining engineers to categorize coals according to their resistance to cutting and grinding (Tiryaki, 2005). HGI is an important index as it can be used to indicate the effectiveness of the mill to grinding different coals, hence their capacity at full scale power plants (Warren Spring Laboratory, 1962; Chelgani *et al.*, 2008; Tichanek, 2008). The Bond work index (WI), which is related to the HGI, in particular is used for this purpose. There are empirical equations which relate these two indices. The Bond WI is defined as the energy required for reducing material of finite size by 80% passing through a 100 micron mesh (Tichanek, 2008). The advantages of determining the grinding nature of coals lie purely in the fact that, if the grinding nature of coals is known, then a proper mill can

be selected for comminution in addition, HGI is indicative of which coals are suitable to be utilized for power generation. HGI and WI are used to assess the rate of comminution (Scieszka, 1996). The power needed to achieve the specific particle size can be determined if the HGI is known, thereby optimizing or simulating the full scale plants (Terchick *et al.*, 1963). This emanates from the fact that a revolution of a laboratory scale mill is equivalent to a specific energy consumed by a plant mill to pulverize a size feed material (Scieszka, 1996). The disadvantage of not knowing the grinding nature of coals will lead to poor performance of mills and poor management put in place, which will mean more money must be put into maintaining the mills (Tlotleng, 2011).

In the past the grindability nature of the coals was determined empirically using the following formula (Raask, 1985):

$$HGI = 6.93W + 13 \quad (2.7)$$

Where W is the weight of material passing the target sieve. HGI can be predicted using the chemical components of coals (De Kock and & Franzidis, 1973).

The survey by Van Vuuren (1978) revealed many coal constituents that affect the grinding nature of South African coals. From the survey it is known that the ash content, volatile matter and moisture content have a great influence on the HGI of coals. Low ash and high volatile matter coals appear to have a low HGI, thus indicating that the coal is hard. Weathering of coals can alter their organic and inorganic constituents (minerals) and can also change their chemical and physical properties.

Reported results are attributed to the fact that these coals contain low volatile matter, are very moist and have a high ash content. Falcon and Falcon (1987) found that the inherent moisture content of coals appears to affect grindability of low rank coal, but did not influence the HGI of high rank coals. It has to be emphasized that this

behaviour is notable only with Southern African coals. This indicates that moisture could be one constituent of coals to be ascertained to establish the grind nature of coals. The three discussed constituents of coals are what form the proximate analyses of coals.

Proximate results have been used to produce linear relationships with HGI; using computer developed programmes like non-linear multivariable regression and GRNNs. Petrographic results also form the primary constituents of coals known to influence the HGI. Following the work of Li *et al.* (2005), Bagherieh *et al.* (2008) developed the artificial NN which incorporates petrographic parameters to predict the HGI of coals. Minerals are observed to influence the HGI of coals. Note that a separate section on petrography is given; it is mentioned here only to indicate how far research goes into trying to correlate many coal constituents to their grinding nature (Tlotleng, 2011).

2.6.4. Grindability and abrasion

Scieszka (1996) was the first to elucidate the relationship between HGI and AI and illustrated their mathematical relationship as presented in Equations 2.7 and 2.8. The two physical properties (HGI and AI) of coal can exist in close proximity and suggested that HGI is sub-group of AI. Using a series of different coals, it was shown that these coal properties exhibit a quadratic relationship when correlated (Terchick *et al.*, 1963). If one looked closely, it was obvious that coal of the same origin had an independent relationship. Briefly, coals being soft (highest HGI) does not mean they are abrasive, and conversely hard coals are not readily abrasive (Tlotleng, 2011). Coals are naturally formed fossil fuels with many different characteristics, being mainly made up

of organic and inorganic matter. One important quality of coal is its burning characteristic, which is induced primarily by its organic matter. Owing to this characteristic, coals are used for different purposes, such as gasification, combustion and in the metallurgical process in South Africa and elsewhere. Typically, electricity is generated from steam turbines in power plants. The turbines are mechanical devices which utilize the thermal energy from steam produced through coal combustion. This is a process in which mechanical energy is converted into electrical energy according to the first law of thermodynamics. Combustion is a chemical reaction in which carbon (coal) reacts with excess oxygen (O_2) to produce steam (H_2O) and carbon dioxide (CO_2). This reaction is exothermic. For the maximum use of the coals fed into a combustion zone, they must be reduced to maximize their surface area. For the boiler to efficiently combust coals, coals are reduced from lump size to small pulverized fuel size. The maximum surface area in combustion facilitates the burning character of the fuel.

This size reduction is achieved by comminution in grinders or mills. All South African power stations use pulverized fuel boilers. Coals therefore have to be pulverized to an efficient burnable size, typically $75\ \mu m$. This specification therefore makes a mill an integral part of any power plant which burns coal. Owing to their characteristics, coals are sometimes soft or hard to grind, which then lead to abrasion during comminution. Abrasion is known to be caused primarily by the presence of some inorganic matter and organic matter, ash content and moisture in coals.

Comminution is a process of reducing solid material into smaller fragments using a mill or grinding machine. A mill is a mechanical device built to grind, cut or shape solid materials into their powder form. Comminution therefore can simply be explained as a mechanical and physical breaking of material during milling or grinding into smaller

fragments. During grinding, mill components, including the grinding elements, suffer abrasive wear or erosion. Mills are therefore constructed from harder materials to enhance their durability and reduce wear, especially where hard materials like minerals and coals are ground. However, some materials are harder than the mill materials and will reduce the mill's longevity through abrasive wear. The mills therefore become cost ineffective in terms of maintenance and material replacement. Replacement of worn out material and power loss constitutes most of the cost in power plants (Spero *et al.*, 1991; Scieszka, 1996). To understand the extent to which material wear occurs in mills during comminution, the abrasive character of coals has to be established.

To study the abrasion of coals, an index termed the AI was established using a YGP test rig. Currently the AI is measured using different methods, which include the AI tester pot which uses four iron blades as cutting elements (Spero, 1990). Mass loss of the blades used during grinding is then divided by the charge mass.

Mathematically this is given as:

$$AI = \frac{M_{Fe}}{\text{Charge Mass}} \quad (2.8)$$

There are two primary forms of abrasive wear that occur during milling, namely: two-body abrasive wear and three-body abrasive wear (Misra & Finnie, 1980; Hutchings, 1992). They are respectively known as sliding and rolling abrasion. For this study, an assumption is made that three-body abrasive wear will result when coals are ground in an AI tester pot. This assumption was made due to the fact that as coal particles are fed into a pot they are loose and become mobile. These particles are then partially trapped by the mill surface and its grinding zone in an enclosed system. There is a wealth of information on two-body abrasive wear as opposed to three-body abrasive wear, but, Scieszka (1996), Misra and Finnie (1980), Rabinowicz *et al.* (1961) and

Toporov (1960) have studied three-body abrasive wear processes; some even going as far as designing equipment for studying it. A full study on three-body abrasive wear is found in the work by Misra and Finnie (1980). Misra and Finnie (1981, 1983) showed that two and three-body abrasive wear was not only concerned with hard material, as material of less hardness than the concerned metal blades can still cause material wear. Spero (1990) revealed that the effects of particles that are less hard than the cutting blades are inconsistent in comparison to harder minerals. Arguably it is known that the only way to proportion the effects of mineral hardness in coals is by combining all abrasive components of coals. These will primarily be the existing minerals, ash contents and organic components in coals. The physical properties of the coals must also be included. In general abrasion can either be determined empirically or by grinder machines (Raask, 1985; Spero, 1990). It is established from literature that abrasion is dependent on some coal properties such as MM (quartz and pyrite), moisture, ash content, bulk density and grindability. Abrasion is not the only physical property of coal that is of concern during comminution. Other physical properties such as coal strength, hardness, friability and grindability are of concern to cutting machines in the coal industry. Coal strength refers to the resistance of coal to grinding or crushing. Friability refers to the ease at which a coal can be compressed. Hardness refers to the resistance of coal to penetration and grindability refers to the resistance of coal to grinding.

Further definitions are given in Falcon and Falcon (1987). Grindability is of importance to this study, because this characteristic may enlighten the researcher on the breaking ability of a coal, and hence its hardness and ease of grinding. Grindability can also be used to establish the power consumed by a mill during comminution, making it possible to understand the abrasiveness and hardness of coals.

Abrasiveness, friability, hardness, strength and grindability of coals are all studied in order to understand their effect on mills and all mechanical equipment used in coal processing. These physical properties of coals reduce the life span of mechanical machines for cutting, grinding or crushing which results in cost effective operation and non-operation during replacement. If known, these characteristics will help with the planning of power plant maintenance. The harder the coal, the longer it takes to grind and the quicker the mill components are worn. The more friable a coal is, the easier it is to grind, the softer and looser it is. The AI and HGI are studied to establish the wear in mills.

2.7 Generalized regression neural network

A GRNN is a variation of the radial basis NNs, which is based on Kernel regression networks (Cigizoglu & Alp, 2005). A GRNN does not require an iterative training procedure such as the BP NN. It approximates any arbitrary function between input and output vectors, drawing the function estimate directly from the training data. In addition, it is consistent that as the training set size increases, the estimation error approaches zero, with only mild restrictions on the function (Cigizoglu & Alp, 2005). A GRNN consists of four layers: input layer, pattern layer, summation layer and output layer (Firat & Gungar, 2009). The number of input neurons in the input layer depends on the total number of observation parameters. The input layer is connected to the pattern layer and in the pattern layer each neuron presents a training pattern and its output. This layer is connected to the summation layer. This layer has two different types of summation, a single division unit and summation units. The summation and

output layer together perform a normalization of the output set. Each pattern layer unit is connected to the two neurons in the summation layer, which has two different types of summation, S and D-summation neurons. The S-summation neuron computes the sum of weighted responses of the pattern layer. On the other hand, the D-summation neuron is used to calculate the unweighted output of pattern neurons. The output layer merely divides the output of each S-summation neuron by that of each D-summation neuron, yielding the predicted value Y_i' to an unknown input vector x as (Firat & Gungar, 2009):

$$D(x, x_i) = \sum_{k=1}^n \left(\frac{x_i - x_{ik}}{\sigma} \right) \quad (2.9)$$

$$Y_i' = \frac{\sum_{i=1}^n y_i \cdot \exp[-D(x, x_i)]}{\sum_{i=1}^n \exp[-D(x, x_i)]} \quad (2.10)$$

Where y_i is the weight connection between the i^{th} neuron in the pattern layer and the S-summation neuron, n is the number of the training patterns, D is the Gaussian function, m is the number of elements of an input vector, x_k and x_{ik} are the j^{th} elements of x and x_i , respectively and σ is the spread of the Gaussian function or also referred as the smoothing factor.

The smoothing factor plays an important role in function approximation (Shuxia *et al.*, 2010). A smaller smoothing factor will lead to a 'steeper' radial basis function, so that the neuron with the weight vector closest to the input vector will provide a much larger output than other neurons. With an increase in the smoothing factor, the radial basis function's slope becomes smoother and more neurons can respond to an input vector. However, a larger smoothing factor will also make the network function less selective. Therefore, there is a need to determine the optimal smoothing factor for GRNNs. In this study, the optimal smoothing factors were determined by comparing the distances

between the prediction and the actual values in the training set. The obtained optimal smoothing factor is 32.1.

2.8 Predicting abrasiveness

Many factors contribute to the abrasiveness of coal. Spero (1990) interpreted abrasion of coal in terms of the mineralogical and physical properties of the coal. For a limited range of coals and their associated relative density fractions he related the AI to the percentage, composition and physical properties of the coal MM, and to the grindability and bulk density of the coal through Equation 2.11:

$$AI = \frac{\sum_{j=1}^n W_j H_j}{PC\gamma B\gamma} \quad (2.11)$$

Where W_j and H_j are the concentration and hardness, respectively of mineral j in the coal, $PC\gamma$ and $B\gamma$ are respectively the grindability factor and bulk density of the coal. The equation requires many inputs for prediction and suffers from the drawback that particle size and shape are not included. However, this equation is the only one which has integrated a number of variables for abrasiveness prediction. In South African coals the major abradant is quartz. Other hard minerals occur in smaller proportions in coal (rutile, pyrite/marcasite etc.), the abundance of which is reflected in the ash. Both have been correlated earlier to the AI of coal, and positive correlations have been found in the literature (Bandopadhyay, 2010b).

The abrasiveness of coal has been described earlier by the empirical Equation 2.12 formulated by Raask (1985):

$$AI = Q_c + 0.5P_c + 0.2A_c \quad (2.12)$$

Where Q_c , P_c and A_c are respectively the mass percentage of quartz, pyrite and ash in coal. The equation has been useful in the design of boilers for power stations (Tickner & Maier, 2005). When reviewing the information on the analysis of coal as presented in standard industry commercial practice, it is rare to find reports covering quartz. Pyrite in contrast is frequently identified and specification sheets always indicate the quantity of ash. In order to compensate for the lack of data, estimates for quartz and pyrite content can be prepared with reasonable accuracy based on formulas employing the reported chemical analysis for SiO_2 , Al_2O_3 and S. The quantity of quartz in coal (Q_c) can then be estimated from Equation 2.13:

$$Q_c = 0.01A_c (\text{SiO}_2 - 1.5\text{Al}_2\text{O}_3) \quad (2.13)$$

Pyrite in coal (P_c) can be estimated by:

$$P_c = 1.3(S - 0.3) \quad (2.14)$$

Equations 2.13 and 2.14 can be used as reasonable substitutes for laboratory data in the AI equation (Raask, 1985; Tickner & Maier, 2005).

Equation 2.12 is applicable to United States of America (US) and United Kingdom (UK) coals with low ash content and a relatively high proportion of pyrite, but is not valid for South African coals with high ash yields and low quartz contents, but low pyrite. Further, Equation 2.12 needs modification for South African coals. Recently Bandopadhyay (2010a) amended the equation and compared quartz obtained from the modified equation to that from an FTIR determination from Indian coal.

It appears from the above that the proportions of ash and quartz are the main factors responsible for abrasion from South African coals. Given the volume of data generated on ash, quartz and the AI for 91 coals studied, simple regression models relating the AI with one or more of the independent variables, A and Q_c can be proposed.

The models proposed by Bandopadhyay (2010a): $AI = 23.6 + 3.05Q_c$ (Model 1), $AI = 1.35A$ (Model 2) and $AI = 1.00A_c + 1.35Q_c$ (Model 3) are all statically significant and show the degrees to which they satisfy the statistical criteria of 'goodness of fit'. Parameters like the R^2 and the adjusted R^2 (for multiple regression) are useful for assessing the aptness of the models in terms of the strength of the relation between the variables, while the standard errors (SE) of the estimate measures the dispersion around the estimating line (in the case of two variables) or the multiple-regression plane (in the case of two variables). For Models 1 and 2, the values of R^2 are respectively 0.61 and 0.79, which signify that 61% of the variation in abrasion is explained by the variation in quartz content in Model 1, while Model 2 can account for 79% of the variation by the variation in ash percentage. The SEs of the estimate for the two models are respectively 8.2 and 6.0. The overall significance of the regression is indicated by the f-test criteria and its p-values, which are satisfied in the case of both Models 1 and 2. The role of the individual variables A_c and Q_c in predicting AI, as indicated by the t-test and p-values, as indicated by Bandopadhyay (2010a), shows that both A_c and Q_c are good predictor variables for the AI of the coal studied.

It is worthwhile to add here that investigators (Livingston & Dugdale, 1998; Foster *et al.*, 2004) have related the AI with A_c , as the latter is quickly and routinely done in a laboratory for characterization. They have derived the following equation from the experimental data related to coals from Britain, South Africa and India and a number of world-traded coals:

$$AI = 3.9 + 1.21A_c \quad (R^2 = 0.80) \quad (2.15)$$

The Equation 2.15 and Model 2 ($AI = 1.35$; $R^2 = 0.79$) derived for Indian coals, are similar and values predicted by both are very close, suggesting both can be used for interpreting abrasion of thermal coals from ash percentages. The model can be

examined using the data of ash yields and abrasion indices of coals reported by Spero (1990). He studied the properties of Walloon coals of Australia *vis-a-vis* their power station performance. For high quartz coals (indicated by a high $\text{SiO}_2/\text{Al}_2\text{O}_3$ ratio) used in power stations, namely, Tarong, Stanwell and Swanbank, predicted values of the AI matched with the experiment in the following manner: The linear correlation shown by the equations (Model 2 and Equation 2.15) between the AI and ash yield is not good enough for predictive purposes and a high R^2 value is a prerequisite for such a purpose. The investigations made so far have clearly identified that both Q_c and A_c are the key predictor variables for abrasion. This also emphasizes that, in order to have a model with better explanatory power to account for the variation in abrasion shown by different coals, both A_c and Q_c should be included and the use of multiple linear regression has been made to develop a model, Model 3 ($AI = 1.00A_c + 1.35Q_c$), which has better explanatory power as anticipated. The adjusted R^2 value for the model is 0.86, indicating that 86% of the variation in the AI can be explained by the variations in A_c and Q_c . Further, the standard deviation of the regression model, i.e., the SE of the estimate, is 4.9, which is less than those for the Models 1 and 2. All these justify the superiority of the model and as the value of R^2 is greater than 0.80, it is a good linear model. Nonetheless, for more accurate predictions the introduction of other factors such as particle size and shape, physical properties of coal like grindability and bulk density should also be explored to achieve higher a R^2 and lower SE than those which characterize the existing model.

Since coal qualities usually vary from seam to seam, it is more difficult and impossible to predict the abrasiveness characteristics for any thermal coal on the AI with a single NN model without compromising the precision of the prediction. In order to overcome this difficulty, we separate the coals into several categories according to the

differences in ratios of volatile matter, ratios of ash content, ratios of dry air moisture and ratios of lower heating values. The NN is then applied to predict the abrasiveness of each type of the coal.

2.9 Review of the application of the GRNN

The GRNN was introduced by Nadaraya (1964) and Watson (1964) and rediscovered by Specht (1991). This model is a generalization of both radial basis function networks and probabilistic NNs that can perform linear and non-linear regression (Zarada, 2001). These FFNNs use a basis function between input and output vectors directly from training samples, and they can be used for multidimensional interpolation (Specht, 1991). Although GRNNs are not as commonly used as radial basis function networks (RBFNs) or BP trained networks, they have been applied to solve a variety of problems including prediction and control (Rutkowski, 2004). The GRNN is often used as a powerful regression tool because it has a high training speed and a strong non-linear mapping capability (Shuxia *et al.*, 2010). The network consists of an input layer, a radial basis layer and a linear output layer. Each neuron in the hidden layer has a radial basis function to perform the non-linear transformation from the input space to the hidden space. The Gaussian function is the common choice for the radial basis neurons and it is represented in Equation 2.16.

$$g(d) = \exp\left(-\frac{d^2}{2\sigma^2}\right) \quad (2.16)$$

Where d is the distance between two vectors and σ is the spread of the Gaussian function or also referred to as a smoothing factor.

The smoothing factor plays an important role in function approximation (Shuxia *et al.*, 2010). A smaller smoothing factor will lead to a 'steeper' radial basis function, so that the neuron with the weight vector closest to the input vector will provide a much larger output than other neurons. With an increase in the smoothing factor, the radial basis function's slope becomes smoother and more neurons can respond to an input vector. However, a large smoothing factor will also make the network function less selective. Therefore, there is a need to determine the optimal smoothing factors for GRNNs (Shuxia *et al.*, 2010).

Spero (1990) assesses and predicts the AI of coal by the following empirical

$$\text{equation: } AI = \frac{\sum_j^n W_j H_j}{PC\gamma B\gamma} \quad (2.17)$$

Where W_j and H_j are the concentration and hardness, respectively, of mineral j in the coal, and $PC\gamma$ and $B\gamma$ are, respectively, the grindability factor and bulk density of the coal. Despite the good results presented, this equation requires many inputs for prediction and suffers from the drawback that particle size and shape are not included. However, this equation is the only one which has integrated many variables for abrasiveness prediction. Raask (1985) described the AI with the following equation:

$$AI = Q_C + 0.5P_C + 0.2A_C \quad (2.18)$$

The quantity of quartz in coal (Q_C) can then be estimated from the Equation 2.19:

$$Q_C = 0.01A_C(SiO_2 - 1.5Al_2O_3) \quad (2.19)$$

Pyrite in coal (P_C) can be estimated by:

$$P_C = 1.3(S - 0.3) \quad (2.20)$$

Equations 2.19 and 2.20 can be used as reasonable substitutes for laboratory data in the AI equation (Raask, 1985; Tickner & Maier, 2005).

Equation 2.18 is applicable to US and UK coals with low ash and a relatively high proportion of pyrite, but is not valid for all Indian and South African coals with high ash yields and high quartz contents, but low pyrite. Further, Equation 2.20 needs modification (Bandopadhyay, 2010a).

Bandopadhyay (2010b) has amended the equation and compared quartz obtained from the modified equation to that from FTIR determination. It appears from above that the proportions of ash and quartz are the main factors responsible for abrasion. Given the volume of data generated on ash (A), quartz (Q) and abrasion index (AI) for the 61 thermal coals studied, three simple regression models relating the AI with one or more of the independent variables, A and Q can be proposed:

$$AI = 23.6 + 3.05Q \text{ (Model 1),}$$

$$AI = 1.35A \text{ (Model 2) and}$$

$$AI = 1.00A + 1.35Q \text{ (Model 3);}$$

which are all statistically significant and show the degree to which they satisfy the statistical criteria of 'goodness of fit'. Parameters like the R^2 and the adjusted R^2 (from multiple regressions) are useful for assessing the aptness of the models in terms of the strength of the relation between the variables. The SE of the estimate measures the dispersion around the estimating line (in case of two variables) or the multiple-regression plane (in case of more than two variables). For Models 1 and 2, the values of R^2 , are respectively, 0.61 and 0.79, which signify that 61% of the variation in abrasion is explained by the variation in quartz content by Model 1. Model 2 can

account for 79% of variation by the variation in ash percentage. The SE of the estimate for the two models are respectively 8.2 and 6.0. The overall significance of the regression is indicated by the f-test criteria and its p-value, which are satisfied in the case of both the Models 1 and 2. A and Q are found to be good predictor variables for AI. It is worthwhile to add here that investigators Livingston and Dugdale (1998); Foster *et al.* (2004) have related the AI with A, as the latter is quickly in laboratory experimental data related to coals from Britain, India and South Africa and a number of world-traded coals:

$$AI = 3.9 + 1.21A \quad (R^2 = 0.80) \quad (2.21)$$

The linear correlation shown by the equations (Model 2 and Equation 2.21) between the AI and ash yield is however, not good enough for predictive purposes, and a high R^2 value is a prerequisite for such purposes. The investigations made so far have clearly identified that both Q and A are the key predictor variables for abrasion. This also emphasizes that, in order to have a model with better explanatory power to account for the variation in abrasion shown by different coals, both A and Q should be included and use of multiple linear regressions has been made to develop such a model. Model 3 has better explanatory power. The adjusted R^2 value for Model 3 is 0.86, indicating that 86% of the variation in the AI can be explained by the variations in A and Q. Further, the standard deviation of the regression model, i.e., the SE of the estimate, is 4.9, which is less than those for Models 1 and 2. All these justify the superiority of the model and it is deemed to be a good linear model as the value of R^2 is greater than 0.80. Nevertheless, for more accurate prediction, introducing other factors, namely, particle size and shape, physical properties of coal like grindability and bulk density should also be explored to achieve a higher R^2 value.

Bandopadhyay (2010b) checked the application of the model developed by himself (Model 1: $AI = 3.9 + 1.21A$) using the data on coal with different origins. His results obtained for predictions agree with the actual values within the prediction range, except for the La Loma coal. The discrepancy in this case was ascribed to factors such as grindability and bulk density of the coal, particle size and shape, which are known to affect the AI but have not been included in the model. As a result accurate predictions could not be made. For coals showing an abnormally high abrasion, especially the morphology of the abrading particles should be given due consideration. Barring this case, it is found that the model is capable of estimating the AI of all coals reasonably well and the results obtained are encouraging.

The regression Model 3 proposed is a simple one and valid for thermal coals containing low pyrite. Bandopadhyay (2010b) found that it was easy for the industry to adopt as all the inputs needed for reasonably good predictions were available. In the absence of experimental data on quartz abundance, however, the empirical equation to estimate quartz content developed by Bandopadhyay (2010a) from the ash analysis may be utilized for Indian coals,

$$Q = 0.01A_C (SiO_2 - 13Al_2O_3) \quad (2.22)$$

Ngoy and Mulaba-Bafubiandi (2013) proposed an analytical model of the coal AI as a function of the mineral composition of coal. They considered the assumption that the resulting amount of abrasion is proportional to the resulting relative hardness as expressed by the following mathematical equation:

$$AI = K \times H_r \quad (2.23)$$

$$AI = K \sum_i C_i X \frac{h_i}{h_b} \quad (2.24)$$

Where K is a constant of proportionality depending on the test method. Equation 2.22 provides a model of the AI that can be evaluated as a linear combination of the mass percentage of mineral components of the coal particle, where the coefficients of linear combination are the respective hardnesses of the mineral components.

$$AI = y \quad (2.25)$$

$$\sum_m C_m h_m = x \quad (2.26)$$

$$\frac{K}{h_b} = A \quad (2.27)$$

According to the model, the experimental value of the AI should be equal to Ax . The above implies that, if the model is valid the experimental AI is linearly correlated to x , inversely if the AI is linearly correlated to x , then the model is valid. Therefore, for experimental verification of the model values of x are computed as per Equation 2.25 and then the linear correlation with respective values of the AI is tested.

Although this proposed model is consistent with empirical models suggested by Bandopadhyay (2010a) and Spero (1990), it does not take into account all the determining factors. NNs are powerful tools that have the ability to identify underlying highly complex relationships of all factors (Haykin, 1999). Generalized Regression Neural Networks (GRNNs) have been suggested to predict the AI of the coal. GRNNs have the advantage of being easily trained and require only one free parameter (Amiri *et al.*, 2010).

2.10 Conclusion

The literature review focused firstly on the effort by different authors to accurately predict the behaviour of the ion-exchange process and the application of NN techniques to different processes. Secondly, published work predicting the AI of coal was reviewed. From this literature review it was clear that there is a need to find an alternative means for modelling and simulating the ion-exchange process and predicting the AI of coal.



CHAPTER 3: EXPERIMENTAL MATERIALS AND METHODS

3.1 Introduction

The goal of this chapter is to give a detailed account of the experimental procedures followed to attain the objectives of this research regarding the ion-exchange process. All experimental and analytical procedures used in this thesis for the ion-exchange process were described by Nyembe (2010) and are also presented. The data generated for loading and elution were then analysed using a NN technique. Results obtained are discussed in Chapters 4 and 5.

3.2 Chemical reagents and materials

All chemicals used in this research with respect to the ion-exchange process, including hydrochloric acid, sodium hydroxide and potassium hydrogen, were of analytical reagent grade (98-99.5%) and were obtained from Sigma Aldrich and Merck. The clinoptilolite (natural zeolite) used was supplied by Pratley South Africa and was sourced from the Vulture Creek, KwaZulu-Natal province of South Africa.

3.3 Preparation of clinoptilolite and synthetic solutions

3.3.1 Preparation and treatment of clinoptilolite

The natural zeolite used (as material for the removal of copper and cobalt ions from synthetic wastewater) was washed with deionized water prior to the treatment with

acid to remove surface adherent particles and soluble materials. It was later dried in an oven at 120°C for 12 hours to remove the moisture content. The dried sample was then crushed with jaw crushers and sieved through screens to a size range of 1-2 mm. The clean sample of zeolite was transferred into a round-bottom flask and a known concentration (0.26-5.73 M) of hydrochloric acid was added at 30°C and stirred for 24 hours. Thereafter, the zeolite was separated from the solution by filtration. The filtrate was titrated with 0.1 M NaOH solution to determine the concentrations using Equation 3.1. A sample was crushed to obtain fine particles (75 µm). There after the solids separated from the solution were dried at 90°C and analysed with XRF.

$$C_{2HCl} = \frac{C_{NaOH} \cdot x V_{NaOH}}{V_s} \quad (3.1)$$

Where: C_{2HCl} is the concentration of HCl after (M), C_{NaOH} is the concentration of NaOH (0.1M), V_{NaOH} is the volume of NaOH required for titration of the sample of filtration (mL) and V_s is the volume of the sample of filtration for titration (10 mL).

3.3.2 Atomic absorption spectroscopy analysis

In atomic absorption spectroscopy (AAS), the solution is atomized in a flame and produces atomic vapour of the element being analysed. Monochromatic light of the same wavelength as the element being analysed is then emitted by a hollow cathode tube containing the same element and is passed through the vaporized sample. The element's atoms absorb the radiant light from a hollow cathode tube and the degree of absorption expresses the amount of the element present in the sample (Skoog *et al.*, 1998).

AAS was used to determine the concentration of Cu (II) and Co (II) in the solution before and after the batch sorption experiments described in detail in a previous section. This was to determine the performance of the zeolite in recovering the targeted metals. The Atomic Absorption Spectrophotometer (a Varian Spectra (20/20)) was used with instrument parameters set at wavelengths for the two metals, Cu (324.7 nm) and Co (240.7 nm), and a spectral band of 0.2 nm for both metals for all AAS analyses. The flame type used was air-acetylene. Standards of 1000 mg/L, 2000 mg/L, 3000 mg/L were then prepared and a calibration curve was drawn using these standards. Dilution was applied stoichiometrically where the concentrations of the unknown solutions of Cu and Co exceeded the concentration range of the standards.

3.3.3 Synthetic solution preparation

For AAS analyses, solutions of copper and cobalt were prepared by dissolving $\text{CoSO}_4 \cdot 7\text{H}_2\text{O}$ and $\text{CuSO}_4 \cdot 5\text{H}_2\text{O}$ in deionised water to generate solutions that contained Cu^{2+} and Co^{2+} concentrations of 0.0020 M, 0.0698 M and 0.2000 M. These concentrations were arbitrarily chosen on the basis of generating low, middle and high concentration solutions. These synthetic aqueous solutions were stored at room temperature (approximately 25°C). The samples were used within 48 hours after preparation to minimize errors from precipitation and container plating of the metal ions. The pH of the solution was adjusted by adding 0.1 M sulphuric acid or 0.1 M sodium hydroxide solution.

3.3.3.1 Non-mixed Co^{2+} and Cu^{2+} solutions

The non-mixed Cu^{2+} and Co^{2+} aqueous solutions of concentrations 0.0020 M, 0.0698 M and 0.2000 M which corresponded to 0.032 g, 1.109 g and 3.177g of Cu^{2+} and 0.030 g, 1.028 g and 2.947 g of Co^{2+} were prepared by dissolving $\text{CoSO}_4 \cdot 7\text{H}_2\text{O}$ and $\text{CuSO}_4 \cdot 5\text{H}_2\text{O}$ salts in deionised water in a 250 ml volumetric flasks.

3.3.3.2 Co/Cu binary synthetic solutions

The possible effects of one cation on the other's removal efficiency were studied by the variation of the metal ion concentration in the solution. Studies on the Co/Cu binary synthetic solutions were done with solutions of copper and cobalt prepared at stoichiometric ratios of Co:Cu - 1:1, 1:5, 1:9, 5:1 and 9:1 which corresponded to these concentrations of Co:Cu - 0.0020:0.0020 M, 0.0020:0.0698 M, 0.0020:0.2000 M, 0.0698:0.0020 M and 0.2000:0.0020 M respectively.

3.3.4 Adsorption studies

For the sorption studies, the amount of metal sorption was computed as follows:

$$\% \text{ metal sorption by clinoptilolite} = \frac{C_i - C_f}{C_i} \times 100 \quad (3.2)$$

Where C_i is the initial concentration and C_f is the final solution concentration.

3.3.5 Verification of sorption mechanism

The following sorption tests were employed to verify the nature of the sorption mechanism. Initially, an exact mass (25 g) of the dried original clinoptilolite was brought into contact with 25 ml of metal solution. The initial concentrations of Cu^{2+} and Co^{2+} were 0.0020 M, 0.0698 M and 0.2000 M. Blank solutions containing no zeolites were also included. The concentration of the remaining metal ions was analysed using AAS. These concentrations were compared with the initial concentrations. Upon comparison of the initial and final concentrations, it was evident that indeed metal adsorption did take place since the final concentration was lower than the initial concentration.

3.4 Experimental procedure

Batch experiments were conducted to determine the effect of pH, operating temperature, initial concentration and contact time on the ion-exchange process of clinoptilolite as the ion-exchange material. The effect of pH was carried out in a pH range of 2-4 and the effect of various operating temperatures ranging from 30, 45, 60 and 90°C was investigated. Temperature adjustments were conducted in the same orbital shaker. Initial concentrations of synthetic solutions were analysed using AAS (Model Varian Spectra (20/20)). The samples were taken at predetermined time intervals (10, 20, 30, 40, 50 and 60 minutes) on the percentage of Cu (II) or Co (II) uptake by the clinoptilolite. In each case, 10 g of the activated clinoptilolite was mixed with one litre of the synthetic solution and held in a closed polyethylene flask at 90°C for 24 hours. Each experiment was performed in duplicate to observe the

reproducibility and the mean value used for each set of values. The percentage of ions removed as the output parameter of the NN model was considered as a measure of the uptake or elution percentage. The uptake or elution efficiency (%) was calculated according to Equation 3.2.

3.5 Data processing

A database is critical when modelling a NN. In the first part (the ion-exchange process), the database was generated by collecting a large number of data points from the ion-exchange experimental data. After evaluating all the experimental results, the collected data were arranged in a set of input vectors as a column in a matrix. Then another set of target vectors was arranged (the correct output vectors for each of the input vectors) to a second matrix in an MS Excel sheet. The input variables were pH, temperature and initial concentration. The corresponding Cu (II) or Co (II) removal or elution efficiency (%) was used as a target. To ensure that all variables in the input data are important, principal component analysis (PCA) was performed as an effective procedure for the determination of input parameters. In this thesis, a multiple-layered perceptron (MLP) type FFNN was used to model the ion-exchange process (loading and elution). All the steps, which are taken to model the system, can be summarized as follows:

- Step 1: the collected and integrated data is stored in a separate data file.
- Step 2: data transformation is done before starting the network training. The pre-processed data is randomly divided by input vectors and target vectors into three different sets: training, testing and validation.

- Step 3; the developed MATLAB programme (NN toolbox V4.0 of MATLAB mathematical software) is used for data transformation, network construction, network training and selecting the best model.

The NN model comparison is mainly used to choose the optimum number of neurons in the hidden layer and identify the type of transfer functions to use in each layer. The performance of the NN during training is measured based on the mean square error.

3.6 Conclusion

In this chapter, the synthetic solutions were prepared in order to load and recover the Cu (II) and Co (II) using the activated clinoptilolite. The data generated were used to create the network and the use of MATLAB NN toolbox software was explained.

CHAPTER 4: FEED-FORWARD NEURAL NETWORK ANALYSIS

4.1 Introduction

This chapter presents the analysis for the ion-exchange process using a FFNN technique. A MLP type FFNN was used for the modelling of the ion-exchange process (loading and elution). For the loading, only copper was used as a heavy metal. It was found in the literature that the removal of copper and cobalt from the aqueous solution using the ion-exchange capacity of the zeolite has the same behaviour (Mamba *et al.*, 2009 and 2010).

4.2 Application of the FFNN technique on loading

Five important aspects that must be determined in the design procedure of NNs are as follows: (1) selection of the BP training algorithm, (2) data distribution, (3) selection of the NN structure, (4) selection of the initial weight and (5) sensitivity analysis (Toma *et al.*, 2004).

4.2.1 Selection of the BP training algorithm

Ten BP training algorithms were compared to select the best suited BP training algorithm. For all BP training algorithms, a three-layer NN with a tangent sigmoid transfer function (*tansig*) at the hidden layer and a linear transfer function (*purelin*) at the output layer were used. The Levenberg-Marquardt back-propagation algorithm

(LMA) with a minimum mean square error (MSE) was found to be the best of 10 BP algorithms as shown in Table 4.1. The benchmark comparison showed a loss on the optimality of the estimates/results produced by some BP training algorithms. The benchmark comparison study resulted in the LMA being able to provide a smaller MSE compared to other BP algorithms such as the resilient back-propagation (RP) algorithm and conjugate gradient algorithms, as shown in Table 4.2. The smallest MSE of about 0.00039 was obtained for the *trainlm* function. The LMA was therefore considered the acceptable training algorithm in this thesis.

Table 4.1: Comparison of 10 BP algorithms

BP algorithms	Function	MSE	IN	R ²	BLE
1. Batch gradient descent	<i>traingd</i>	0.55739	100	0.864	$y = 0.719x + 23.6$
2. Batch gradient descent with momentum	<i>traingdm</i>	0.61835	100	0.585	$y = 0.350x + 55.3$
3. BFGS quasi-Newton back-propagation	<i>trainbfg</i>	0.07200	16	0.879	$y = 0.768x + 19.5$
4. Fletcher-Reeves conjugate gradient back-propagation	<i>traincgf</i>	0.16533	14	0.822	$y = 0.742x + 20.8$
5. Levenberg-Marquardt back-propagation	<i>trainlm</i>	0.00039	24	0.930	$y = 0.946x + 4.05$
6. One step secant back-propagation	<i>trainoss</i>	0.18571	20	0.826	$y = 0.724x + 22.6$
7. Polak-Ribiere conjugate gradient back-propagation	<i>traincgp</i>	0.14871	18	0.842	$y = 0.805x + 15.9$
8. Powell-Beale conjugate gradient back-propagation	<i>traincgb</i>	0.15984	13	0.812	$y = 0.698x + 25.0$

9. Scaled conjugate gradient back-propagation	<i>trainscg</i>	0.14274	19	0.888	$y = 0.846x + 12.6$
10. Variable learning rate back-propagation	<i>traingdx</i>	0.6563	38	0.499	$y = 0.265x + 62.8$

MSE: mean squared error, R²: correlation coefficient, BLE: Best linear equation, IN: iteration number.

Another important factor in NN design is the type of transfer function. NNs owe their non-linear capability to the use of non-linear transfer functions. Different transfer functions can be used for neurons in the different layers. Different transfer functions were examined in each layer, separately and with respect to the MSE of testing data where after the proper transfer functions were chosen. MSE is calculated as in Equation 4.1:

$$MSE = \frac{\sum (SP_{cal} - SP_{exp})^2}{N} \quad (4.1)$$

Where subscripts *cal* and *exp* denote calculated and experimental values of *SP*, respectively. *N* is the number of validation and training data.

The most widely used criteria included MSE, root mean square error (RMSE), correlation coefficient (R), coefficient of determination (R²) and mean square relative error (MSRE) for training, validation and testing data sets and are given in Table 4.2.

Table 4.2: Statistical criteria for the evaluation of the NN model

Criterion	Training data	Validation data	Testing data	Total NN
MSE	0.018	0.250	0.333	0.102

RMSE	0.127	0.409	0.555	0.219
R	0.988	0.988	0.988	0.988
R ²	0.988	0.987	0.987	0.988
MSRE	0.003	0.001	0.011	0.003

In probability theory and statistics, R indicates the strength and direction of a linear relationship between two variables. In general statistical usage, R refers to the departure of two variables from independence. A number of different coefficients are used for different situations. The best known is the Pearson product-moment correlation coefficient which is explained as in Equation 4.2.

$$R = \frac{\sum_N (SP_{cal} - SP_{cal,ave})(SP_{exp} - SP_{exp,ave})}{\sqrt{\sum_N (SP_{cal} - SP_{cal,ave})^2} \sqrt{\sum_N (SP_{exp} - SP_{exp,ave})^2}} \quad (4.2)$$

R^2 can have only positive values ranging from $R^2 = +1.0$ for a perfect correlation (positive or negative) down to $R^2 = 0.0$ for a complete absence of correlation.

The advantage of R is that it provides a measure of the strength of the correlation. It can be said that R^2 represents the proportion of the data that is the closest to the line of best fit (Sadrzadeh *et al.*, 2009).

Among different transfer functions available in MATLAB, the log sigmoid function was selected for all neurons due to its better prediction performance than other transfer functions. The log sigmoid function is bounded between 0 and 1. Therefore the input and output data should be normalized to the same range as the transfer function used. In other words, the logarithmic sigmoid transfer function gives scaled outputs (SP) in this range (0-1).

4.2.2 Data distribution

A training set of ninety experimental data sets: 70%, 15% and 15% for training, validation and testing respectively, was selected to develop the model. The NN model based on the BP algorithm for experimental data was applied to train the NN.

During training, the output matrix is computed by a forward pass in which the input matrix is propagated forward through the network to compute the output value of each unit. The output matrix is then compared with the desired matrix which results in an error signal for each output unit. In order to minimize the error, appropriate adjustments were made for each of the weights of the network. The training was stopped after 24 iterations for the LMA. This was done to give the desired output for a given input matrix because the differences between training errors and validation errors started to increase. Figure 4.1 illustrates training, validation and test MSE for the LMA.

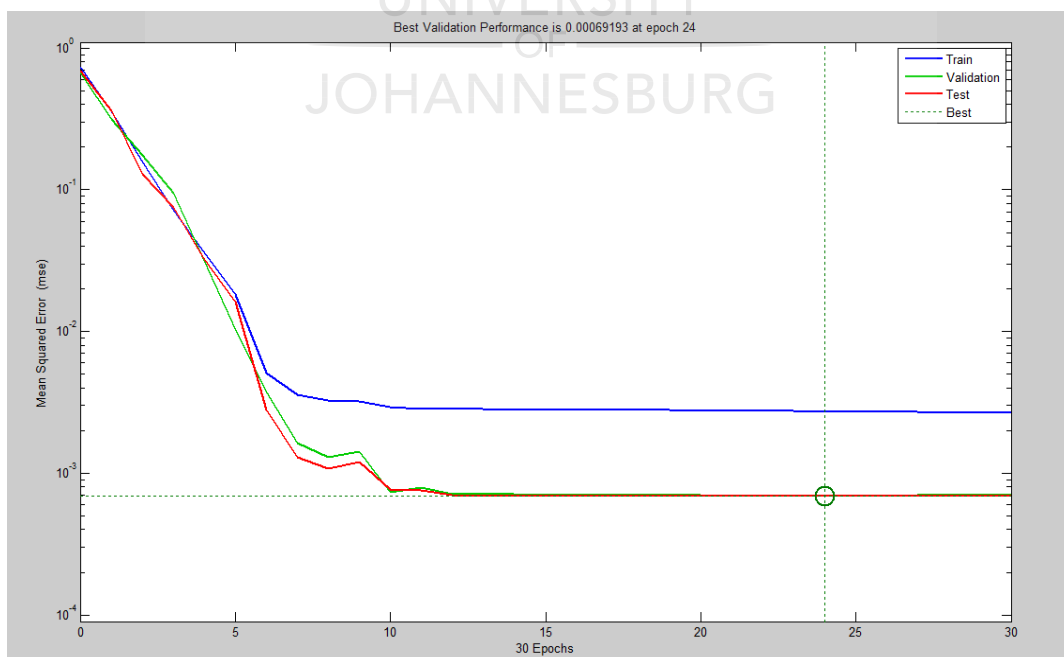


Figure 4.1: Training, validation and test MSEs for the LMA

A regression analysis of the network response between the NN outputs and the corresponding target was performed. The graphical output of the network was plotted the non-linear dependence of the data, linear regression shows a good agreement between the NN outputs, predicted data and the corresponding targets (experimental values). The figure contains two lines, one is the perfect fit $y = T$ (predicted data = experimental data) and other is the best fit indicated by a solid line with best linear equation, correlation coefficient (R^2) 0.999 and MSE 0.000365. This agrees well with the correlation coefficient reported in the literature with a correlation coefficient of 0.985 for the prediction of nitrogen oxides removal by TiO_2 photo catalysis (Toma *et al.*, 2004); 0.998 for the prediction of methyl tert-butyl ether (MTBE) by UV/ H_2O_2 process (Salari *et al.*, 2005); 0.966 for the prediction of polyvinyl alcohol degradation in aqueous solution by the photo-Fenton process (Giroto *et al.*, 2006); 0.995 for the removal of humic substances from the aqueous solutions by ozonation (Oguz *et al.*, 2008); 0.98 for the decoloration of Acid Orange 52 dye by the UV/ H_2O_2 process (Guimaraes *et al.*, 2008); and 0.997 for the COD removal from antibiotic aqueous solution by the Fenton process (Elmolla *et al.*, 2010).

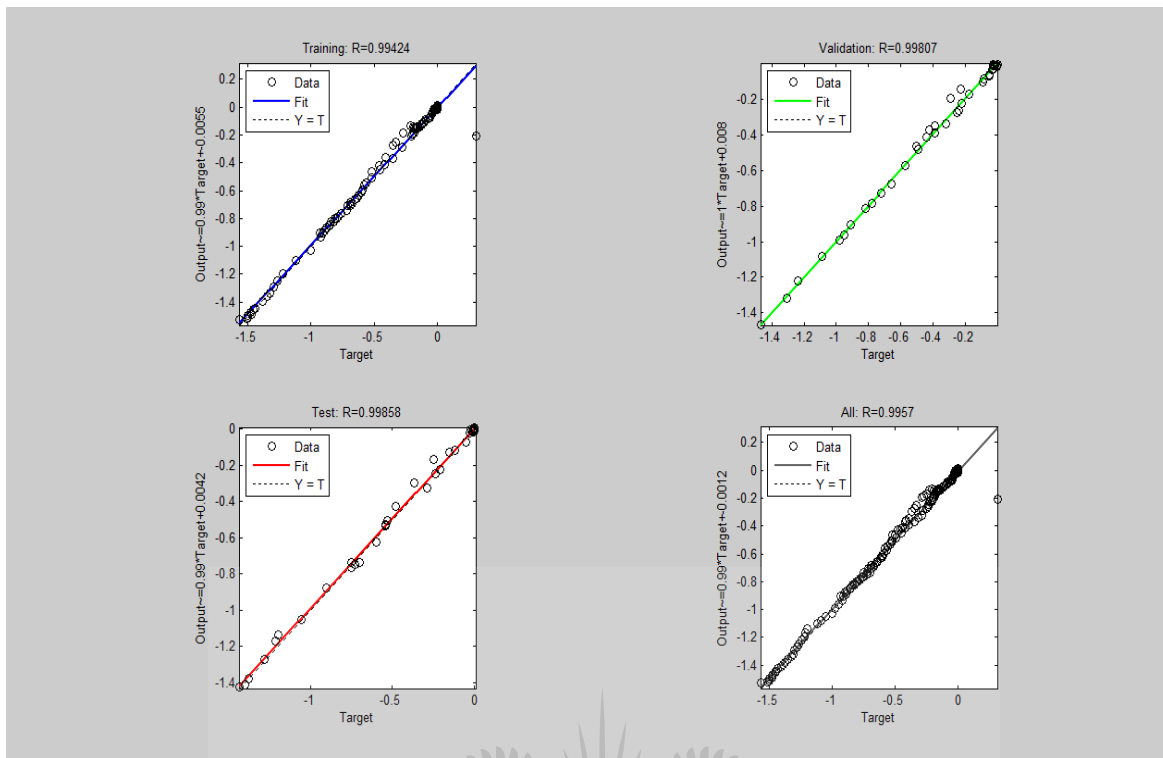


Figure 4.2: Regression analysis of the network response between NN output and the corresponding targets

4.2.3 Selection of the NN structure

The optimum number of neurons was determined based on the minimum value of MSE of the training and prediction set. The optimization was done by using LMA as a training algorithm and varying the neuron number in the range 1-15. The optimal number of hidden layers and the optimal number of nodes in each layer are case dependent and there is no straightforward method for determining them. Hornik *et al.* (1989) showed that MLP FFNNs with one hidden layer and sufficiently large neurons can map any input to each output to an arbitrary degree of accuracy. However, *et al.* (1994) reported that many functions are difficult to approximate well with one hidden layer. They revealed that the use of more than one hidden layer provides greater flexibility and enables the approximation of complex functions with fewer neurons.

Baughman and Liu (1995) established that adding a second hidden layer improves the network prediction capability significantly without having any detrimental effects on the generalization of the data testing set. It was observed that adding a third hidden layer results in a prediction capability similar to that of a two hidden layer network, but it requires longer training times due to its more complex structure.

The optimal architecture of the NN model and its parameter variation was determined based on the minimum value of the MSE of the training and prediction set. In optimization of the network, two neurons were used in the hidden layer as an initial guess. With an increase in the number of neurons, the network gave several local minimum values and different MSE values were obtained for the training set. Figure 4.3 illustrates the dependence between the neuron number and MSE for the LMA selected as the best BP algorithm. Figure 4.3 depicts that the MSE of the network was much higher for the 2 (MSE 0.151843) and decreased to the minimum value of 0.000365 when 11 neurons were used. Increasing the neurons to more than 11 did not significantly decrease the MSE.

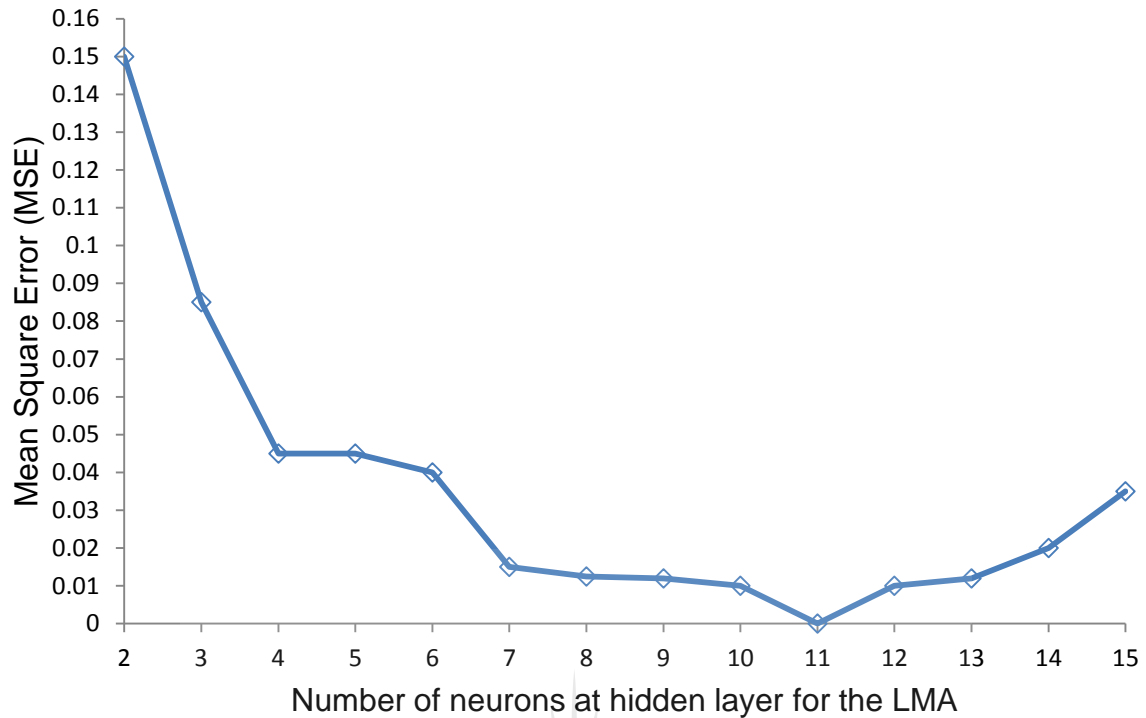


Figure 4.3: Relationships between MSE and number of neurons at the hidden layer for the LMA

The increment can be attributed to the characteristics of the MSE performance index and the input vector [p] used (Yetilmezsay & Demired, 2008). Hence, 11 neurons were selected as the best number of neurons. Figure 4.3 shows the optimized NN structure (3-11-1). It has a three-layer NN, with *tansig* at the hidden layer with 11 neurons and *purelin* at the output layer.

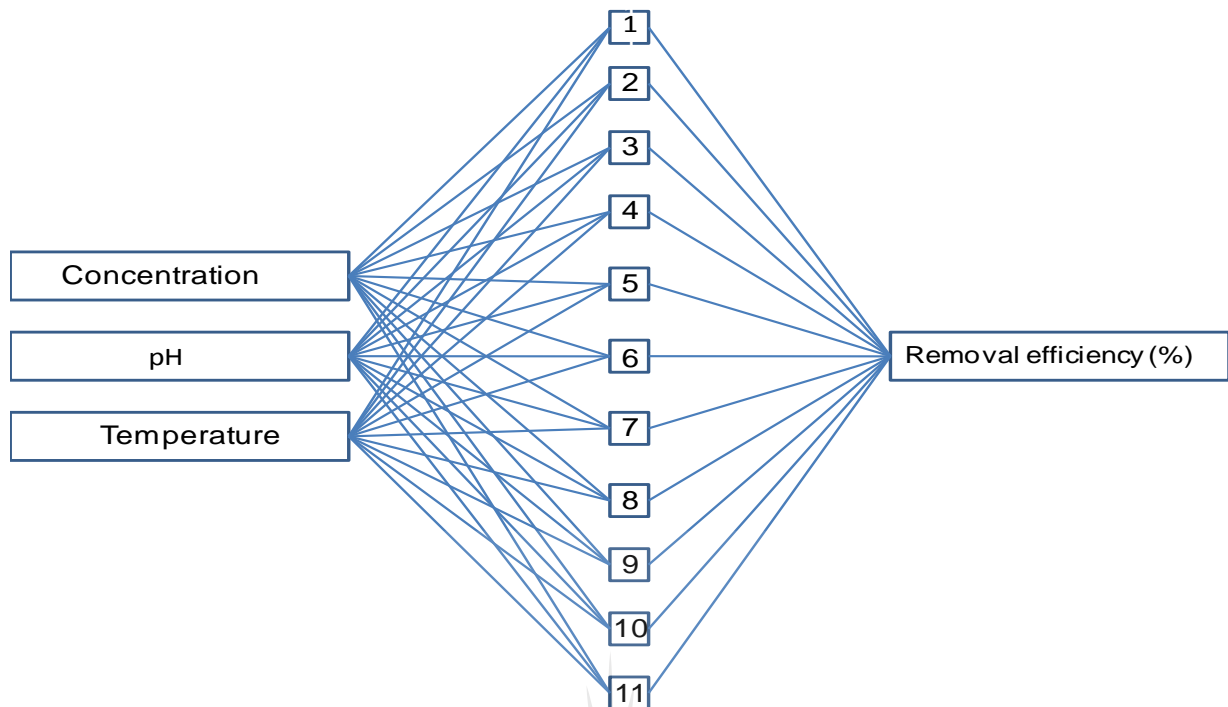


Figure 4.4: Structure of the NN for the removal

4.2.4 Selection of initial weight

An important problem encountered when training a NN is the determination of the appropriate initial values for the connection weights. Effective weight initiation is associated with performance characteristics such as the time needed to successfully train the network and the generalization ability of the trained network (Adam *et al.*, 2014). The wrong choice of initial weights can lead to an increase in the training time or can even cause the non-convergence of the training algorithm. In order to prevent these phenomena, 25 runs were performed using different random values of initial weights and the best training network was then selected.

4.2.5 Sensitivity analysis

In order to assess the relative importance of the input variables, two evaluation processes were used. The first one was based on the NN weight and Garson equation (Aber *et al.*, 2009). Garson proposed an equation (4.3) based on the partitioning of the connection weights:

$$I_j = \frac{\sum_{m=1}^{m=N_h} \left(\left(\left(|W_{jm}^{ih}| / \sum_{k=1}^{N_i} |W_{km}^{ih}| \right) x |W_{mn}^{ho}| \right) \right)}{\sum_{k=1}^{k=N_i} \left\{ \sum_{m=1}^{m=N_h} \left(\left(|W_{km}^{ih}| / \sum_{k=1}^{N_i} |W_{km}^{ih}| \right) x |W_{mn}^{ho}| \right) \right\}} \quad (4.3)$$

Where, I_j is the relative importance of the j th input variable on the output variable, N_i and N_h are the number of input and hidden neurons, respectively and W is the connection weight. The superscripts 'i', 'h' and 'o' refer to input, hidden and output layers, respectively and subscripts 'k', 'm' and 'n' refer to input, hidden and output neurons, respectively.

Table 4.3 shows the relative importance of the input variables calculated by Equation 4.3. All variables have a strong effect on Cu (II) or Co (II) removal. The initial concentration appears to be the most influential variable and the pH has the low relative importance. The second evaluation process is based on the possible combination of variables (Salari *et al.*, 2005). The performance of the groups of one, two and three variables was tested by the optimal NN structure using the LMA with 11 hidden neurons. The input variables were defined in this form: P_1 , pH; P_2 , initial Cu (II) ions or Co (II) concentration; P_3 , temperature.

Table 4.3: Relative importance of input variables

Input variable	Importance
pH	42.6
Initial ions concentration	36.7
Temperature	20.7

Table 4.3 shows the results of the sensitivity analysis for different combinations of variables. The sensitivity analysis showed that P_1 (pH) was found to be the most effective parameter among those considered in the group of one variable. As shown in Table 4.4, the MSE value (264.4249) significantly decreased to 0.349342, which is the minimum value of the group of two variables when P_1 was used in combination with P_3 . The MSE (0.349342) decreased to 0.307253, which is the minimum value of the group of three variables when all three variables were combined. It can be concluded that pH is the most influential variable. In addition, all variables have a strong effect on Cu (II) or Co (II) removal and it agrees well with the sensitivity analysis using Equation 4.2.

Table 4.4: Performance evaluation of combinations of input variables

CN	Combination	MSE	R ²	IN	BLE
1	P_1	368.505	0.375	10	$y = 3.75x+785$
2	P_2	276.165	0.523	8	$y = 7.59x+746$
3	P_3	264.4249	0.642	12	$y = 8.91x+659$
4	P_1+P_2	0.884074	0.404	8	$y = 0.405x+28.7$
5	P_1+P_3	0.349342	0.642	9	$y = 0.452x+29.2$
6	P_2+P_3	0.663052	0.531	7	$y = 0.412x+27.1$

7	$P_1+P_2+P_3$	0.307253	0.862	8	$y = 0.767x+17.6$
---	---------------	----------	-------	---	-------------------

CN, combination number; MSE, mean square error; IN, iteration number; R^2 , correlation coefficient; BLE, best linear equation; P_1 , pH; P_2 , initial Cu (II) ions or Co (II) ions concentration; P_3 , temperature.

4.2.6 Effect of pH on removal efficiency

To examine the effect of pH, experiments were conducted by varying the pH in the range 2-4 at different initial concentrations of copper in the solution. Figures 4.5 to 4.8 show a comparison between the predicted and experimental values of the Cu (II) removal at pH 2, 2.5, 3 and 4. The results show that pH significantly influences Cu (II) removal. A decrease in Cu (II) removal at a pH higher than 3 may be due to the fact that a high concentration of H^+ ions competes with Cu (II) for active sites at low pH, with an apparent preponderance of H^+ ions. This results in the suppression of Cu (II) adsorption on the surface of clinoptilolite. The uptake capacity of clinoptilolite was found to be a maximum at pH 4 and at an initial concentration of 0.361 mg/L. Figures 4.5 to 4.8 show that predicted values are in good agreement with the experimental results.

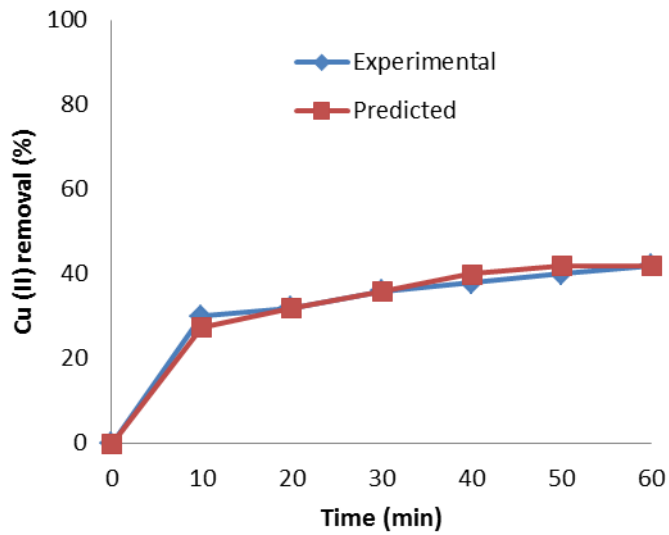


Figure 4.5: Comparisons between NN outputs and experimental data for initial pH 2 and temperature 30°C

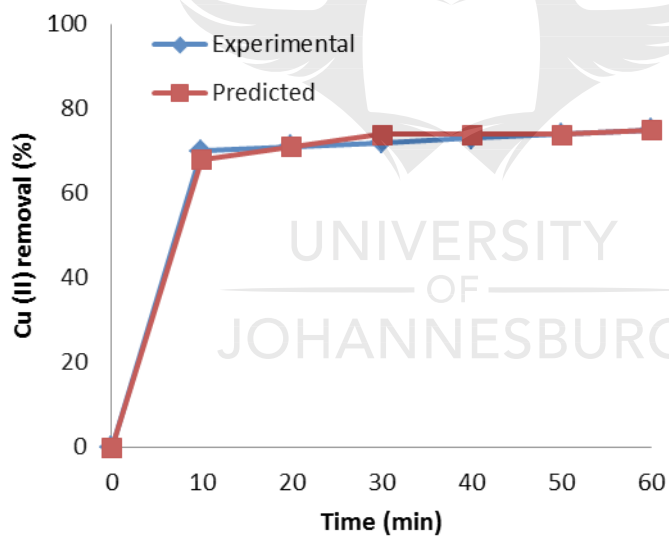


Figure 4.6: Comparisons between NN outputs and experimental data for initial pH 2.5 and temperature 30°C

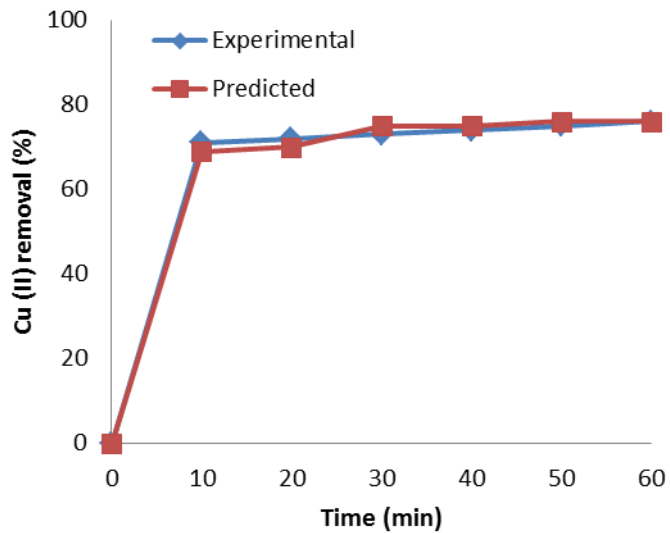


Figure 4.7: Comparisons between NN outputs and experimental data for initial pH 3 and temperature 30°C

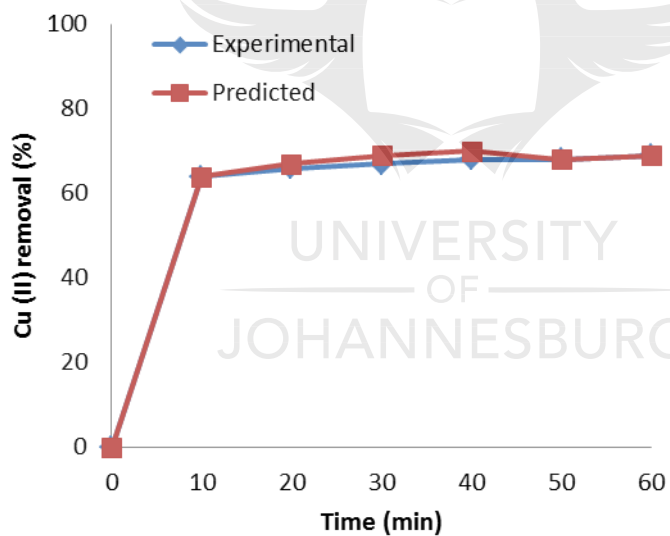


Figure 4.8: Comparisons between NN outputs and experimental data for initial pH 4 and temperature 45°C

4.2.7 Effect of temperature on removal efficiency

The effect of the temperature on adsorption of Cu (II) was studied by conducting different sets of experiments at initial concentrations of 0.361, 1.099, 1.969 and 2.748 mg/L at the following temperatures (30, 45, 60, 90°C). An increase in temperature was expected to increase the movement of cations since at higher temperature electrostatic interaction becomes weaker which causes the ions to become smaller promoting the adsorption of the ions onto the surface of the adsorbent. The results also indicate that the lower the initial concentration, the better the performance. For instance at 30°C, the percentage removal is 74% when initial concentration is 2.748 mg/L compared with 96.59% at an initial concentration of 0.361mg/L. The effects of temperature on the removal can be attributed to the activation of the Cu (II) at a higher temperature which enhances the adsorption of Cu (II) onto the coordinating sites of the treated clinoptilolite. Figures 4.9 to 4.12 show that predicted values are in good agreement with the experimental results.

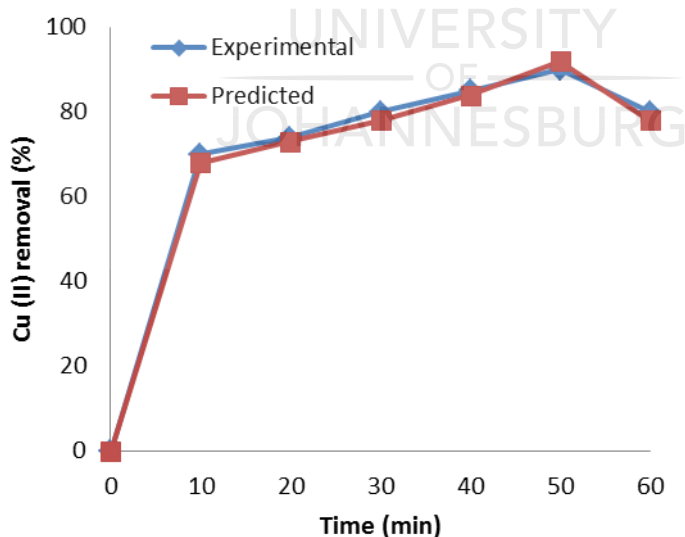


Figure 4.9: Comparisons between NN outputs and experimental data for temperature 30°C and pH 4

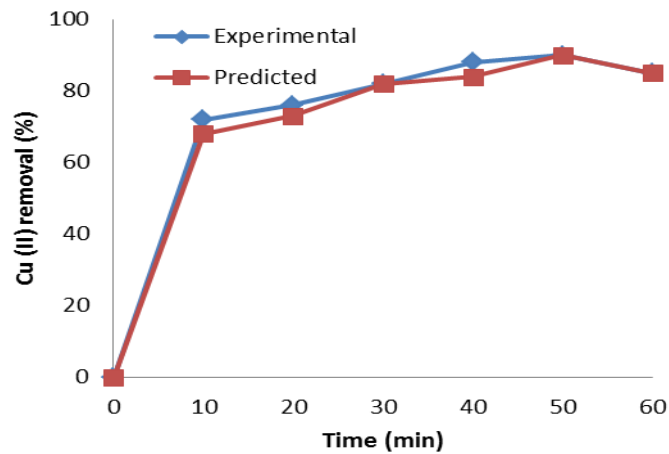


Figure 4.10: Comparisons between NN outputs and experimental data for temperature 45°C and pH 4

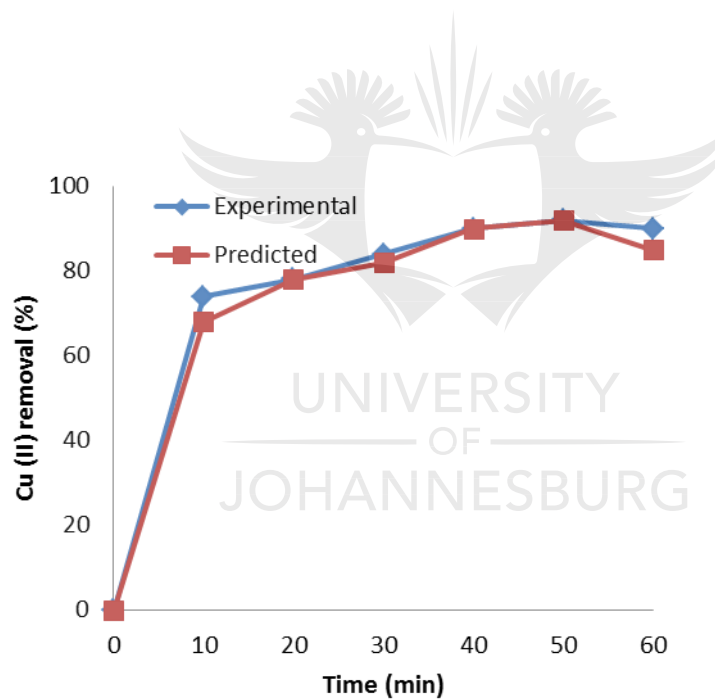


Figure 4.11: Comparisons between NN outputs and experimental data for temperature 60°C and pH 4

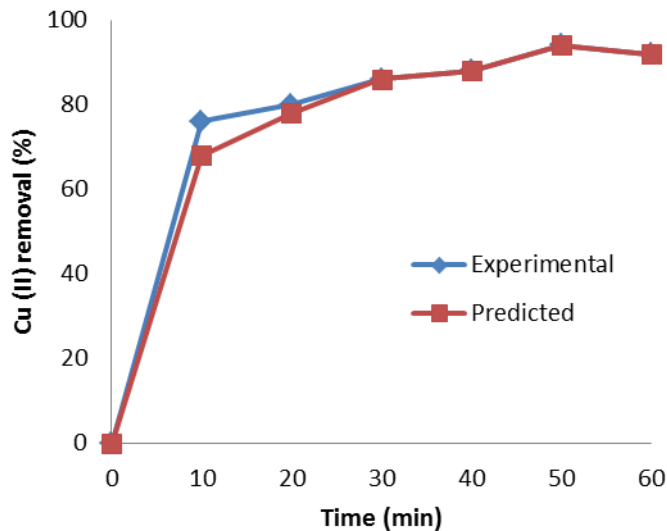


Figure 4.12: Comparisons between NN outputs and experimental data for temperature 90°C and pH 4

4.2.8 Effect of initial concentration of Cu (II) ions on loading efficiency

To observe the effect of the initial concentration of Cu (II) ions, experiments were conducted by varying the initial concentration of copper in the solution. The corresponding concentrations were 0.361, 1.099, 1.969 and 2.748 mg/L. The operating conditions were pH 4 and temperature 30°C. Figure 4.13 shows a comparison between the predicted and experimental values of Cu (II) removal. The results indicate a marginal decrease in Cu (II) removal with an increase in concentration. Sensitivity analysis also confirmed that the initial concentration is the lowest influential variable. In terms of the relationship between the experimental results and the predicted values of Cu (II) removal by the model, Figures 4.13 to 4.16 show that the predicted values are in good agreement with the experimental results.

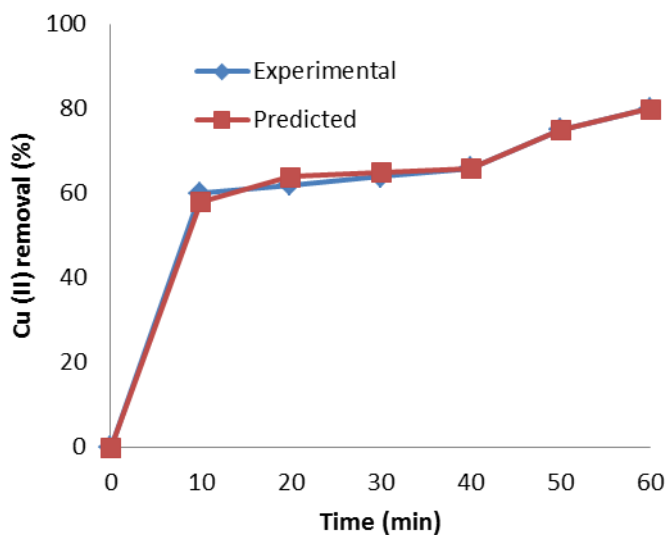


Figure 4.13: Comparisons between NN outputs and experimental data for initial concentration of 0.361 mg/L

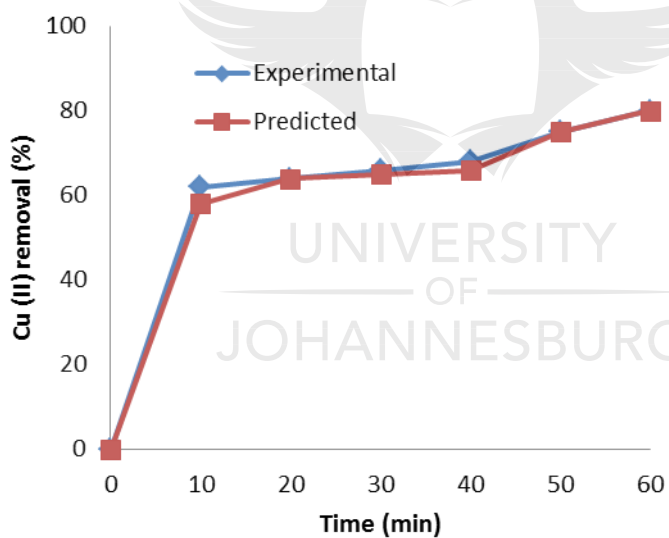


Figure 4.14: Comparisons between NN outputs and experimental data for initial concentration of 1.099 mg/L

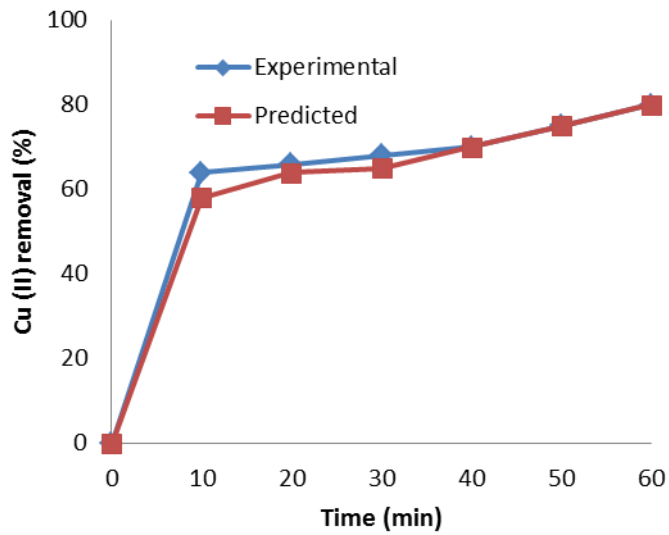


Figure 4.15: Comparisons between NN outputs and experimental data for initial concentration of 1.969 mg/L

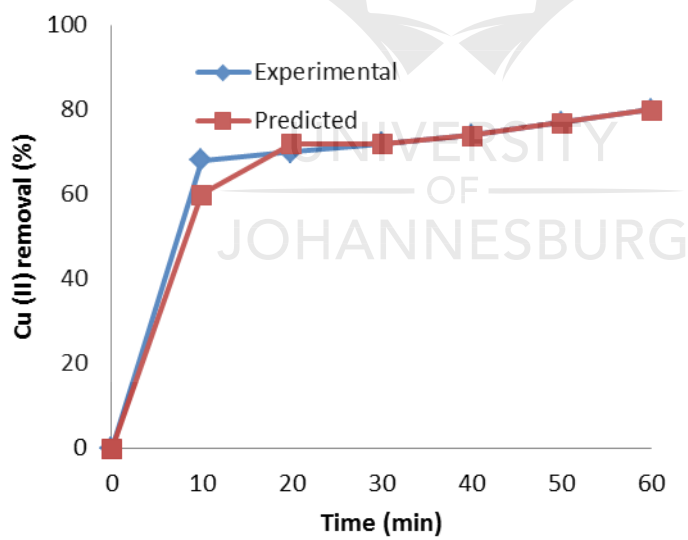


Figure 4.16: Comparisons between NN outputs and experimental data for initial concentration of 2.748 mg/L

4.2.9 Testing the NN generalization

The statistical significance of the quadratic model was evaluated with the ANOVA. The experiment sequence was randomized to minimize the effects of the uncontrolled factors. Each response was used to develop a mathematical model that correlates with the loading percentage to the experimental variable through the regression model equation:

$$Y = 62.9 + 1.3X_1 + 8.5X_2 - 4.8X_3 + 0.01X_1^2 + 64.2X_2^2 + 0.9X_3^2 - 8.9X_1X_2 + 8.4X_1X_3 + 6.1X_2X_3 \quad (4.4)$$

Where: X_1 , X_2 , X_3 represent pH, temperature and initial concentration.

The magnitude of the coefficient in Equation 4.4 denotes the intensity while the sign indicates the nature of the influence (positive or negative) of the particular variable on the response. A positive effect of a factor means that the response is improved when the factor level increases, and a negative effect of the factor reveals that the response is inhibited when the factor level decreases.

Table 4.5: ANOVA for the regression model

Source	Sum of squares	Degrees of freedom	Mean of squares	F-test
Model	201.2	9	300.5	48.4
X_1	10.1	1	100.1	25.9
X_2	120.1	1	1200.1	17.3
X_3	80.9	1	80.9	48.6
X_1^2	34.9	1	34.9	62.2
X_2^2	27.2	1	27.2	41.2
X_3^2	12.3	1	12.3	21.1
X_1X_2	12.1	1	13.1	20.7

X_2X_3	14.3	1	14.3	24.2
X_1X_3	11.2	1	11.5	22.3
Residual	11.5	20	0.6	-

Prob > F (0.05) which shows that the second order quadratic model is significant for ANOVA. The high value of the determination of the coefficient ($R^2 = 0.91$) indicates that 91% of the variability in the response is explained by the model. Table 4.5 indicates that the regression model is reliable in predicting the copper loading percentage. It was observed that among the three individual variables studied, the pH (X_1) has an enormous effect. The initial concentration (X_2) has a similar effect and temperature (X_3) also has a significant effect on the copper loading percentage.

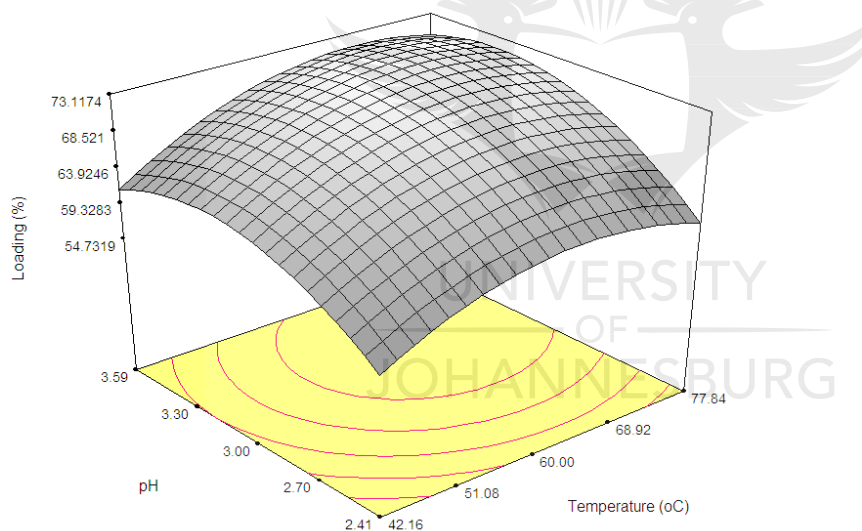


Figure 4.17: Generalization performances of optimal NN: effect of temperature and pH

As one can see in Figure 4.17, a rise in temperature resulted in an increase in the loading of the metal as expressed as a percentage. The enhancement of the adsorption capacity when temperature is increased could be due to increased mobility

and diffusion of ionic species. Since diffusion is an endothermic process, it would be expected that an increased solution temperature would result in the enlargement of pore size due to activated diffusion causing the micro pore to widen and deepen and create a great surface area. The pH on the loading percentage was carried out as per the selected model with selected ranges of temperature and pH to investigate their combined effects on the system. Figure 4.17 shows that if temperature is increased from 42.16 to 77.84°C, keeping the initial concentration (0.361 mg/L) constant, the percentage loading increases from 54.73% to 68.52%. This can be attributed to the fact that the attraction forces between material surface and metal ions are weakened and the removal decreases above a certain temperature threshold. Similarly, Aksu and Kutsa (1991) found that the thickness of the boundary layer decreases at relatively high temperatures, due to the increased tendency of the metal ion to escape from the clinoptilolite material surface to the solution, which results in a decrease in the removal.

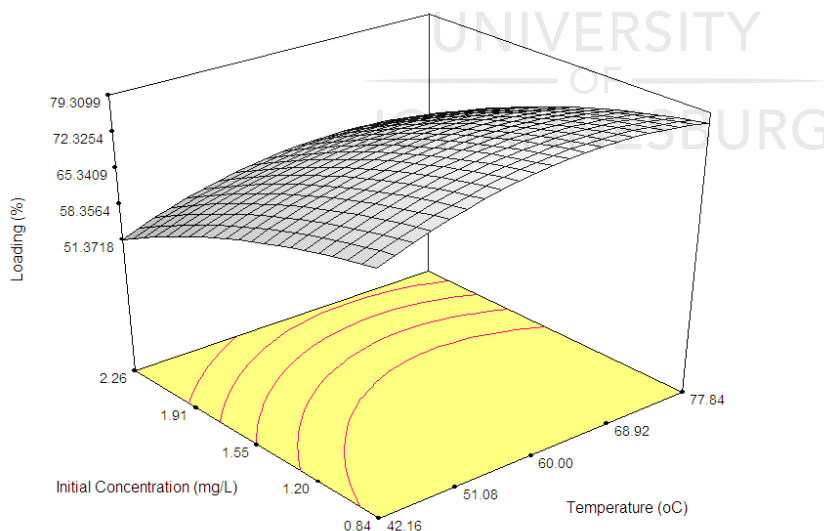


Figure 4.18: Generalization performances of optimal NN: effect of temperature and initial concentration

The effect of temperature on adsorption of Cu (II) ions was studied by conducting different sets of experiments at initial concentrations 0.84 to 2.22 mg/L at different temperatures between 42.16 to 77.84°C, keeping the pH 4 constant, and the results obtained are presented in Figure 4.18. The increase in temperature is expected to increase the movement of cations, since electrostatic interaction becomes weaker at higher temperatures, which causes the ions to become smaller and promotes the adsorption of the ions onto the surface of the clinoptilolite. It can be observed from the results that adsorption of Cu (II) ions increases with an increase in temperature at different initial concentrations of the Cu (II) as shown in Figure 4.18. The results also indicate that the lower the initial concentration of Cu (II), the better the performance of the clinoptilolite. For instance, at 45°C, the loading percentage of Cu (II) is 53.625% when the initial concentration is 2.22 mg/L, compared with 72.125% loading when the initial concentration is 0.84 mg/L. The effects of temperature on the removal of Cu (II) from the aqueous solution can be attributed to the activation of the Cu (II) at higher temperatures which enhanced the adsorption of Cu (II) onto the coordinating sites of the treated clinoptilolite.

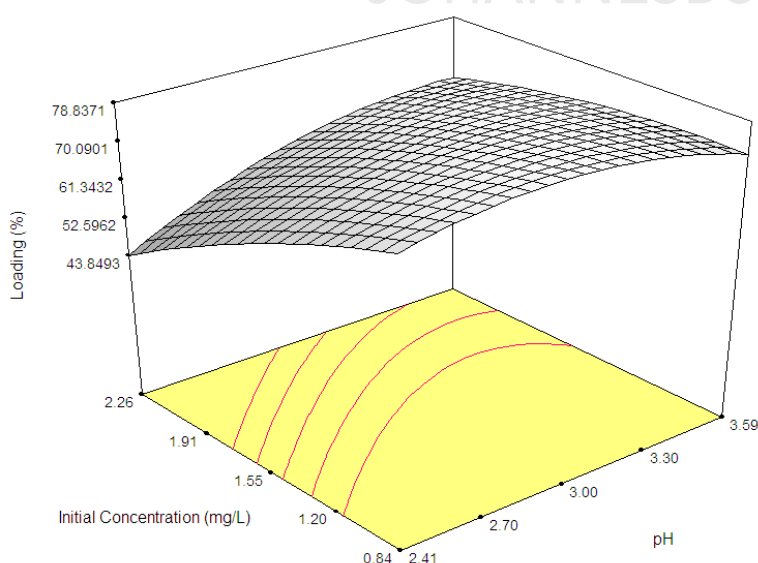


Figure 4.19: Generalization performances of optimal NN: effect of pH and concentration

Figure 4.19 illustrates the combined effect of pH and initial concentration while keeping the temperature (90°C) constant. The pH value of the solution is an important controlling parameter in the adsorption process. The initial pH value of the solution has a greater influence than the final pH, which influences both the adsorbent surface metal binding sites and the metal chemistry in water (Waranusantigul *et al.*, 2003). The pH of the feed solution was examined at different pH levels, covering a range of 2.41 to 3.59. In the case of Cu (II) the maximum adsorption was obtained at pH 3.59 for 2.26 mg/L. The removal of Cu (II) onto the activated clinoptilolite is pH dependent, as shown in Figure 4.19. At pH < 2.70, H⁺ ions compete with Cu (II) ions for the surface of the adsorbent which would hinder Cu (II) ions from reaching the binding sites of the sorbent because of the repulsive forces. At pH > 3.30, the Cu (II) gets precipitated due to hydroxide anions forming a lead hydroxide precipitate. For this reason the maximum pH value was selected to be 3.59. The highest efficiency was observed with a 70.9 % loading level at pH of 3.59 for 0.84 mg/L. Horsfall and Spiff (2002) reported that adsorption sites take up available metal more quickly at low concentrations. However, at high concentrations metals need to diffuse to the clinoptilolite surface by intraparticle diffusion. Greatly hydrolysed ions will diffuse at a slower rate because of the saturation of the active site available on the clinoptilolite for interaction with metal ions. It can be concluded that the loading efficiency increases with decreasing metal concentration in aqueous solutions.

Based on the developed NN model, the optimization of process variables was carried out in order to establish the optimal conditions that ensure the maximal loading efficiency.

It is usually found necessary to check the fitted model to ensure that it provides an adequate approximation to the real system. Unless the model shows an adequate fit, proceeding with investigation and optimization of the fitted response surface is likely to give poor or misleading results.

4.2.10 Mathematical model (MaMo)

Modelling helps to better understand a process and it is usually a simplified system that reflects only selected properties of the process. In order to assess the reliability of the mathematical model (MaMo), the calculated results were compared with the measured experimental data (Tomczak, 2011).

The process description is based on the mass balance (mass exchange between fluid and clinoptilolite) for differential bed height dx .

$$u_o \frac{\partial c(x,t)}{\partial x} + (1-\varepsilon)\rho_s \frac{\partial q(x,t)}{\partial t} + \varepsilon \frac{\partial c(x,t)}{\partial t} = \varepsilon D_{eff} \frac{\partial^2 c(x,t)}{\partial x^2} \quad (4.5)$$

In the literature Equation 4.5 can be solved analytically or numerically, but simplifying assumptions are necessary (Engell & Toumi, 2005). The most difficult problem is to define the expression $\frac{\partial q(x,t)}{\partial t}$ in Equation 4.5. For instance, if the main mass transfer resistance is assumed to be on the liquid side, i.e. the resistance of mass transfer from

the liquid to the adsorbent granule determines the rate, then $\frac{\partial q(x,t)}{\partial t}$ can be described using Equation 4.6.

$$(1 - \varepsilon)\rho_s \frac{\partial q}{\partial t} = \beta a(C - C_e) \quad (4.6)$$

In this thesis, expression $(\frac{\partial q}{\partial t})$ can be approximated from sorption kinetics equations.

In order to investigate adsorption, various kinetic models have been suggested. In recent years, numerous kinetics-based models have described the reaction order of adsorption systems based on solution concentrations. These include first-order and second-order reversible or irreversible reaction kinetics. Reaction (pseudo-first order and pseudo-second order) based on the capacity of the sorbent has also been presented in this work, such as Lagergren's pseudo-first order and pseudo-second order equations, Ho's second-order expression and the Elvovich equation (Tomczak, 2011).

If we assume that the sorption kinetics depend mainly on chemisorption, as it was proved by Benguella and Benaissa (2002), changes in the sorbate (content in sorbent particle) can be described by Equation 4.7.

$$\frac{dq}{dt} = k_2(q^* - q)^2 \quad (4.7)$$

Where q is the adsorption (mg/g), q^* is the equilibrium adsorption (mg/g) and k_2 is the coefficient in the pseudo second-order equation (g/mg min).

If the sorption kinetics are determined by physical adsorption, then this equation has the following form:

$$\frac{dq}{dt} = k_1(q^* - q) \quad (4.8)$$

Where: k_1 is the coefficient in the pseudo first-order equation (1/min)

For two points in the column at different distances from the input, concentrations of ions both in liquid and adsorbent are different and changes of the concentration are delayed in time. This is the reason why the following equation is proposed:

$$\xi = \{u_0 t - x \text{ for } u_0 t \geq x; 0 \text{ for } u_0 t < x\} \quad (4.9)$$

This substitution has been used in the literature in the analysis of multi-component adsorption (Tomczak, 2010). Every process could be considered from the Lagrange's point of view or Euler's point of view (a motionless observed). When the variable in form (Equation 4.9) is assumed, the adsorption process can be followed from Lagrange's point of view i.e., electrostatic interaction becomes weaker.

From Equation 4.9 the following transformations are valid

$$\frac{\partial c(x,t)}{\partial x} = -\frac{dC(\xi)}{d\xi} \quad (4.10)$$

$$\frac{\partial C(x,t)}{\partial t} = u_0 \frac{dC(\xi)}{d\xi} \quad (4.11)$$

$$\frac{\partial^2 C(x,t)}{\partial x^2} = \frac{d^2 C(\xi)}{d\xi^2} \quad (4.12)$$

The assumption of the new variable (Equation 4.9) offers a possibility of transforming Equation 4.5 to the form of the ordinary second-order differential equation of one variable.

Upon substitution of Equations 4.10, 4.11 and 4.12; Equation 4.5 takes the following form:

$$\frac{\varepsilon D_{\text{eff}}}{u_o(1-\varepsilon)} \frac{d^2 C}{d\xi^2} + \frac{dC}{d\xi} = \rho_s \frac{dq}{d\xi} \quad (4.13)$$

An analytical or numerical solution of Equation 4.13 is possible provided that the expression of component $\rho_s \frac{dq}{d\xi}$ is known.

Assuming that at every site of the column, sorption kinetics can be described by Equation 4.7 or 4.8, we can find relation $q = f(\xi)$ after a relevant modification of the variable.

$$\frac{\partial q}{\partial t} = k_2 (q^* - q)^2 = u_o \frac{dq}{d\xi} \quad (4.14)$$

After the separation of variables and integration of Equation 4.14 within the range $[\xi_o, \xi]$ and $[q(\xi_o), q(\xi)]$ we will have the form:

$$q(\xi) = \frac{q^* \alpha \xi}{1 + \alpha \xi} \text{ for } u_o t \geq x \quad \text{and } q(\xi) = 0 \text{ for } u_o t < x \quad (4.15)$$

$$\text{Where: } \alpha = \frac{q^* k_2}{u_o} \quad (4.16)$$

A similar transformation can be done for Equation 4.8 or for another form which described the sorption kinetics.

The derivative $\frac{dq}{d\xi}$ can be calculated from Equations 4.14 and 4.15. It has the following form:

$$\frac{dq}{d\xi} = \frac{q^* \alpha}{(1 + \alpha\xi)^2} \quad (4.17)$$

Equations 4.13 and 4.15 can be used to identify the adsorption column. The identification will consist of calculations of the coefficients k , q^* and D_{eff} by solving Equation 4.13 with the use of input-output data measured in the column in definite time intervals (e.g. to time of breakthrough and above).

The integration of Equation 4.13 in the range from ξ_0 to ξ gives the following result:

$$\frac{\varepsilon D_{eff}}{u_o(1-\varepsilon)} \int_{\xi_0}^{\xi} \frac{d^2C}{d\xi^2} d\xi + \int_{\xi_0}^{\xi} \frac{dC}{d\xi} d\xi = \rho s \int_{\xi_0}^{\xi} \frac{dq}{d\xi} d\xi \quad (4.18)$$

After relevant transformations we get:

$$\frac{\varepsilon D_{eff}}{u_o(1-\varepsilon)} \left(\frac{dC}{d\xi}(\xi) - \frac{dC}{d\xi}(\xi_0) \right) + C - C_o = \rho s q^* \left(\frac{\alpha\xi}{1+\alpha\xi} - \frac{\alpha\xi_0}{1+\alpha\xi_0} \right) \quad (4.19)$$

$\frac{dC}{d\xi}(\xi)$ can be approximated in the following way:

$$\frac{dC}{d\xi}(\xi) = \rho s \frac{dq}{d\xi}(\xi) \quad (4.20)$$

For this purpose Equation 4.19 should be used.

$$\frac{dC}{d\xi}(\xi) = \frac{q^* \alpha \rho s}{(1 + \alpha \xi)^2} \quad (4.21)$$

Taking into account Equations 4.16 and 4.18, the final equation takes the following form:

$$C = C_o + \rho s q^* \left(\frac{\alpha \xi}{1 + \alpha \xi} - \frac{\alpha \xi_o}{1 + \alpha \xi_o} \right) - \frac{\varepsilon D_{eff} q^* \alpha \rho s}{u_o (1 - \varepsilon)} \left(\frac{1}{(1 + \alpha \xi)^2} - \frac{1}{(1 + \alpha \xi_o)^2} \right) \quad (4.22)$$

For $u_o t \geq x$

$C = 0$ for $u_o t < x$

Equations 4.22 and 4.14 enable the calculation of the concentration distribution along the column in both the solution and the adsorbent, depending on time and distance from the inlet. A similar analysis can be carried out for a multi-component mixture. In such a case, each component will have individual coefficients q^* , k and D_{eff} (Tomczac, 2010).

Mathematical model values and experimental data are depicted in Figures 4.20 and 4.21. It should be noted that, although experimental values and MaMo curves do not completely coincide with each other (significant deviations are observed in some cases), they properly describe the trend of the behaviour. Obviously, it can be said that MaMo is of great importance because

- it satisfies experimental data to a moderately sufficient degree of correlation coefficient;
- it can be used for different scales;
- it can be easily used to calculate copper removal at different operational conditions;
- it can be used for scale up.

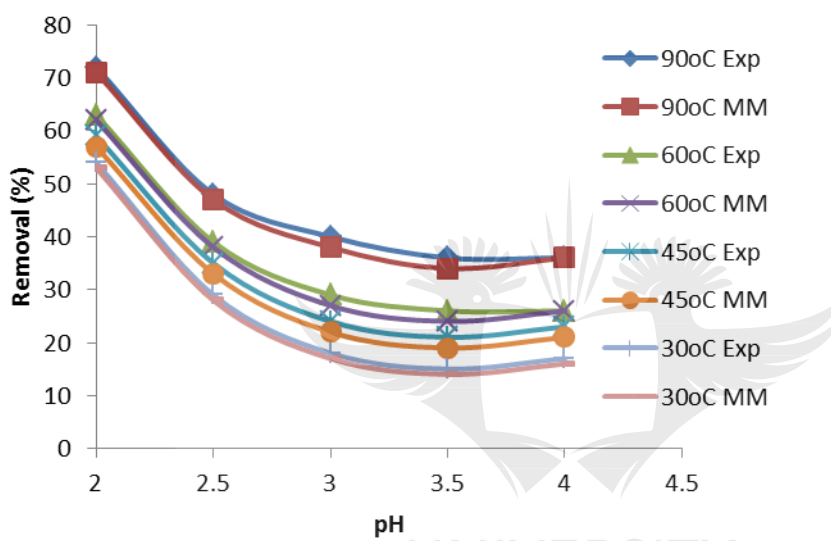


Figure 4.20: MaMo prediction values compared with experimental data: effect of pH on the percentage removal at the different temperatures

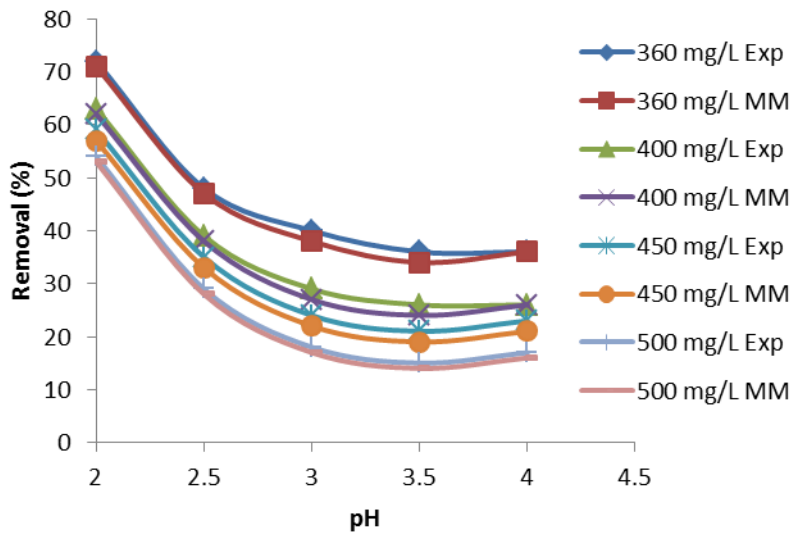


Figure 4.21: MaMo prediction values compared with experimental data: effect of pH on the percentage removal at the different concentrations

4.2.11 Comparing the MaMo and NNs

The MaMo and NN modelling predictions and experimental data are juxtaposed in Figures 4.22 to 4.23. As can be seen, the NN can predict copper removal at various operational conditions much better than the MaMo.

Excellent agreement between NN results and experimental data indicates the capacity of NN to model the complicated process. Figures 4.22 to 4.24 confirm that MaMo tends to describe the non-linear behaviour of the ion-exchange process in an almost linear manner. According to Figures 4.22 to 4.24, increasing pH, concentration and temperature increases the value of the removal. It is obvious due to the fact that increasing temperature and concentration decreases the solution resistance, while increasing the pH increases the driving force.

Taking a closer look at Figures 4.22 to 4.24, it is found that the differences between the removal value regarding medium and high levels of parameters are negligible compared to those regarding low and medium levels, i.e. at higher values of parameters, almost constant values of removal are achieved.

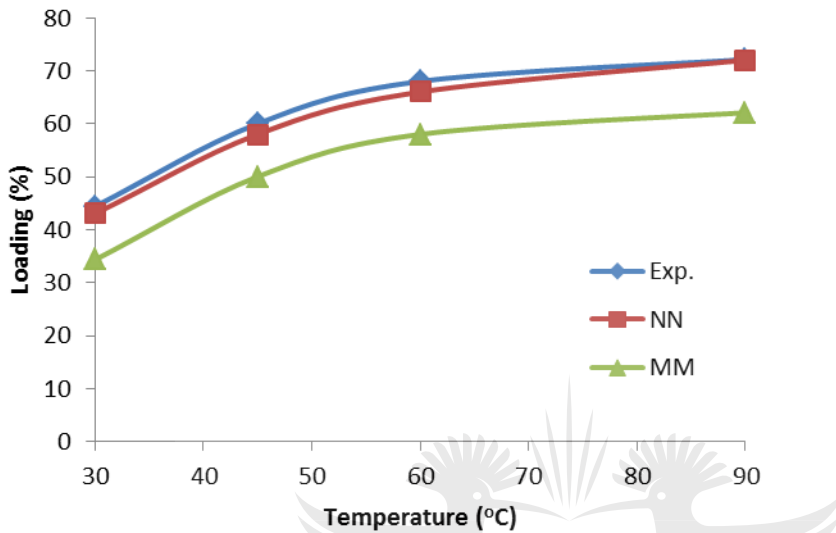


Figure 4.22: Comparisons between MaMo, NN and experimental data: effect of temperature on the removal

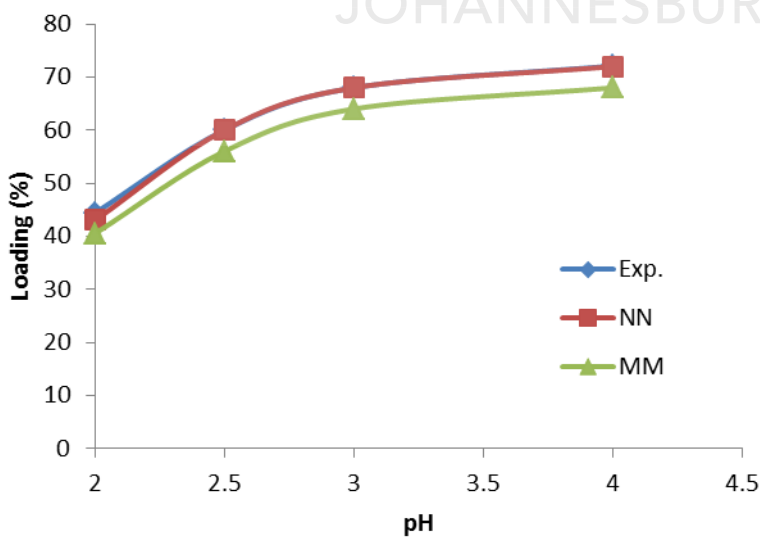


Figure 4.23: Comparisons between MaMo, NN and experimental data: effect of pH on the removal

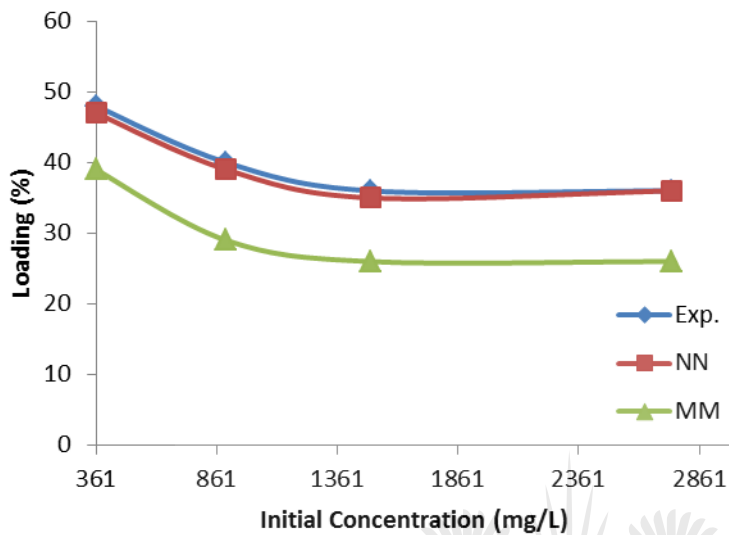


Figure 4.24: Comparisons between MaMo, NN and experimental data: effect of initial concentration on the removal

The better performance of the NN model was confirmed by comparing the MSE, RMSE and MSRE of two models in Table 4.6.

Table 4.6: Comparison between the MaMo and the NN

Error	NN	MaMo
MSE	0.9697	0.768
RMSE	0.9520	0.658
MSRE	0.9527	0.665

4.2.12 Confirmation of experiments

To support the optimized data given by numerical modelling under optimized conditions, the confirmatory experiments were conducted with the parameters as suggested by the model, and the loading was found to be 80%. The effect of pH, temperature and initial concentration were studied to support the results, and the data is in accordance with the results obtained from optimized conditions.

4.2.13 Conclusion on the loading

MaMo and NN modelling were employed for the prediction of the ion-exchange process in aqueous solutions in terms of Cu (II) removal. A (3-11-1) FFNN model with a tangent sigmoid transfer function (*tansig*) at the hidden layer with 11 neurons and a linear transfer function (*purelin*) at the output layer was proposed to predict the efficiency of copper loading. The developed NN model showed a good prediction of the experimental data with a satisfactory result. The NN predicted results are very close to the experimental results with $R^2 = 0.997$ and $MSE = 0.000376$.

A MaMo was obtained to correlate the experimental variables with the loading percentage using multiple regression analysis. The analysis of the response surface showed that the experimental variables have a significant effect on the loading percentage. The NN successfully tracked the non-linear behaviour of removal versus pH, temperature, concentration with MSEs, R and MSREs of 0.102, 0.999 and 0.004, respectively. The LMA was found to be the best BP algorithm with a minimum MSEs for training at 0.00039.

The NN modelling technique was found to have many favourable features such as efficiency, generalization and simplicity, which make it an attractive choice for the modelling of highly complex systems and non-linear processes, such as the ion-

exchange process.

4.3 Application of the FFNN technique on elution

In this part of the thesis, the effects of acid concentration, contact time and bed volume on the recovery of copper from clinoptilolite were investigated.

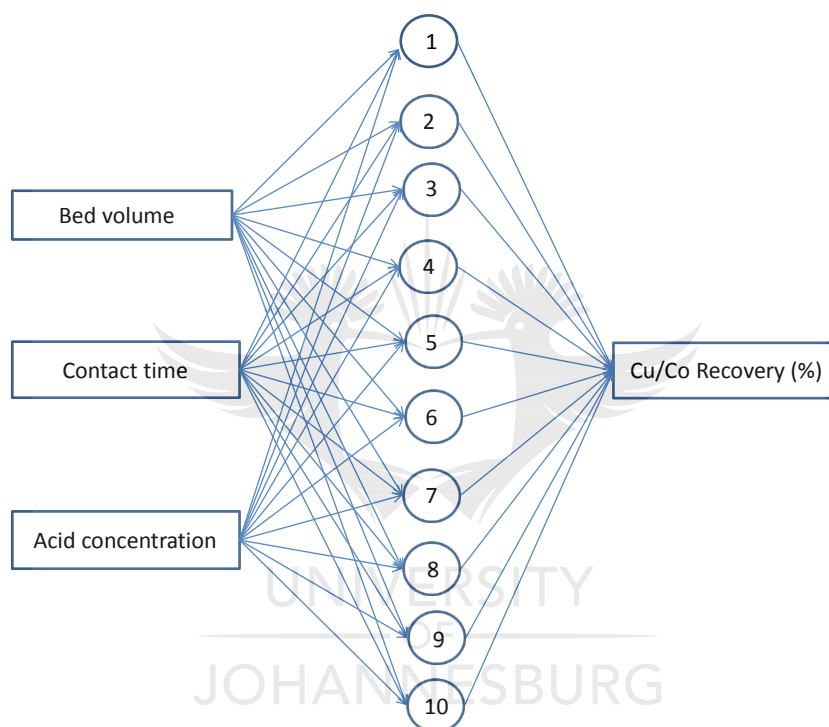


Figure 4.25: The optimized NN structure for elution

A three layer neural network with a tangent sigmoid transfer function (*tansig*) at the hidden layer, and a linear transfer function (*purelin*) at the output layer were used. Figure 4.25 presents the proposed network structure. Levenberg-Marquardt back-propagation (*trainlm*) was selected for training the designed networks. The data obtained from the experimental values for Cu/Co recovery were applied for network training to construct the network model for the elution prediction of percentage values

from the input using the MATLAB NN toolbox software. All experimental data were divided randomly into three groups (training, testing and validation). The input parameters are bed volume, contact time and acid concentration, while the recovery percentage was applied as the output parameter. All the data for NN models were normalized between 0 and 1 to avoid numerical overflows due to very large or small weights (Ghaedi *et al.*, 2014). The normalization equation applied is as follows:

$$y = (x_i - x_{\min}) / (x_{\max} - x_{\min}) \quad (4.23)$$

where y is the normalized value of x_i , the x_{\max} and x_{\min} are the maximum and the minimum values of x_i , respectively.

The optimal number of hidden layers and the optimal number of neurons in each layer are case dependent and there is no straightforward method for their determination. In this work, one hidden layer is used because a significant improvement in performance by increasing the number of hidden layers was not observed. Several iterations were conducted with different numbers of epochs and neurons of the hidden layer to determine the optimal NN structure. The optimum number of neurons or epochs in the hidden layer was iteratively determined by changing the number of neurons or epochs. The learning curve for training is given in Figure 4.26.

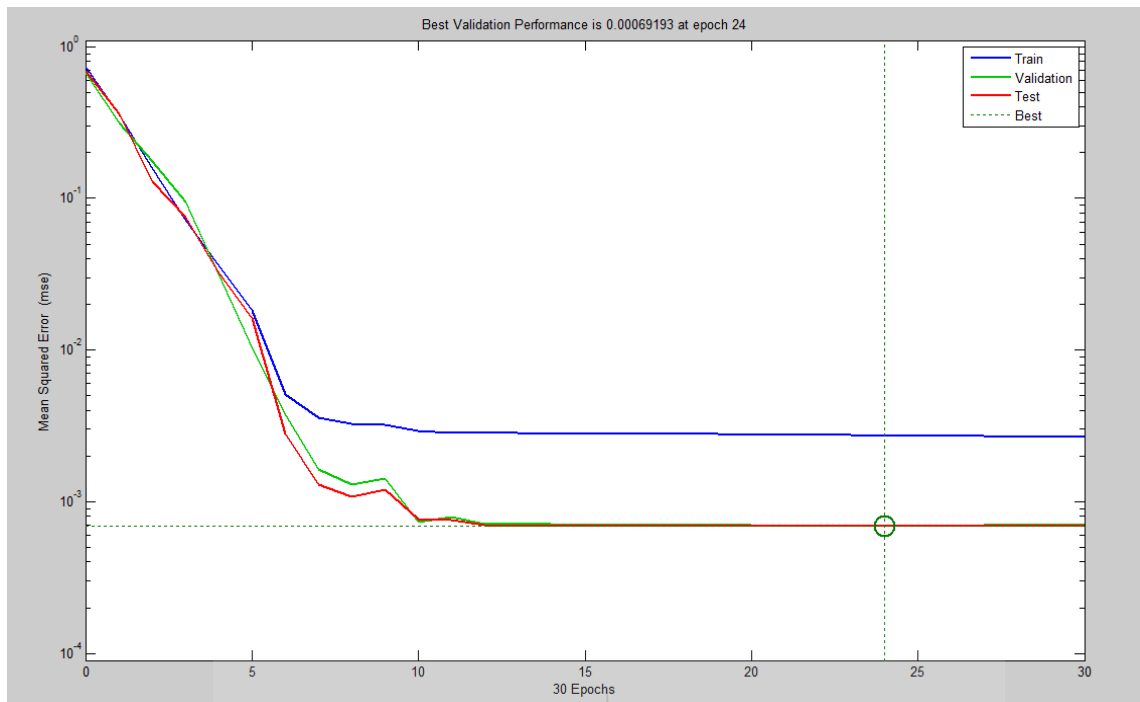


Figure 4.26: Learning curves for training, validation and testing

As can be seen in Figure 4.16, the MSE decreases initially and then it becomes constant at epoch 24. Therefore, the least MSE was obtained with 10 neurons and 30 epochs in the hidden layer. Therefore, the optimal structure of the network with 10 neurons in the hidden layer and 30 epochs was 3-10-1. The tangent sigmoid transfer function (*tansig*) at the hidden layer with 10 neurons and the linear transfer function (*purelin*) at the output layer were used. During the training process, the values of weights between individual neurons were assigned. To determine how a NN is performing during iterative training, the value of errors was calculated.

The trained network was used to estimate the response of 26 experimental points. R^2 between actual and estimated responses was determined as 0.9957 for all (training, validation and testing) (Figure 4.26). The optimum condition is obtained by the NN as the optimized technique is shown in Table 4.7. As can be seen, there is more than one

point with a quantitative recovery. However, the optimum condition with the lowest amount of bed volume is selected to obtain the higher concentration factor. The summary of the optimum condition which is obtained by three different optimization methods, are listed in Table 4.7.

Table 4.7: Effect of the number of neurons on MSE, mean absolute error (MAE) and regression coefficient (R)

Neurons	MSE	MAE	R
2	61.3410	7.832	0.76
4	245.2670	15.661	0.56
6	422.3030	20.550	0.70
8	0.0635	0.252	0.98
10	0.0014	0.038	1.00
12	0.0051	0.072	1.00
14	0.0074	0.086	1.00

In order to investigate the elution behaviour of Co (II) and Cu (II) from the loaded clinoptilolite, elution experiments were conducted in which the acidity of the eluent was increased (Lee & Nichol, 2007). The elution of Co (II) and Cu (II) from the loaded clinoptilolite was carried out using sulphuric acid and hydrochloric acid.

4.3.1 Effect of H₂SO₄ and HCl on the elution of Co (II) and Cu (II)

The concentrations of H₂SO₄ and HCl in the solution were varied from 0.2 M to 2 M. Figures 4.27 to 4.28 illustrate the effect of the acid concentrations (H₂SO₄, HCl) on the elution of metals (Co, Cu). Observing the plots one can see that HCl elution is best accomplished with a concentration of 2 M which provided the sharpest elution curve.

It was able to extract 40% of Cu and Co at 2 bed volumes. The other eluents were not as efficient, presenting a slower elution rate. As shown in Figures 4.27 and 4.28, HCl was a very powerful metal-desorbing agent compared to H_2SO_4 as is seen in Figures 4.27 and 4.29. An acid concentration higher than 2 M was not tested as it was feared that the stability of the clinoptilolite might be affected (Riveros, 2010). Figure 4.27 shows that the Co is easily eluted when compared to Cu in Figure 4.29 due to its low charge density. Low charge density exhibits a high need for hydration. Therefore, the high affinity of Co for the aqueous phase leads to a faster elution.

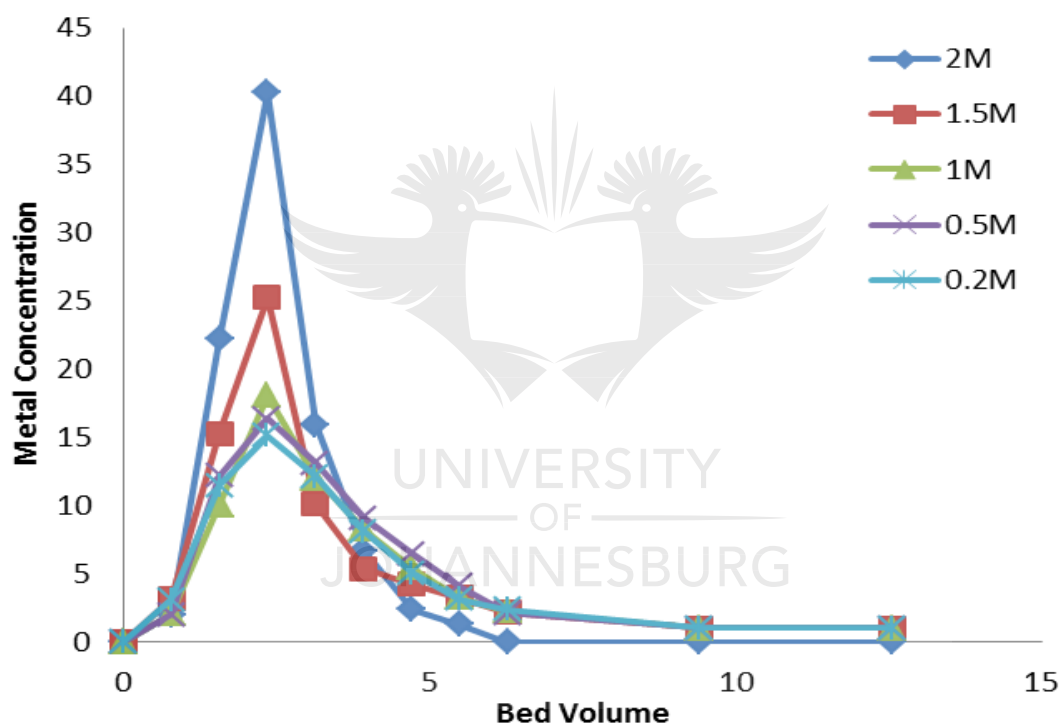


Figure 4.27: Effect of the H_2SO_4 concentration on the elution of Co

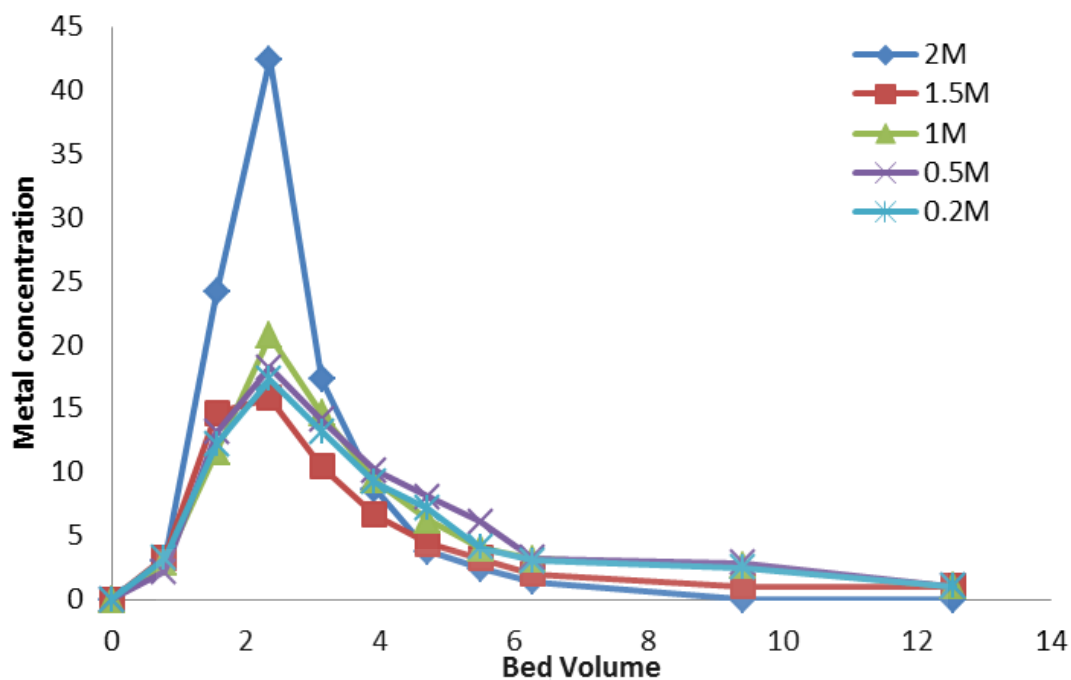


Figure 4.28: Effect of the HCl concentration on the elution of Co

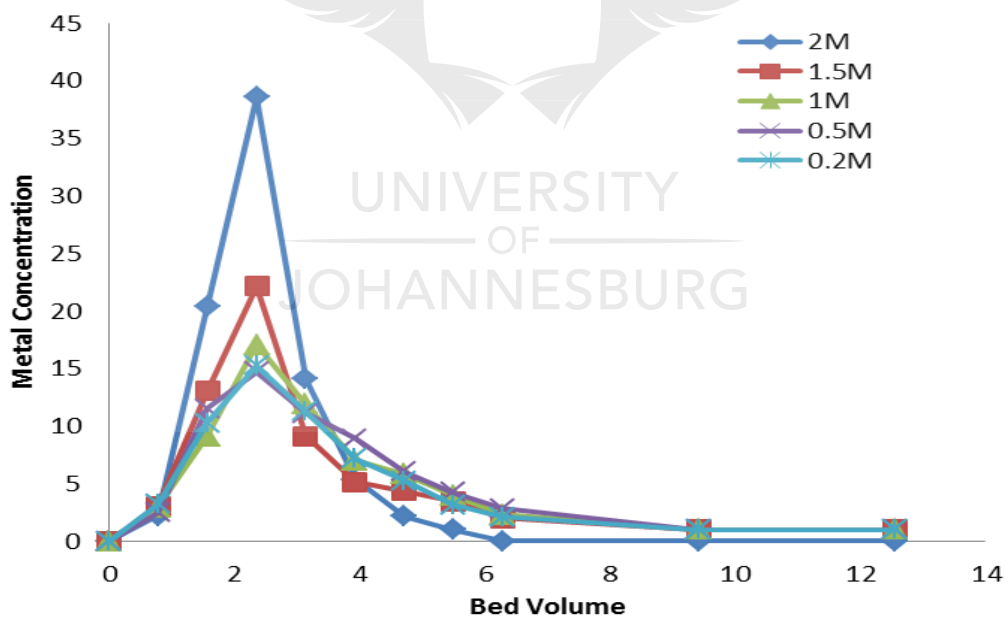


Figure 4.29: Effect of the H₂SO₄ concentration on the elution of Cu

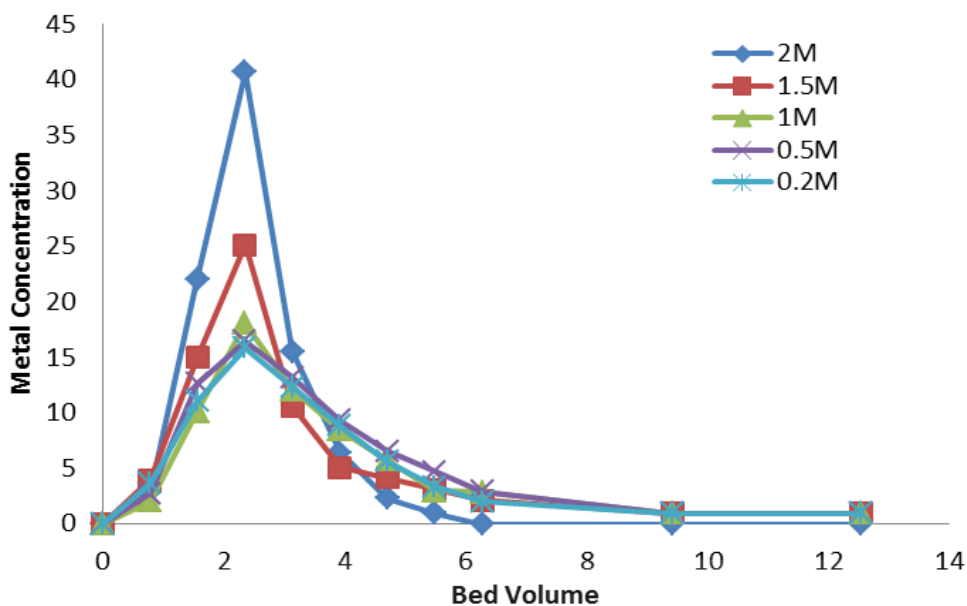


Figure 4.30: Effect of the HCl concentration on the elution of Cu

4.3.2 NN model for elution

In a parametric method of equilibrium modelling such as the multi-component Freundlich isotherm, it is necessary to know the mathematical form of the expressions involved. Only in this way can the empirical parameters be estimated from batch equilibrium adsorption/desorption data, or from column data as described earlier (Riveros, 2010; Van Deventer *et al.*, 1994). Inherent disadvantages of these parametric methods are that the selected mathematical forms of the equilibrium expressions are not necessarily valid. All relevant variables are not necessarily included in the mathematical expressions, and some related processes are ill-defined to such an extent that they defy explicit mathematical representation. For example, the pre-soaking step is still poorly understood (Van Deventer *et al.*, 1994), and the change in the adsorptive capacity of cobalt and copper due to the possible formation of a surface compound cannot be modelled adequately by using explicit expressions (Van

der Merwe, 1991).

Therefore, a non-parametric method such as a NN should be used instead to relate the equilibrium loading of a species to all the possible variables such as solution phase concentrations, temperature and the loading of the clinoptilolite. The main advantage is that no functional form needs to be specified *a priori*, and even semi-quantitative data such as the age of the clinoptilolite or the conditions of acid washing could be included as inputs. Especially in multi-component elution, it becomes very difficult to estimate independently the dependence of the various metals on process conditions. When neural nets are used this step-wise estimation of parameters becomes unnecessary. The MATLAB computing environment was chosen to generate the NN model from the data using the NN toolbox. The hyperbolic tangent (*tansig*) (being a sigmoid transfer function) was chosen for the input to the hidden layer mapping while a purely linear transfer function (*purelin*) was chosen for the hidden layer to the output layer mapping. A number of training runs were performed to identify the best possible weights in the error BP framework.

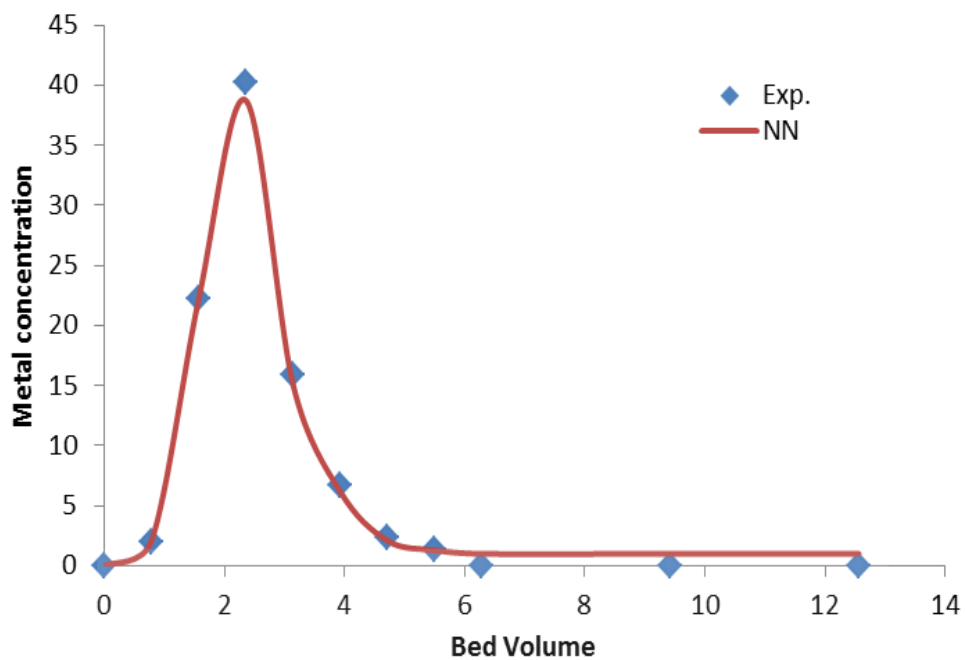


Figure 4.31: Comparison of experimental data and NN model for Co using H_2SO_4

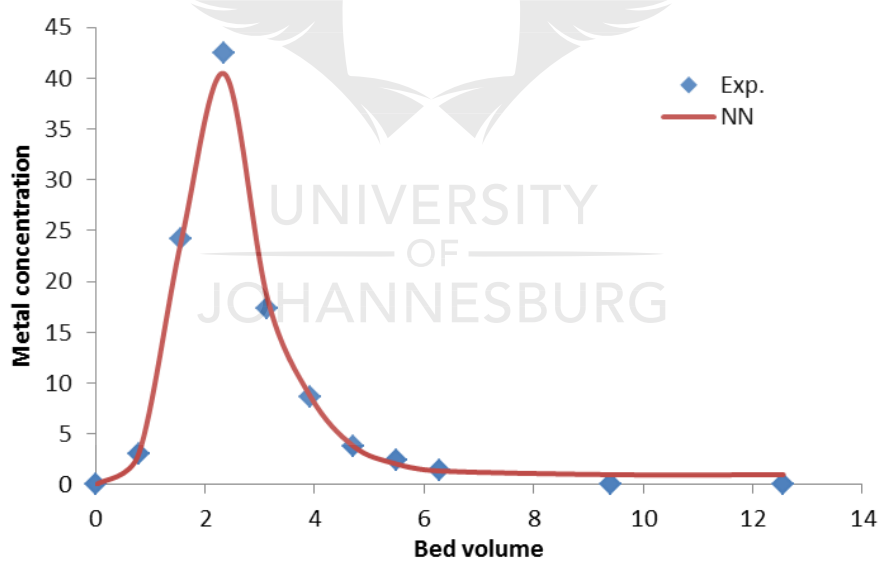


Figure 4.32: Comparison of experimental data and NN model for Co using HCl

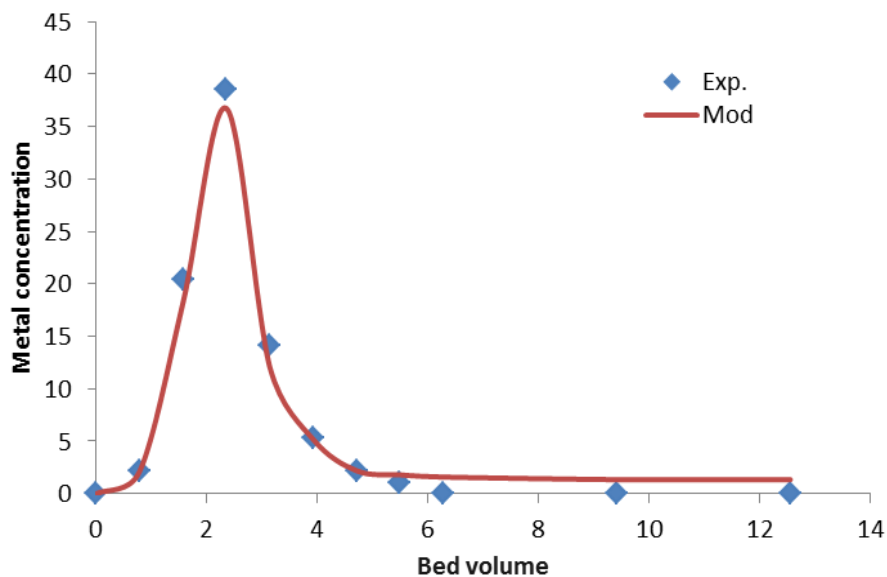


Figure 4.33: Comparison of experimental data and NN model for Cu using

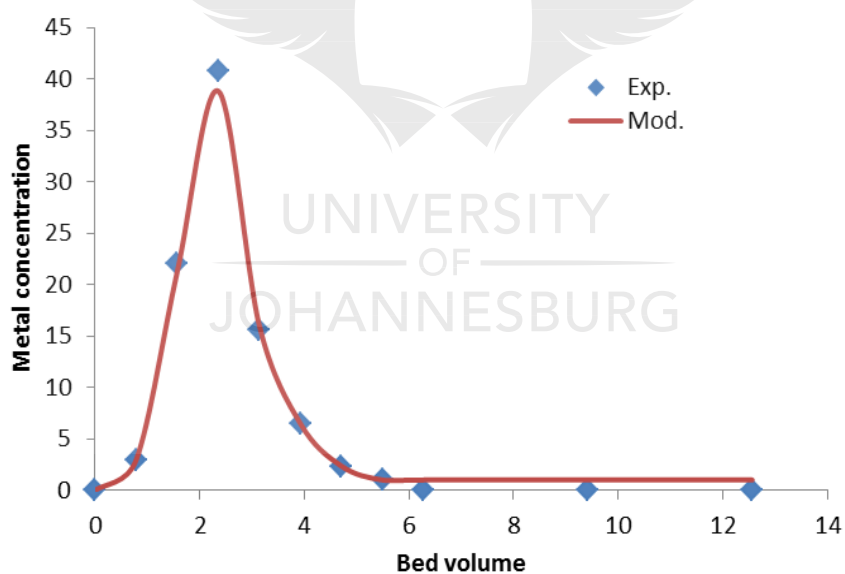


Figure 4.34: Comparison of experimental data and NN model for Cu using HCl

4.3.3 Conclusion on the elution

The configuration of the FFNN resulting in the smallest MSE was LMA (3-10-1) with a

tangent sigmoid transfer function (*tansig*) at the hidden layer with 10 neurons and a linear transfer function (*purelin*) at the outer layer. The NN predicted results are very close to the experimental results with $R^2 = 0.997$ and $MSE = 0.000376$.

The NN successfully tracked the non-linear behaviour of the Co/Cu percentage recovery versus bed volume, contact time, acid concentration with an MSE, R and MAE of 0.0014, 1.00 and 0.038, respectively. The NN modelling technique was found to have many favourable features such as efficiency, generalization and simplicity, which make it an attractive choice for the modelling of highly complex systems and non-linear processes, such as the ion-exchange process.

4.4 Conclusion

All the other chapters have a final conclusion for the whole chapter. I suggest you summarize what you have established about the FFNN analysis. It is required for the sake of consistency.

CHAPTER 5: GENERALIZED REGRESSION NEURAL NETWORK ANALYSIS

5.1 Application of the GRNN to the coal AI

This chapter presents the analysis of the determination of the coal AI using GRNN technique. This technique was employed to investigate the AI of thermal coal.

5.1.1 Experimental data on the coal AI

In this study, the proximate analysis data and AI values of more than 67 coal samples obtained from different South African thermal power stations were used. See Appendix C for more details (Lombard & Potgieter, 2008). Different types of coal are supplied to the power stations. They include large nut, small nut, pea, duff and cobble types. Each coal sample has specific percentages of H₂O, ash, SiO₂, pyrite, CaCO₃ and remaining MM (unidentified mineral matter). Documented values of the AI were used to develop and validate the NN based models.

5.1.2 Minerals influencing the abrasiveness quality of coals

Coal contains a wide range of minerals, but it is generally acknowledged that quartz and pyrite are the main components in the coal responsible for the wear and abrasion. Quartz was established to be twice as abrasive as pyrite by Raask (1985). Carbonates are known to be soft and therefore do not contribute to the abrasive quality of coals. Only those minerals that are released from the coal during the grinding process, MM

that is termed “excluded” will cause abrasive damage. Minerals that remains within the coal particles, known as “included” MM, will not be abrasive, nor will the carbonaceous material which acts as a lubricant during the grinding process (Wells *et al.*, 2004).

Quartz is two times more abrasive than pyrite on a weight percentage basis in coal. This factor was attributed to quartz which is generally found as large “excluded” particles, whereas the pyrite is often “included” in the soft clays and the coal matrix (Raask, 1985).

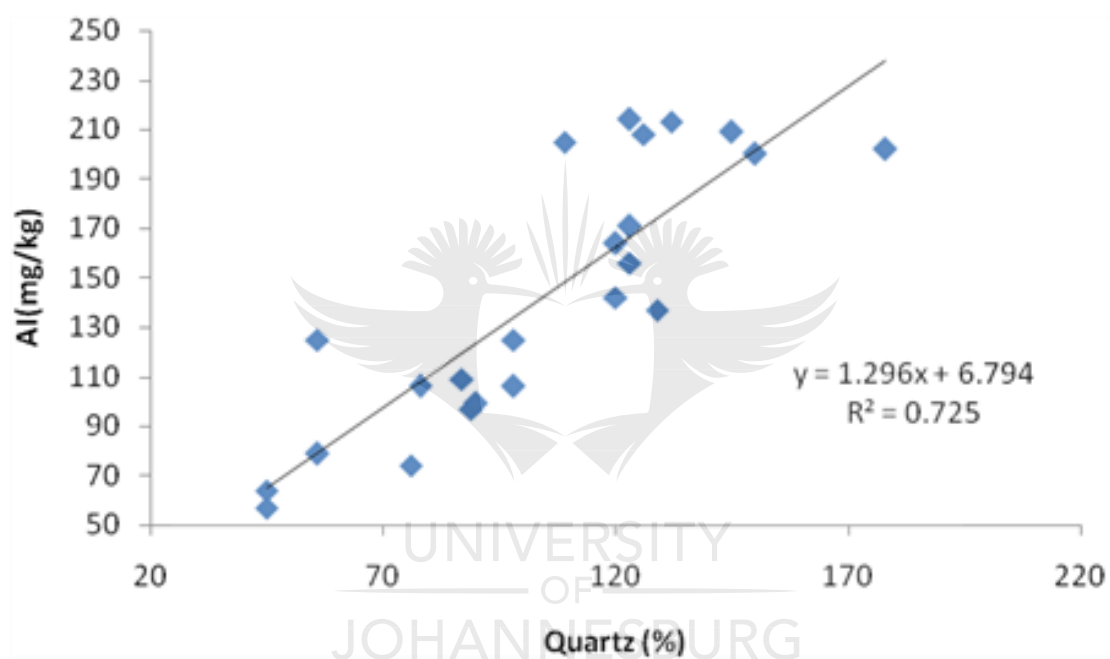


Figure 5.1: Effects of quartz on the Al of coal

Figure 5.1 illustrates the effects of quartz on the Al using the data from Lombard and Potgieter (2008). Quartz is the hardest common mineral associated with coal (Bandopadhyay, 2010a). The relationship between the Al and quartz in the coal is represented in Figure 5.1. Although there is a considerable scatter of data and a relatively poor correlation ($R^2 = 0.725$), Figure 5.1 still shows a positive trend. This indicates that the concentration of quartz is not the only factor contributing to abrasion.

Such scattering of data has also been reported by Spero (1990), Sliger (1996) and Bandopadhyay (2010a).

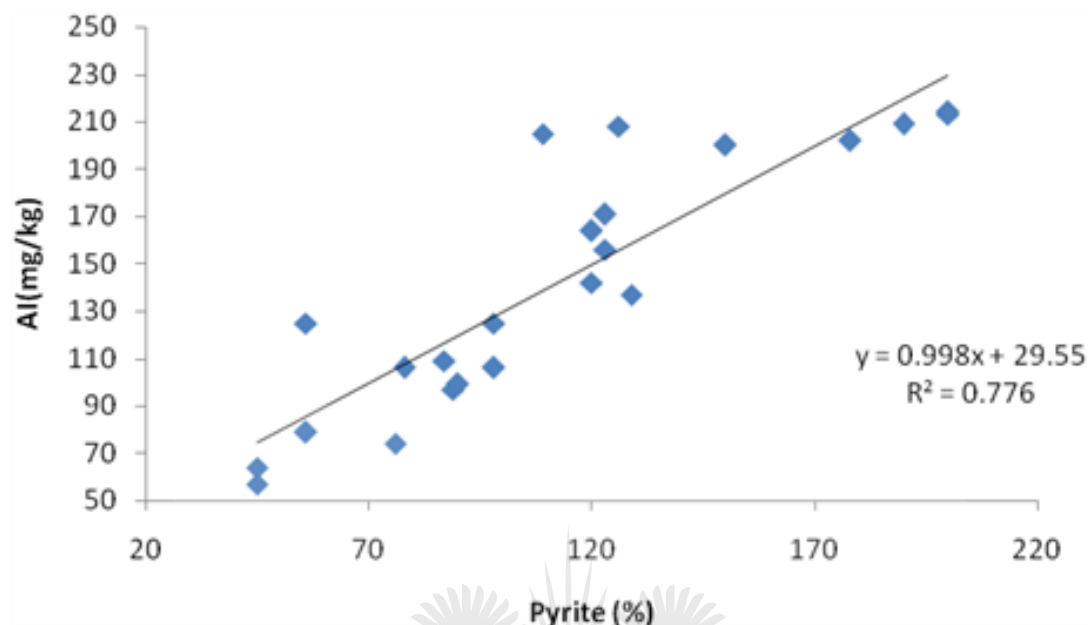


Figure 5.2: Effects of pyrite on the Al of coal

Figure 5.2 illustrates the effects of pyrite on Al. The relationship between the Al and pyrite in the coal is represented in Figure 5.2. Although there is a considerable scatter of data and a relatively poor correlation ($R^2 = 0.776$), Figure 5.2 shows a positive trend. This indicates that the concentration of pyrite is not the only factor contributing to abrasion.

The correlation between the Al and ash percentage has been reported earlier in literature (Livingston & Dugdale, 1998; Foster *et al.*, 2004 ; Bandopadhyay, 2010a). A linear relationship was found between the two variables, with $R^2 = 0.805$ in Figure 5.3. A good deal of scatter in the data was observed, which was ascribed *inter alia* to variations in quartz and pyrite content of the coals. The ash yield essentially reflects the non-combustible residues of the different minerals associated with the coal.

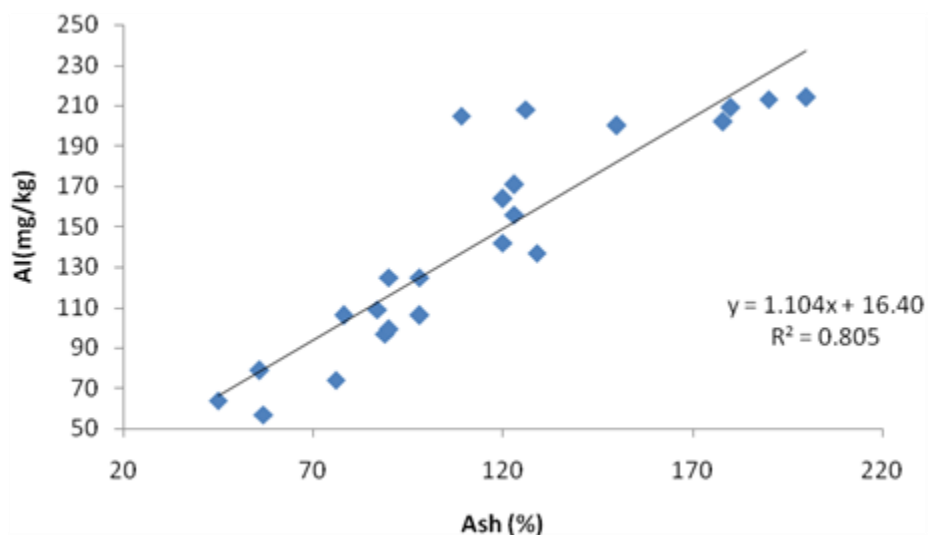


Figure 5.3: Effects of ash on the Al of coal

Figure 5.4 shows that CaCO_3 does not have an effect on the Al of coal indicated by the R^2 as 0.021. Carbonate (CaCO_3) is known to be soft and least abrasive and hence it does not add to the abrasive quality of coal (Falcon & Falcon, 1987).

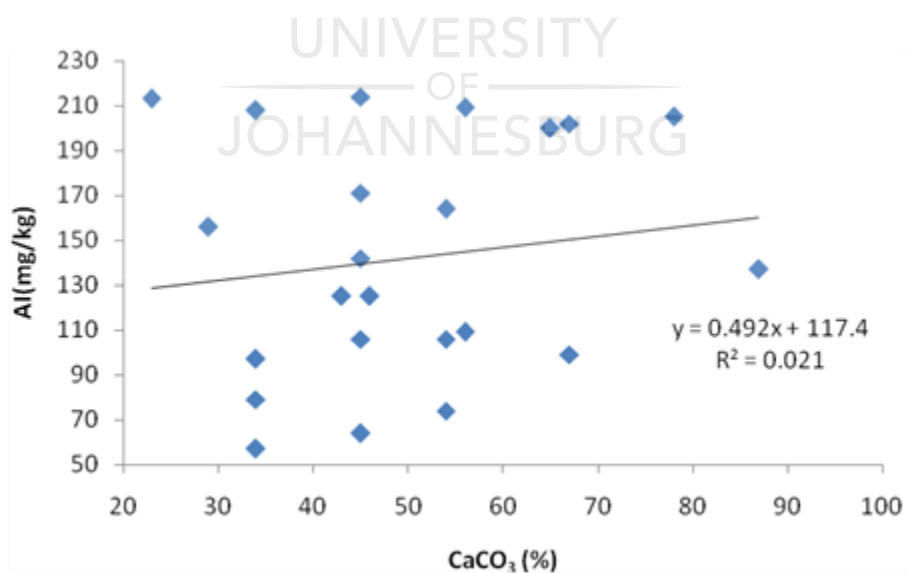


Figure 5.4: Effects of CaCO_3 on the Al of coal

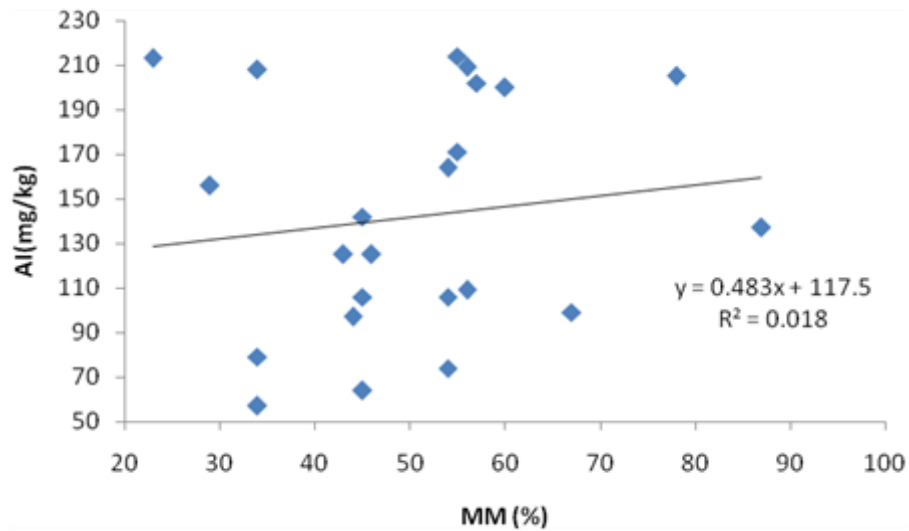


Figure 5.5: Effects of MM on the Al of coal

Figure 5.6 shows the relationship between free moisture and the Al of coal. A linear relationship was found between the two variables, with $R^2 = 0.762$. Moisture is a typical coal constituent that is known to cause abrasive wear (Eswaraiah *et al.*, 2008).

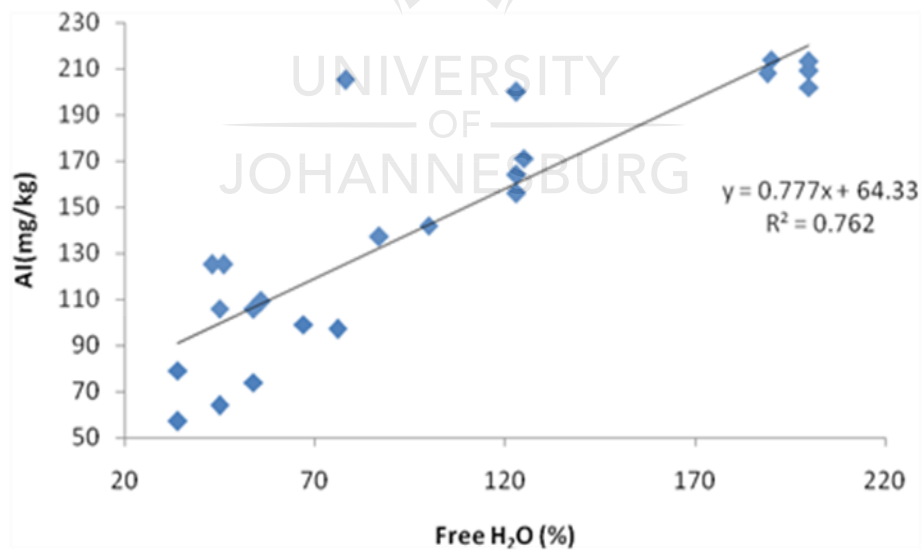


Figure 5.6: Effects of free H₂O on the Al of coal

High moisture content constituents of coals influenced the AI of coal. Spero (1990), using three sets of coals, established the evidence of a linear and exponential increase respectively between the AI and total moisture (which includes both free and inherent moisture).

Abrasiveness refers to the capacity of coal to wear away or erode the surfaces with which it comes into contact. The factors affecting the wear rate or abrasion rate are not well understood. It has been suggested that a high content of MM and the presence of hard minerals like quartz and pyrite contribute to the abrasive qualities of coal (Snyman & Botha, 1993). Meintjies (1965) suggested that there is only a general relationship between abrasion and ash content (this is quite likely when high proportions of soft clay comprise the ash forming minerals). It was also suggested that the nature of the minerals is the major factor governing abrasiveness. The oxides of silicon and aluminium form the major part of the ash of the coal studied and a useful estimate of the quartz content of the coals can be deduced from these bulk oxides found in the ash analysis. The quartz content of the ash of the coals can be related to the major element oxides (SiO_2 and Al_2O_3) through the empirical formula (Raask, 1985).

5.1.3 Application of the NNs on the AI of coal

The GRNN was used to predict the AI of coal to minerals. In this type of NN, the network consists of six input neurons and one output neuron. The six input neurons represent H_2O , ash, SiO_2 , pyrite, CaCO_3 and MM. The output layers had a single neuron to represent the AI.

5.1.4 Prediction results of abrasiveness based on GRNN

The data of 67 groups of coals were used to manage the training of the design and testing of the model. After training the parameters to the allowable range of error, the validity of the model was verified by the remaining 30 groups of data. The performances of the GRNN model for training and testing data were evaluated according to some statistical parameters such as correlation coefficient (R^2) and RMSE:

$$R^2 = \frac{\sum_{i=1}^N (O - \bar{O})(P - \bar{P})}{\sqrt{\sum_{i=1}^N (P - \bar{P})^2 \cdot (O - \bar{O})^2}} \quad (5.1)$$

$$RMSE = \sqrt{\sum_{i=1}^N \frac{(O - P)^2}{N}} \quad (5.2)$$

Where P is the predicted value, O is the observed value, \bar{P} is the average of the predicted value, and \bar{O} is the average of the observed value of the abrasiveness characteristic of coal.

The performances of the model are given in Table 5.1.

Table 5.1: The performance of the model

Testing data set		Training data set	
RMSE	R^2	RMSE	R^2
48.11	0.903	28.13	0.937

The correlation coefficient (R^2) is a commonly used statistic and provides information on the strength of the linear relationship between observed and computed values. The values of R^2 close to 1.0 indicate good model performance (Firat & Gungar, 2009).

Theoretically, if RMSE equals zero then the model represents the perfect fit, which is not possible at all.

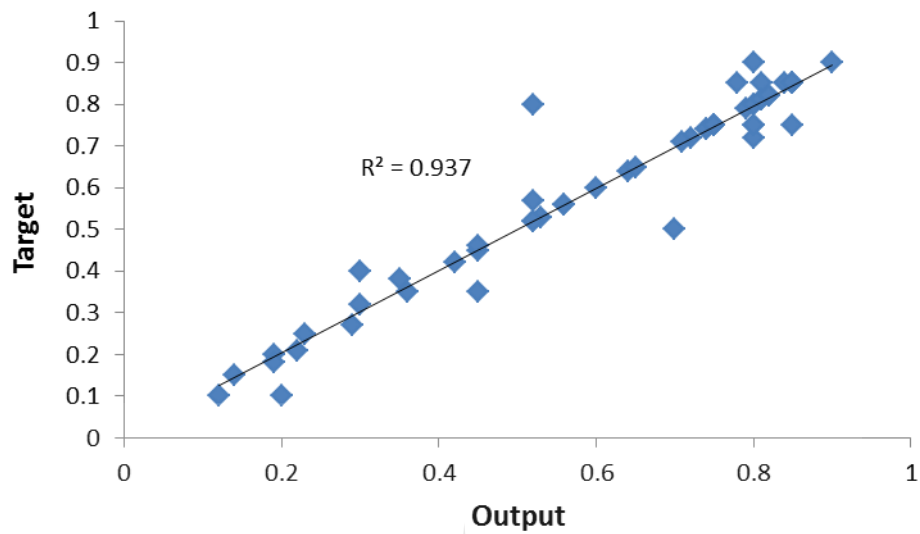


Figure 5.7: AI target of the GRNN in the training process versus output

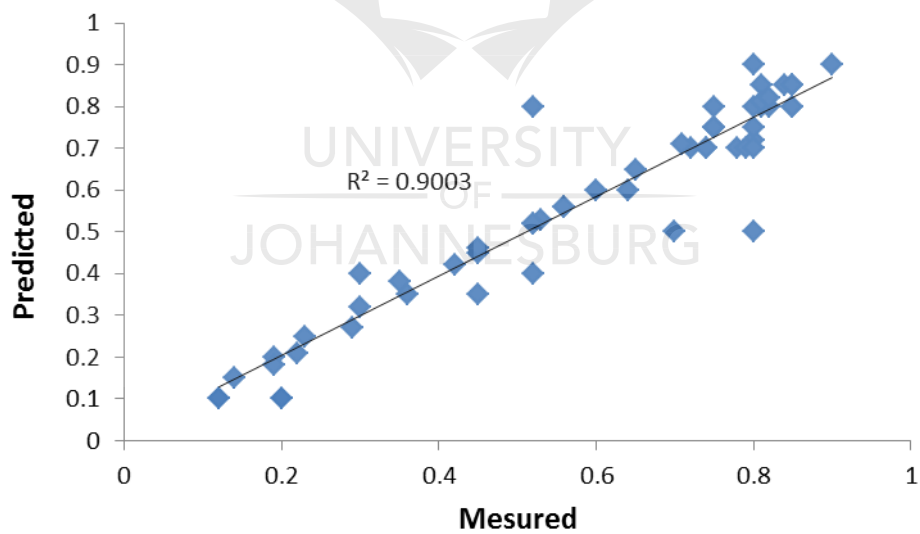


Figure 5.8: AI predicted by GRNN in the testing process versus actual measured

The results of the GRNN model presented in Figures 5.7 and 5.8 and in Table 5.1 demonstrate that the GRNN can be successfully applied to establish an accurate and reliable AI prediction model.

5.1.5 Estimation of abrasiveness characteristics of thermal coal on the AI using NNs

The following inputs were used to train the neural network: H₂O%, ash %, free SiO₂ %, pyrite %, CaCO₃ %, remaining MM %. The individual network for predicting the abrasiveness of coal, K takes the following form:

$$K = f(\text{H}_2\text{O}, \text{Ash}, \text{SiO}_2, \text{Pyrite}, \text{CaCO}_3, \text{MM}) \quad (5.3)$$

Here, $f(\cdot)$ is the underlying non-linear function defined by the networks. To avoid the saturation of the neurons, all the input and output values were normalised to numbers between 0 and 1.

A GRNN was used to develop NN models for the estimation of abrasiveness characteristics of thermal coal on the AI. Sixty seven batches of data obtained from different collieries were randomly divided into three groups, each containing 30, 17, 20 batches for training, validation and testing, respectively. The network giving the least error on the test data was selected. During network training, the training algorithm continuously checks the network error on the test data set. The training was terminated at the point where the network error on the test data was at a minimum. Early stopping is implicit to implement regularisation, which can improve model robustness (Sjoberg *et al.*, 1995). The training strategy implemented has the advantages of speed and not over-fitting the noise in the data.

5.1.6 Comparing work on empirical equations

In order to set an accurate and reliable comparison and evaluation, the model has also been tested by the AI prediction equation proposed by Raask (1985). Snyman, Van Vuuren and Barnard (1984) suggested that a high content of MM and the presence of hard minerals like quartz and pyrite contributes to the abrasive qualities of coal. Raask (1985) generated the following predictive equation for the abrasiveness of coal:

$$AI = Q_c + 0.5P_c + 0.2A_c \quad (5.4)$$

Although there are several newer empirical linear formulas in the literature for predicting the AI within narrow rank ranges (Stachowiak & Stachowiak, 2001; Bandopadhyay, 2010a), the above-mentioned formula is more compatible with variables in the present proposed approach. Therefore, this empirical formula was used for the comparison.

Table 5.2: Comparison of performances of the prediction model and Raask equation

	Testing data set	
	RMSE	R ²
GRNN	48.11	0.937
Raask equation	92.70	0.684

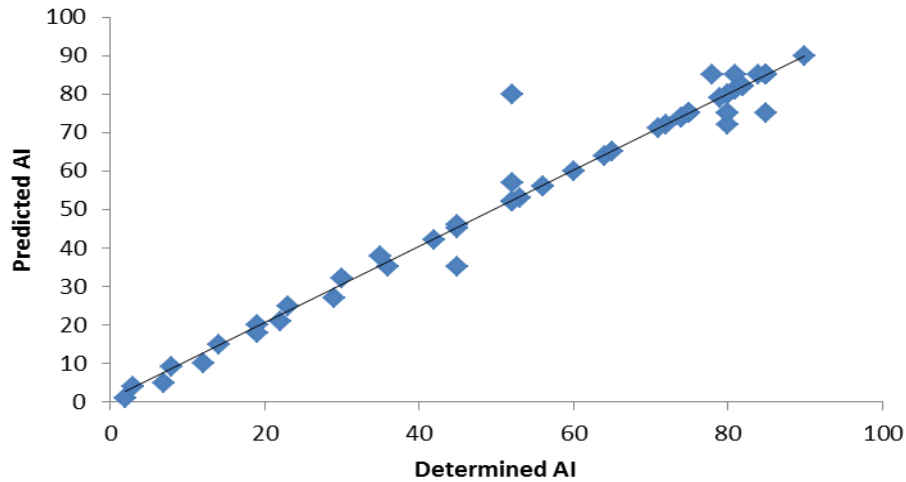


Figure 5.9: Prediction of the AI based on Equation 5.4

A comparison between the performances of GRNN and the Raask equation are given in Table 5.2 and Figure 5.9 which has shown that the value of the RMSE of the GRNN is lower than that of the Raask equation.

The prediction of data sets of networks (training data set and testing data sets) based on Equation 5.4 is shown in Figure 5.9. It is clear from Figures 5.9 and 5.10 and the comparison of R^2 of NN-predicted and regression predicted (Equation 5.4) AIs that the latter equation has a significantly lower accuracy compared to NN results. The prediction was based on a complex set of coals.

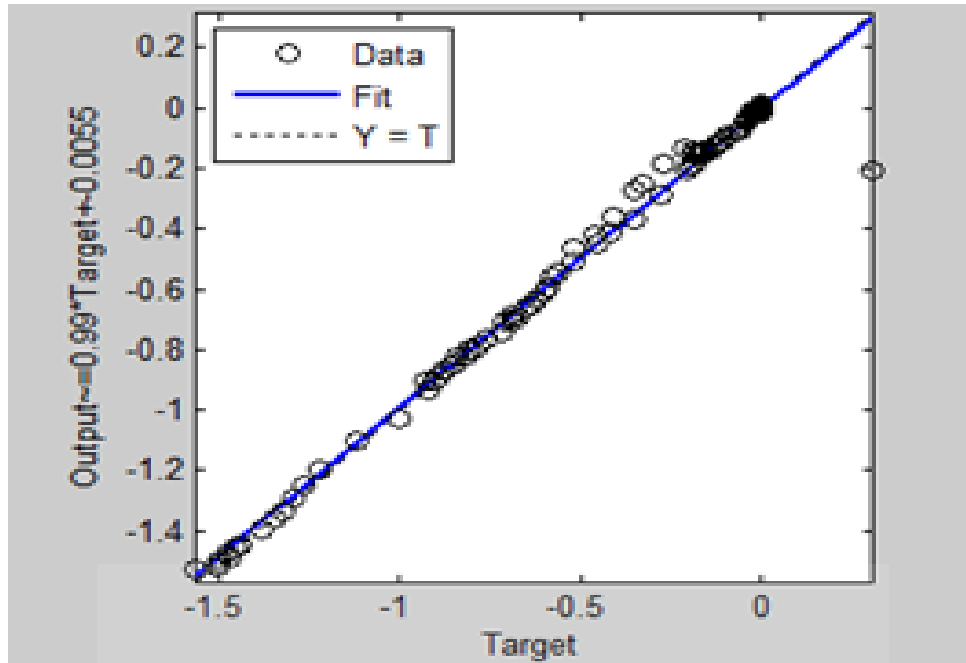


Figure 5.10: Target of the GRNN versus the output

The comparison of the training and test results with the data is shown in Figure 5.10, which demonstrates that in general the predictions from the GRNN fit reasonably well with the data, although there are some discrepancies.

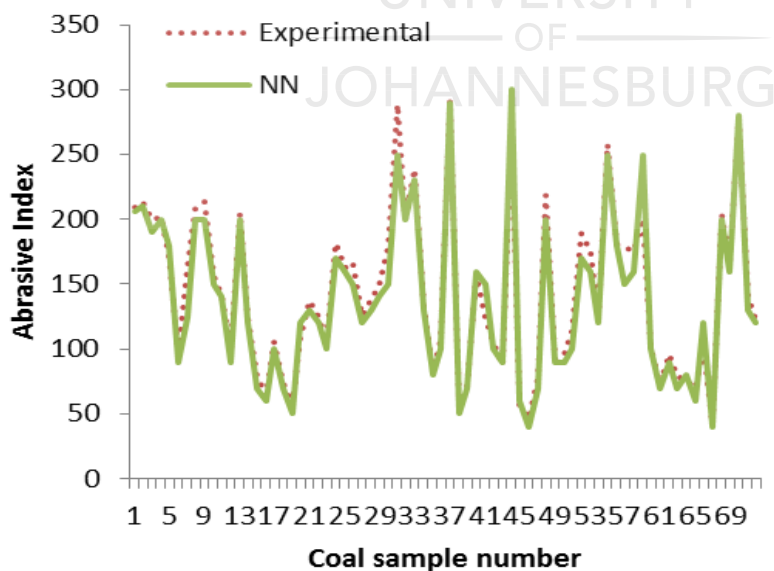


Figure 5.11: Comparison of the training results with experimental values

In this study, the neuron transfer function $f(x)$ for calculating the weights is in the form:

$$f(x) = \log [1/1+\exp (-x)] \quad (5.5)$$

NNs are increasingly being used to construct empirical non-linear models for inferential estimation and control (Bhat & McAvoy, 1990; Willis *et al.*, 1991). An important requirement of inferential estimators is that they should not only provide satisfactory estimation accuracy but also be robust to new data. The accuracy and robustness of a GRNN model is strongly influenced by the availability of training data. In this case, to build an accurate and robust GRNN, ideally a large amount of training data must be obtained from coals. To overcome the problem of limited training data available, Breiman (1992) and Wolpert (1992) proposed stacked GRNN to improve both the accuracy and robustness of a NN model. Since each GRNN model can behave differently in different regions of the input space, model accuracy over the entire input space can be improved by combining several GRNN models. This combination or aggregation of several GRNN models has been termed stacking. The data are randomly re-sampled to form a number of different training and test data sets. A number of GRNN models are then developed based on each re-sampled training and test data set. Instead of selecting a perceived 'best' single GRNN for prediction purposes, several networks are combined (aggregated) and the aggregated predictor is used as the overall model. Results have shown that improved estimations can be achieved by using stacked NNs (Sridhar *et al.*, 1996; Zhang *et al.*, 1997).

A further criterion to ensure the robustness of a GRNN model is the knowledge of the magnitude of the underlying prediction error, especially when predictions are made outside the region where suitable training data are available. The standard error of predictions can be estimated using bootstrap techniques (Efron & Tibshirani, 1993; Tibshirani, 1996). Based on the estimated SE, confidence bounds for GRNN

predictions can be calculated. A benefit of using the boot-strap re-sampled data sets is that the confidence bounds of the model predictions can be calculated automatically. Two approaches to the generation of realistic confidence bounds were described and compared by Shao *et al.* (1997).

Since good training results do not guarantee reliable predictions on unseen data, explicit error bars should be placed on model predictions to provide the user with a clearer idea of how confident he can be of the model. GRNN predictions encompassed by confidence bounds provide a more robust and credible model of the forecast, and provide the users with greater confidence when using such models.

In industrial applications, the abrasive properties of coal can lead to serious operational problems at a power station. Wear of pulverising mills can reduce the size control of the pulverised coal particles and may ultimately lead to mechanical failure of mill components. Expensive maintenance programmes are required to keep a utility operating efficiently (Wells *et al.*, 2004). Understanding the abrasive and erosive properties of specific coals is thus very important, allowing the frequency of maintenance work to be optimized minimising the risk of failures requiring unscheduled outages of the machinery.

A separate GRNN model based on values of different parameters other than training data needs to be developed for predictions of abrasiveness characteristics of thermal coal on the AI in industrial applications.

5.1.7 Sensitivity analysis

In this study, the influence of the characteristics of quartz (Q_c), ash (A_c), pyrite (P_c) and water (H_c) are found to be the main components in the coal responsible for the wear

and abrasion. Four different models are constructed to investigate these parameters. The first one, called the GRNN 1 model, includes Q_c , P_c , H_c and $CaCO_3$ as input variables. The second model called GRNN 2, includes Q_c , P_c , A_c and H_c as input variables. The third model called GRNN 3, includes P_c , A_c , H_c and $CaCO_3$. The last model called GRNN 4, includes Q_c , A_c , H_c and $CaCO_3$. These models are trained and tested by the GRNN.

Table 5.3: Comparison of performances of GRNN models

Models	Testing data set		Training data set	
	RMSE	R ²	RMSE	R ²
GRNN 1	48.01	0.873	28.13	0.924
GRNN 2	52.68	0.787	37.28	0.876
GRNN 3	62.21	0.732	38.31	0.865
GRNN 4	92.30	0.482	50.85	0.667

As can be seen from Table 5.3, the performance of the GRNN 1 model is better than the other models. It can be said that A_c is the least influential component in coal responsible for the wear and abrasion. It appears that the effect of Q_c on model performance is significant because the GRNN 3 model, which does not include Q_c as input variable, is worse than other models. As a result, it can be said that Q_c is the most influential variable on performance in the AI prediction models.

5.2 Conclusion

An evaluation of the effectiveness of the use of a NN model was made to predict the

efficiency of copper and cobalt ions removal from aqueous solutions. The effect of operational parameters such as adsorbent dosage, concentration of copper and cobalt ions, solution of the pH, operating temperature and contact time were studied to optimize the conditions for the maximum removal of copper and cobalt ions. For the loading the experimental results showed that a contact time of 45 minutes was generally sufficient to achieve equilibrium. After BP training combined with principal component analysis, the NN model was able to predict adsorption efficiency with a tangent sigmoid transfer function (*tansig*) at a hidden layer with 11 neurons and a linear transfer function (*purelin*) at the outer layer. The LMA was found as the best of 11 BP algorithms with a minimum MSE of 0.00069193 at epoch 24. The efficient result for the metal adsorption was expressed as an absolute value.

The elution of Co (II) and Cu (II) from clinoptilolite with HCl and H₂SO₄ at different concentrations was investigated. It was found that HCl at 2M has a high elution rate compared to the H₂SO₄. An effort has been made to model the elution of the Co (II) and Cu (II) process using the NN approach. The NN model (3-10-1) developed from the limited experimental data scored fairly well on the validation experiments.

The result of the GRNN model demonstrates that the GRNN can be successfully applied for predicting the abrasiveness characteristics of thermal coal. In order to evaluate the performance of the GRNN model, the Raask equation taken from literature was used. Comparing the results of the methods, it was seen that the performance of the GRNN technique is better than other techniques.

In this study, moreover, sensitivity analysis was conducted to determine the influences of the input variables on the performance of the model. For this, four different models were trained and tested with GRNN techniques using the same training and testing data set. The result showed that quartz is the component in coal with the highest

responsibility for wear and abrasion, while ash is found to be the component least likely to cause abrasive wear. The performance of the GRNN for the prediction of abrasiveness characteristics of thermal coal was found to be impressive.



CHAPTER 6: CONCLUSIONS AND RECOMMENDATIONS

6.1 Introduction

Two objectives were pursued in this thesis. The first was to assess the ability of NNs to model the ion-exchange process using the activated clinoptilolite, and the second to investigate the possibility of the prediction of abrasiveness characteristics of thermal coal expressed in the AI.

The results of the investigations and recommendations for further research studies are summarized in the following paragraphs.

6.2 Conclusions

6.2.1 The ion-exchange process

A three-layer FFNN was optimized to predict the ion-exchange process in aqueous solutions in terms of Cu/Co (II) removal. The configuration of the FFNN giving the smallest MSE was LMA (3-11-1), with a tangent sigmoid transfer function (*tansig*) at the hidden layer with 11 neurons and a linear transfer function (*purelin*) at the outer layer for loading. The NN predicted results are very close to the experimental results, with $R^2 = 0.997$ and $MSE = 0.000376$. The sensitivity analysis showed that all variables studied (initial concentration, pH and temperature) have a marked effect on the process. For elution, the configuration of the FFNN giving the smallest MSE was LMA (3-10-1), with a tangent sigmoid transfer function (*tansig*) at the hidden layer with 10

neurons and a linear transfer function (*purelin*) at the outer layer. The NN predicted results are very close to the experimental results, with $R^2 = 0.997$ and $MSE = 0.000376$. The NN successfully tracked the non-linear behaviour of Co/Cu percentage recovery versus bed volume, contact time, acid concentration with an MSE, R and MAE of 0.0014, 1.00 and 0.038, respectively.

The NN results showed that NN techniques could effectively simulate and predict the behaviour of the ion-exchange process.

6.2.2 The coal AI

From the review of published work related to the prediction of coal, we show the need to develop NN models for predicting the abrasiveness characteristics of thermal coal. The following inputs were used to train the NN: H₂O%, ash %, free SiO₂ %, pyrite %, CaCO₃ % and remaining MM %. In the individual network for predicting the abrasiveness of coal, k takes the following form: $k = f(\text{H}_2\text{O}, \text{Ash}, \text{SiO}_2, \text{Pyrite}, \text{CaCO}_3 \text{ and MM})$. Here, $f(\cdot)$ is the underlying non-linear function defined by the networks. To avoid saturation of the neurons, all the input and output values were normalised to numbers between 0 and 1.

The GRNN was used to develop NN models for the estimation of abrasiveness characteristics of thermal coal on the AI. The result of the GRNN model demonstrates that the GRNN can be successfully applied for predicting the abrasiveness characteristics of thermal coal. In order to evaluate the performance of the GRNN model, the Raask equation from literature was used comparing the results of the methods. It was seen that the performance of the GRNN technique is better than other techniques. In this study, moreover, sensitivity analysis was conducted to determine the influences of the input variables on performance of the model. For this, four

different models were trained and tested by GRNN techniques using the same training and testing data set. The result showed that quartz (Q_c) is the most influential component in coal responsible for wear and abrasion while ash is found to be the component to be the least probable to cause abrasive wear. The performance of the GRNN technique for the prediction of abrasiveness characteristics of thermal coal was found to be impressive.

6.3 Recommendations

We have shown that the NN can accurately predict the non-linear behaviour of the ion-exchange process. We recommend this study to be extended to use more input parameters. The number of parameters should be increased in order to increase the accuracy of prediction.

We have assessed the ability of the NN to predict the abrasiveness characteristics of thermal coal. Since the possibility of NNs to predict the AI of coal has been proven, we recommend the use of the parameters such as liptinite, vitrinite and sulphur content on the AI which has the potential to improve the accuracy of modelling results.

APPENDICES

Appendix A: Physical Properties of Clinoptilolite

1. Main phase: 80-85% clinoptilolite (XRD, BET & analysis)
2. Main impurities: Paline Cristobalite, K-Feldspar & trace of Sanidine
3. Refractive index: 1.484
4. Density or Specific gravity: 2.2 g/cm³
5. Bulk density of the ore: 1.92 g/cm³
6. Packing density: 0.99 kg/m³
7. Thermal stability: it can be heated to over 700°C before the alumina-silicate framework collapses
8. Acid and alkaline stability: stable from pH 3 to 12
9. Colour: reflection white: 80% [MgO = 85%]
10. Hardness: hardness is 3.5-4.0 MOH pore size
11. Pore size: 3.5-6 Angstroms [3.5 Å]
12. Pore volume: approximated 5-10%, the bulk density of the rock as determined by immersion in mercury is 1.92 g/ml³.

Appendix B: Atomic Absorption Spectroscopy: Results for Loading and Elution

Loading

Co

Co:Cu

Time	0.5:1	1.5:1	2:1	1:1	1:2	1:1.5	1:2
0	296.0848	282.4247	282.8222	282.7631	282.1653	281.9453	282.2021
10	210.7113	234.8125	228.8817	218.5620	193.2690	215.6950	199.2654
20	210.8552	234.7880	228.7658	218.3260	193.0291	214.6952	199.3650
30	210.4760	234.6872	228.1005	218.0597	192.3654	214.2365	197.9532
40	210.4124	234.5613	227.4147	217.8560	192.1321	212.3021	196.5827
50	209.9958	234.2392	227.0950	216.9650	192.0329	202.0396	196.5640
60	209.7430	234.0923	226.8572	216.5321	191.9985	200.9653	195.3654

Cu

Co:Cu

Time	0.5: 1	1.5 :1	2:1	1:1	1:2	1:1.5	1:2
0	298.2897	298.5117	298.2748	298.102	297.6214	297.2336	297.1168
10	201.6660	224.9125	226.5227	208.9375	193.7099	224.5856	209.7291
20	201.4145	224.7980	226.4298	208.0874	193.2317	224.4529	209.5172
30	201.3823	224.6888	226.1464	208.4044	193.7141	224.7346	208.1461
40	201.2865	224.6613	226.1336	208.1581	193.5009	224.2106	207.9765
50	201.1801	224.3392	226.0881	208.4989	193.4634	201.3865	206.8784
60	201.1020	224.0911	225.9868	208.1527	193.3649	202.1168	206.2748

Elution 2 M (HCl)**Co****Co:Cu**

Time	0.5:1	1.5:1	2:1	1:1	1:2	1:1.5	1:2
0							
10	15.039	14.5538	17.326	15.943	16.159	14.195	21.826
20	15.383	14.3638	17.312	15.860	16.265	14.177	21.802
30	11.241	14.3259	17.337	15.854	16.181	14.244	21.745
40	12.486	14.2827	17.299	16.259	15.117	14.226	21.665
50	14.614	14.2739	17.001	16.256	15.163	14.252	21.629
60	14.506	12.5117	16.934	16.233	15.102	14.246	21.612

Cu**Co:Cu**

Time	0.5: 1	1.5 :1	2:1	1:1	1:2	1:1.5	1:2
0							
10	14.106	15.3488	19.303	17.943	18.100	16.195	23.826
20	14.080	15.3578	19.312	17.860	18.059	16.177	23.802
30	14.070	15.3218	19.336	17.854	18.111	16.244	23.786
40	14.057	15.2927	19.299	18.259	16.117	16.217	23.665
50	14.070	15.2739	18.001	18.256	16.163	16.252	23.635
60	14.056	12.5117	17.934	18.233	16.102	16.246	23.659

1M (HCl)**Co****Co:Cu**

Time	0.5: 1	1.5 :1	2:1	1:1	1:2	1:1.5	1:2
0							
10	14.039	14.5538	16.326	14.943	14.559	13.195	21.826
20	14.383	14.3638	16.312	14.860	14.265	12.177	21.702
30	13.241	13.3259	15.356	14.754	14.181	11.244	21.645
40	12.486	12.2827	15.299	14.259	13.117	11.226	21.665
50	12.614	12.2739	15.001	13.256	12.163	11.248	21.629
60	12.506	11.5117	13.934	13.233	12.102	11.246	21.612

Cu**Co:Cu**

Time	0.5: 1	1.5 :1	2:1	1:1	1:2	1:1.5	1:2
0							
10	13.106	13.3488	17.783	15.943	16.189	14.195	22.826
20	12.880	13.5678	17.312	15.860	16.059	14.177	21.802
30	12.070	13.3218	16.336	15.854	15.111	13.244	21.786
40	12.057	13.2927	16.299	14.259	14.117	13.217	21.665
50	12.070	12.2739	15.001	14.256	13.163	12.252	20.635
60	12.056	11.5117	14.934	14.233	13.102	12.246	19.659

0.5M (HCl)**Co****Co:Cu**

Time	0.5: 1	1.5 :1	2:1	1:1	1:2	1:1.5	1:2
0							
10	13.039	13.5538	15.326	13.943	13.559	12.195	20.826
20	13.383	13.3638	15.312	13.860	13.265	12.177	21.702
30	12.441	12.3259	14.356	13.754	13.181	11.244	21.645
40	11.486	11.2827	14.299	13.259	13.117	11.226	21.665
50	10.614	11.2739	14.001	13.256	12.163	11.248	21.629
60	10.506	11.1117	13.934	13.233	12.102	11.246	21.612

Cu**Co:Cu**

Time	0.5: 1	1.5 :1	2:1	1:1	1:2	1:1.5	1:2
0							
10	12.106	12.3488	16.783	14.943	15.189	13.195	20.826
20	11.880	11.5678	16.312	14.860	15.059	12.177	20.802
30	11.070	11.3218	15.336	13.854	14.111	11.244	19.786
40	11.057	11.2927	15.299	13.259	13.811	13.217	19.665
50	10.070	10.8739	15.001	12.256	13.163	12.252	19.635
60	10.056	10.5117	14.934	12.233	13.102	12.246	18.659

Elution 2M (H₂SO₄)

Co

Co:Cu

Time	0.5:1	1.5:1	2:1	1:1	1:2	1:1.5	1:2
0							
10	14.0391	13.8538	16.9268	15.9565	16.1590	14.1959	21.8265
20	14.3834	13.3838	16.6528	15.8605	16.2659	14.1779	21.8026
30	12.2419	13.3289	16.3378	15.8545	16.1810	14.2445	21.7459
40	12.4869	13.2927	16.2996	14.2599	15.1170	14.2269	21.6659
50	11.6140	13.2889	16.0019	14.2565	15.1639	14.2523	21.6291
60	11.5064	12.5117	15.9349	14.2336	15.1020	14.2467	21.6126

Cu

Co:Cu

Time	0.5: 1	1.5 :1	2:1	1:1	1:2	1:1.5	1:2
0							
10	13.1062	15.3488	19.3038	17.9435	18.1000	16.1959	23.8265
20	13.0803	15.3578	19.3128	17.8605	18.0590	16.1779	23.8026
30	12.0701	15.3218	19.3364	17.8545	18.1110	16.2445	23.7869
40	12.0574	15.2927	19.2996	18.2599	16.1170	16.2179	23.6659
50	12.0706	15.2739	18.0019	18.2565	16.1639	16.2523	23.6351
60	12.0561	12.5117	17.9349	18.2336	16.1020	16.2467	23.6596

1M (H₂SO₄)

Co

Co:Cu

Time	0.5: 1	1.5 :1	2:1	1:1	1:2	1:1.5	1:2
0							
10	13.0391	14.5538	16.3268	14.9435	14.5590	13.1959	21.8265
20	13.3834	14.3638	16.3128	14.8605	14.2659	12.1779	21.7026
30	12.2419	13.3259	15.3568	14.7545	14.1810	11.2445	21.6459
40	11.4869	12.2827	15.2996	14.2599	13.1170	11.2269	21.6659
50	10.6140	12.2739	15.0019	13.2565	12.1639	11.2483	21.6291
60	10.5064	11.5117	13.9349	13.2336	12.1020	11.2467	21.6126

Cu

Co:Cu

Time	0.5: 1	1.5 :1	2:1	1:1	1:2	1:1.5	1:2
0							
10	12.1062	13.3488	17.7838	15.9435	16.1890	14.1959	22.8265
20	11.8803	13.5678	17.3128	15.8605	16.0590	14.1779	21.8026
30	12.0701	13.3218	16.3364	15.8545	15.1110	13.2445	21.7869
40	11.0574	13.2927	16.2996	14.2599	14.1170	13.2179	21.6659
50	11.0706	12.2739	15.0019	14.2565	13.1639	12.2523	20.6351
60	11.0561	11.5117	14.9349	14.2336	13.1020	12.2467	19.6596

0.5M (H₂SO₄)**Co****Co:Cu**

Time	0.5: 1	1.5 :1	2:1	1:1	1:2	1:1.5	1:2
0							
10	12.0391	13.5538	15.3268	13.9435	13.5590	12.1959	20.8265
20	12.3834	13.3638	15.3128	13.8605	13.2659	12.1779	21.7026
30	11.4419	12.3259	14.3568	13.7545	13.1810	11.2445	21.6459
40	10.9869	11.2827	14.2996	13.2599	13.1170	11.2269	21.6659
50	10.6140	11.2739	14.0019	13.2565	12.1639	11.2483	21.6291
60	10.5064	11.1117	13.9349	13.2336	12.1020	11.2467	21.6126

Cu**Co:Cu**

Time	0.5: 1	1.5 :1	2:1	1:1	1:2	1:1.5	1:2
0							
10	12.1062	12.3488	16.7838	14.9435	15.1890	13.1959	20.8265
20	11.8803	11.5678	16.3128	14.8605	15.0590	12.1779	20.8026
30	11.0701	11.3218	15.3364	13.8545	14.1110	11.2445	19.7869
40	11.0574	11.2927	15.2996	13.2599	13.8117	13.2179	19.6659
50	10.0706	10.8739	15.0019	12.2565	13.1639	12.2523	19.6351
60	10.0561	10.5117	14.9349	12.2336	13.1020	12.2467	18.6596

Appendix C: Proximate Analysis of Coal (Lombard & Potgieter, 2008)

No	Ash (%)	Free SiO₂ (%)	Pyrite (%)	CaCO₃	Remain MM (%)	AI
1	27.1	2.8	1.8	4	23.9	236
2	29.3	6.6	0.8	4.4	23.3	431
3	22.4	4.4	1.1	4.9	16.5	190
4	11.5	0.1	1.1	3.4	9.3	89
5	11.2	0.1	0.9	2.8	9.7	68
6	20.9	3.1	1.1	0.6	20.3	86
7	19.2	3	1.1	0.6	18.4	74
8	20	2.9	2.8	0.2	18.1	116
9	18.9	2.6	2.7	0.5	17	127
10	18.8	3.4	1.1	0.5	17.6	172
11	16.1	0.8	0.9	3.8	13.8	86
12	7.1	0.4	0.3	1.5	6.2	61
13	11.1	2.9	0.4	0.1	9.9	109
14	13.3	4	0.6	0.1	11.02	152
15	11	3.9	0.5	0.1	8.7	132
16	9.5	2.9	0.2	0.1	8.2	138
17	23.4	4.7	1.1	3.4	18.9	206
18	18.5	2.1	2.4	5	12.4	142
19	16.6	1.9	1.5	5	11.6	122
20	16.2	2	1.4	4.7	11.3	104

21	15.2	2.1	1	3.9	11.2	79
22	15.3	2.2	0.6	3.9	11.7	115
23	18.2	3.1	1.1	4	13.6	134
24	20.2	5.9	1.2	0.2	16.9	354
25	19.2	5.4	0.9	0.5	16.2	350
26	16.5	4.1	0.8	0.3	14.5	357
27	17.9	1.6	1.2	4	14.7	187
28	16.9	1.1	0.7	3.3	14.8	127
29	18	2.9	0.9	3.2	14.6	229
30	17.7	3.2	0.7	2.8	14.5	231
31	14.1	2.2	0.3	35	10.9	180
32	14.3	1	1.9	4.4	9.9	161
33	15	1.8	0.9	2.5	12.8	133
34	13.4	1.5	0.4	2.5	11.8	98
35	24.9	4.6	1.4	0.7	23.2	340
36	10.2	0.3	0.8	1.1	10	65
37	9.5	0.3	0.5	0.7	9.9	49
38	9.5	0.5	0.2	1.2	9.5	41
39	9.6	0.6	0.2	1.2	9.5	50
40	9	0.4	0.3	1.4	8.7	38
41	16.5	2	1.7	1.6	14.5	112
42	12.5	0.8	1	3	10.2	106
43	6.6	0.4	0.5	1.2	5.8	55
44	14.8	0.3	0.9	3.9	12.7	42

45	15.1	0.3	0.7	3.8	13.3	44
46	17.3	2.1	0.5	3.7	14.4	124
47	11.4	0.3	0.4	3.6	9.4	58
48	7.9	0.1	0.4	1.2	7.8	50
49	12.6	1.2	0.6	3.4	10	132
50	13.1	0.8	0.8	3.4	10.7	101
51	6.1	0.3	0.4	1.1	5.4	42
52	16.1	1.4	1.3	0.2	16.3	147
53	15.7	1.7	1.9	0.1	15.1	185
54	15.9	1.5	2.2	0.1	15.3	159
55	23	3.9	2.4	0.2	21.1	375
56	14.6	1.8	0.7	2	13	173
57	9.6	0.2	0.6	2.8	7.9	73
58	14.9	0.7	0.7	3.3	13.2	79
59	7.1	0.2	0.4	1	6.9	60
60	16.9	2.4	3.6	4.4	9.9	203
61	16.6	2.8	3.3	3.8	10	200
62	18.2	3.1	2	3.9	12.9	180
63	24.3	3.1	0.3	0.1	25.6	135
64	25.2	2.8	0.5	0.2	26.8	133

REFERENCES

Abdel Rahman, R.O., Ibrahim, H.A. Abdel Monem, N.M. (2009). Long-term performance of zeolite A–X blend as backfill material in near surface disposal vault. *Chemical Engineering Journal*, **149**, 143-152.

Aber, S., Amani-Ghadim, A.R. & Mirzajani, V. (2009). Removal of Cr (VI) from polluted solutions by electrocoagulation: modeling of experimental results using artificial neural network. *Journal of Hazardous Materials*, **171**, 484-490.

Abusafa, A. & Yucel, H. (2002). Removal of ^{137}Cs from aqueous solutions using different cationic forms of a natural zeolite: clinoptilolite. *Separation and Purification Technology*, **28**, 103-116.

Adam, S.P., Karras, D.A., Mogoulas, F.D. & Vrahatis, M.N. (2014). Solving the linear interval tolerance problem for weight initialization of neural networks. *Neural Networks*, **54**, 17-37.

Adeleke, A.A., Ibitoye, S.A., Afonja, A.A. & Chagga, M.M. (2011). Multistage caustic leaching de-ashing of Nigerian Lafia-obi coal. *Petroleum & Coal*, **53**, 259-265.

Aksu Z. & Kutsa, T.A. (1991). A bioseparation process for removing Pb (II) ions from wastewater by using *C. vulgaris*. *Journal Chemical Technology and Biotechnology*, **52**, (1), 108-118.

Al-Degs, Y., Tutunji, M. & Baker, H. (2003). Isothermal and kinetic sorption behavior of Pb^{2+} ions on natural silicate minerals. *Journal of Clay Mineral*, **38**, 501-509.

Al-Enezi, G., Hamoda, M.F. & Fawzi, N. (2004). Ion exchange extraction of heavy metals from wastewater sludges. *Journal of Environmental Science Health A Toxic Hazard Substance Environmental Engineering*, **39**, 455-464.

Ambaw, A. (2005). *Modelling chemical engineering processes using artificial neural networks*. PhD dissertation. Addis Ababa: Addis Ababa University.

Appelo, C.A.J. & Postma, D. (1999). Variable dispersivity in a column experiment containing MnO_2 and $FeOOH$ -coated sand. *Journal of Contaminant Hydrology*, **40**, 95-106.

Bagherieh, A.H., Hower, J.C., Bagherieh, A.R. & Jorjani, E. (2008). Studies of the relationship between petrography and grindability for Kentucky coals using artificial neural network. *International Journal of Coal Geology*, **73**, 130-138.

Bailey, J.G. & Esterle, J.S. (1996). Insights into the grindability of coal microlithotypes. 30th Newcastle Symposium, March 1996, 135-142.

Bandopadhyay, A.K. (2010a). Determination of quartz content for Indian coals using an FTIR technique. *International Journal of Coal Geology*, **81**, 73-78.

Bandopadhyay, A.K. (2010b). A study on the abundance of quartz in thermal coals of India and its relation to abrasion index: Development of a predictive model for abrasion. *Coal Geology*, **84**, 63-69.

Baughman, D.R. & Liu, Y. A. (1995). *Neural Networks in Bioprocessing and Chemical Engineering*. San Diego, California: Academic Press.

Benguella, B. & Benaissa, H. (2002). Cadmium removal from aqueous solutions by Chitin: Kinetic and equilibrium studies. *Water Research*, **36**, 2463-2474.

Benson, S.A. & Holm, P.L. (1985). The composition of inorganic constituents in three low rank coals. *Industrial and Engineering Chemistry, Product, Research and Development*, **24**, 145-149.

Bhat, N.V. & McAvoy, T.J. (1990). Use of neural nets for dynamic modelling and control of chemical process systems. *Computers and Chemical Engineering*, **14**, 469-479.

Bhattacharjee C. & Singh, M. (2002). Studies on the applicability of artificial neural network (ANN) in continuous stirred ultrafiltration. *Chemical Engineering and Technology*, **25**, 1187-1192.

Borba, C.E, Silva, E.A. Spohr, S., Santos, G.H.F. & Guirardello, R. (2011). Application of the mass action law to describe ion exchange equilibrium in a fixed-bed column. *Chemical Engineering Journal*, **172**, 312-320.

Breck, D.W. (1974). *Zeolite molecular sieves: Structure, chemistry and use*. New York: Wiley & Sons.

Breiman, L. (1992). Technical Report no. 367, Department of Statistics, University of California at Berkeley, USA.

Brigatti, M.F., Franchini, G., Frigieri, P., Gardinali, C., Medici, L. & Poppi, L. (1999). Treatment of industrial wastewater using zeolite and sepiolite, natural microporous materials. *Canadian Journal of Chemical Engineering*, **77**, 163-168.

Callcott, T.G. (1956). Coal grindability – A standardized procedure for the determination of coal grindability and a survey of the grindabilities of British coals. *Journal of the Institute of Fuel*, **29**, 207-217.

Castaldi, P., Santona, L., Enzo, S. & PietroMelis, P. (2008). Sorption processes and XRD analysis of a natural zeolite exchanged with Pb^{2+} , Cd^{2+} and Zn^{2+} cations. *Journal of Hazardous Materials*, **156**, 428-434.

Chelgani, S.C., Hower, J.C., Jorjani, E., Mesroghlia, Sh. & Bagherieh, A.H. (2008). Prediction of coal grindability based on petrography, proximate and ultimate analysis using multiple regression and artificial neural network models. *Fuel Processing Technology*, **89**, 13-20.

Chen, H. & Wang, A. (2007). Kinetic and isothermal studies of lead ion adsorption onto palygorskite clay. *Journal of Colloid Interface Science*, **307**, 309-316.

Chojnacki, A., Chojnacka, K., Hoffmann, J. & Goreck, H. (2004). The application of natural zeolites for mercury removal: From laboratory tests to industrial scale. *Minerals Engineering*, **17**, 933-937.

Cigizoglu, H.K. & Alp, M. (2005). Generalized regression neural network in modelling river sediment yield. *Advanced Engineering Software*, **37**, 63-68.

Cinar, O., Hasar, H. & Kinaci, C. (2006). Modeling of submerged membrane bioreactor treating cheese whey wastewater by artificial neural network. *Journal of Biotechnology*, **123**, 204-209.

Cobzaru, (2005). Mathematical modeling of the ion-exchange processes of sodium clinoptilolite with heavy metals from residual water. *Chemical Industry and Chemical Engineering Quarterly*, **11**, (4), 209-212.

Cote, M., Grandjean, B.P.A., Lessard, P. & Thibault, J. (1995). Dynamic modeling of the activated sludge process: improving prediction using neural networks. *Water Research*, **29**, 995-1004.

Creelman, R.A. & Ward, C.R. (1996). A scanning electron microscope method for automated, quantitative analysis of mineral matter in coal. *International Journal of Coal Geology*, **30**, 249-269.

Dabrowski, A., Hubicki, Z., Podkoscielny, P. & Robens, E. (2004). Selective removal of the heavy metal ions from waters and industrial waste waters by the ion-exchange method. *Chemosphere*, **56**, 91-106.

Daneshvar, N., Kahataee, A. R. & Djafarzadeh, N. (2006). The use of artificial neural networks (ANN) for modelling of decolorization of textile dye solutions containing C.I. basic Yellow 28 by electrocoagulation processes. *Journal of Hazardous Materials*, **B 137**, 1788-1795.

De Kock, J.W. & Franzidis, J.P. (1973). The estimation of some properties of South African coals from proximate analyses. *Journal of the South African Institute of Mining and Metallurgy*, 421-427.

Dhermendra, K., Tiwari, J., Behari, S. & Prasenjit, S. (2008). Application of nanoparticles in wastewater treatment. *Journal of World Applied Sciences*, **3**, 417-433.

Dubini, M.M., radushkevich, L.V. (1947). The quatum of the characteristic curve of the activated charcoal. *Proc. Acad. Sci USSR Phys. Chem. Sect.* **55**, 331-337.

Efron, B. & Tibshirani, R. (1993). *An Introduction to the Bootstrap*. New York, London: Chapman and Hall.

El-Kamash, A.M. (2008). Evaluation of zeolite a for the sorptive removal of Cs⁺ and Sr²⁺ ions from aqueous solutions using batch and fixed bed column operations. *Journal of Hazardous Materials*, **151**, 432-445.

Elmolla, E.S., Chaudhuri, M. & Eltokhy, M.M. (2010). The use of the artificial neural network (ANN) for modelling of COD removal from antibiotic aqueous solution by the Fenton process. *Journal of Hazardous Materials*, **179**, 127-134.

Engell, S. & Toumi, A. (2005). Optimization and control of chromatography. *Computers and Chemical Engineering*, **29**, 1243-1252.

Eswaraiah, C., Gupta, A., Nagarajan, R., Rajavel, M. & Nandakumar, K. (2008). Minimization of fines generation in size reduction of coals by impact crusher. *Fuel Processing Technology*, **89**, 704-714.

Fagundes-Klen, M.R., Ferri, P., Martins, T.D., Tavares, C.R.G. & Silva, E.A. (2007). Equilibrium study of the binary mixture of cadmium-zinc ions' biosorption by the *sargassum filipendula* species using adsorption isotherm models and neural networks. *Biochemical Engineering Journal*, **34**, 136-146.

Falcon, L.M. & Falcon, R.M.S. (1983). The application of coal petrography to certain beneficiation techniques on South African coal. *Special Publication. Geological Society of South Africa*, **7**, 137-148.

Falcon, L.M. & Falcon, R.M.S. (1987). The petrographic composition of Southern African coals in relation to friability, hardness and abrasion indices. *Journal of the South African Institute of Mining and Metallurgy*, **87**, (10) 323-336.

Falcon, R.M.S. & Ham, A.J. (1988). The characteristics of Southern African coal. *Journal of the South African Institute of Mining and Metallurgy*, **88** (5) 145-161.

Falcon, R.M.S. (1989). Macro and micro factors affecting coal-seam quality and distribution in southern Africa with particular reference to the no. 2 seam, Witbank Coalfields, South Africa. *International Journal of Coal Petrology*, **12**, 681-731.

Firat, M. & Gungor, M. (2009). Generalized regression neural networks and feed forward neural networks for prediction of scour depth around bridge piers. *Advances in Engineering Software*, **40**, 731-737.

Flood, I. & Kartam, N. (1994). Neural networks in civil engineering: Systems and application. *Journal of Computing in Civil Engineering*, ASCE, **8** (2) 131-148.

Foster, D.J., Livingston, W.R., Wells, J., Williamson, J., Gibb, W.H. & Bailey, D. (2004). Particle impact erosion and abrasion wear – predictive methods and remedial measures. Report No COAL R241 DTI/Pub URN 04/701, 43.

Freundlich, H.M.F. (1906). Over the adsorption in solution. *Journal of Phys. Chem.*, **57**.

Ghaedi, M., Zeinali, N., Ghaedi, A.M., Teimuori, M. & Tashkhourian, J. (2014). Artificial neural network - genetic algorithm based optimization for the adsorption of methylene blue and brilliant green from aqueous solution by graphite oxide nanoparticle. *Spectrochimica Acta Part A: Molecular and Biomolecular Spectroscopy*, **125**, 264-277.

Gilchrist, J.D. (1989). *Extraction Metallurgy*. Pergamon Press

Giroto, J.A., Guardani R., Teixeira, A.C.S.C. & Nascimento, C.A.O. (2006). Study on the photo-Fenton degradation of polyvinyl alcohol in aqueous solution. *Chemical Engineering Process*, **45**, 523-532.

Given, P.H. & Spackman, W. (1978). Reporting of analyses of low rank coals on the dry, mineral-matter free base. *Fuel*, **57**, 319.

Gontarski, C.A., Rodrigues, P.R., Mori, M. & Prenem, L.F. (2000). Simulation of an industrial wastewater treatment plant using neural networks. *Computers and Chemical Engineering*, **24**, 1719-1723.

Gougar M.L.D. (2004). Fission product ion exchange between zeolite and a molten salt. PhD dissertation. Pennsylvania: Pennsylvania State University.

Hamachi, M., Cabassud, M., Davin, A. & Mietton Peuchot, M. (1999). Dynamic modeling of crossflow microfiltration of bentonite suspension using recurrent neural network. *Chemical Engineering and Processing*, **38**, 203-210.

Harvey, R.D. & Ruch, R.R. (1986). Mineral matter in Illinois and other US coals. In *Mineral matter in coal. Ash and Coal*. Edited by K.S. Vorres. *American Chemical Society Symposium Series*, **30**, 10-40.

Haykin, S. (1994). *Neural networks, a comprehensive foundation*. 2nd ed. City of publication: Prentice Hall, USA.

Helferich, F. (1962). *Ion-exchange*. New York: McGraw-Hill.

Hernandez, M.A. (2000). Nitrogen-sorption characteristics of the micro porous structure of clinoptilolite-type zeolites. *Journal of Porous Materials*, **7**(4), 443-454.

Hong, S.H., Lee, M.W., Lee, D.S. & Park, J.M. (2007). Monitoring of sequencing both reactors for nitrogen and phosphorus removal using neural networks. *Biochemical Engineering Journal*, **35** (3), 365-370.

Hornik, K., Stinchcombe, M. & White, H. (1989). Multilayer feedforward networks are universal approximators. *Neural Network*, **2**, 359-366.

Huggins, F.E. (2002). Overview of analytical methods for inorganic constituents in coal. *International Journal of Coal Geology*, **50**, 169-214.

Hutchings, I.M. (1992). *Tribology: Friction and wear of engineering materials*. Boca Raton, FL: CRC Press.

Hutchings, I.M. (2002). Abrasion processes in wear and manufacturing. Processing Institute of Mechanical Engineering. *Part I: Journal of Engineering Tribology*, **216**, 55-62.

Inglezakis, V.J. & Grigoropoulou, H. (2004). Effect of pore clogging on kinetics of lead uptake by clinoptilolite. *Journal of Hazardous Materials*, **B112**, 37-43.

Khashei, M. & Bijari, M. (2012). Hybridization of the probabilistic neural networks with feed-forward neural networks for forecasting. *Engineering Application of Artificial Intelligence*, **25**, 1277-1288.

Korkuna, O., Leboda, R., Skubiszewska-Zieba, J., Vrublevs'ka, T., Gun'Kovn & Ryczkowski, J. (2006). Structural and physicochemical properties of natural zeolites: Clinoptilolite and moderdenite. *Microporous Mesoporous Materials*, **87**, 243-254.

Kuronen, M., Weller, M., Tounsend, R. & Harjula, R. (2006). Ion exchange selectivity and structural changes in highly aluminous zeolites. *Reactive and Functional Polymers*, **66**, 1350-1361.

Langmuir, I. (1918). The adsorption of gases on plane surfaces of glass, mica and platinum. *Journal of American Chemical Society*, **40**, 361-1403.

Lee, M.M. & Nicol, M.J. (2007). Removal of iron from cobalt sulfate solutions by ion exchange with Diphonix resin and enhancement of iron elution with titanium (III). *Hydrometallurgy*, **86**, 6-12.

Lessard, P. & Beck, M.B. (1993). Dynamic modeling of the activated sludge process: a case study. *Water Research*, **27**, 963-978.

Lexa, D. & Johnson, I. (2001). Occlusion and ion exchange in the molten (lithium chloride-potassium chloride-alkali metal chloride) salt + zeolite 4A system with alkali metal chlorides of sodium, rubidium, and cesium. *Metallurgical and Materials Transactions B*, **32B**, 429-435.

Li, P., Xiong, Y., Yu, D. & Sun, X. (2005). Prediction of grindability with multivariable regression and neuron network in Chinese coal. *Fuel*, **84**, 2384-2388.

Livingston, W.R. & Dugdale, K.L. (1998). Modern coal mill design and performance. Proceedings of the Conference and Exhibition POWER-GEN Asia, 801-822.

Lombard, F. & Potgieter, C.J. (2008). Report on an abrasive index investigation, 30 January 2008.

Luccarini, L., Porra, E., Spagni, A., Ratini, P., Grilli, S., Longh, S. & Bortone, G. (2002). Soft sensors for control of nitrogen and phosphorus removal from wastewaters by neural networks. *Water Science and Technology*, **45** (4-5), 101-107.

Madejova, J. (2003). FTIR techniques in clay mineral studies. *Vibrational Spectroscopy*, **31** (1), 1-10.

Mamba, B.B., Nyembe, D.W. & Mulaba-Bafubiandi, A.F. (2009). The effect of conditioning with NaCl, KCl and HCl on the performance of natural clinoptilolite's removal efficiency of Cu²⁺ and Co²⁺ synthetic solutions. *Water SA*, **36** (4) 437-444.

Meintjes, A.A. (1965). The grindability and abrasive properties of South African coals. *Journal of the South African Institute of Mining and Metallurgy*, **65**, 629-646.

Misra, A. & Finnie I. (1980). A classification of three-body abrasive wear and design of a new tester. *Wear*, **60**, 111-121.

Misra, A. & Finnie I. (1981). Correlations between two-body and three-body abrasion and erosion of metals. *Wear*, **68**, 33-39.

Misra, A. & Finnie I. (1983). An experimental study of three-body abrasive wear. *Wear*, **85**, 57-68.

Moral, H., Aksoy A. & Gakcay C.F. (2008). Modeling of the activated sludge process by using artificial neural networks with automated architecture screening. *Computers and Chemical Engineering*, **32**, 2471-2478.

Nadaraya, E.A. (1964). On estimating regression. *Theory Probability and its Application*, **10**, 186-190.

Ng, E.P. & Mintova, S. (2008). Nanoporous materials with enhanced hydrophilicity and high water sorption capacity. *Microporous Mesoporous Materials*, **114**, 1-26.

Ngoy, E.K. & Mulaba-Bafubiandi, A.F. (2013). An analytical model of coal abrasiveness index in a function of the mineral composition of coal. International Conference on Chemical and Engineering (ICCEE 2013). April 15-16, 2013, Johannesburg (South Africa). 79-83.

Nikkah, K. (2002). Dynamic modeling for design of ion exchange systems. *The Minerals, Metals & Materials Society*, Canada.

Nyembe, D.W. (2010). *Natural clinoptilolite for the removal of cobalt and copper from aqueous solutions*. PhD thesis. Johannesburg, South Africa: University of Johannesburg.

Ogata, A. & Banks, R.B. (1961) A solution of the differential equation of longitudinal dispersion in porous media, *US Geology Surv. Prof. Paper*, 411-A, 1-9.

Oguz, E., Tortum, A. & Keskinler, B. (2008). Determination of the apparent rate constants of the degradation of humic substances by ozonation and modeling of the removal of humic substances from the aqueous solutions with neural network. *Journal of Hazardous Materials*, **157**, 455-463.

Ozturk, H.U. (2005). Discharge predictions using ANN in sloping rectangular channels with free overfall. MSc thesis.

Pai, T.Y., Tsai, Y.P., Lo, H.M., Tsai, C.H. & Lin, C.Y. (2007). Grey and neural network prediction of suspended solids and chemical oxygen demand in hospital wastewater treatment plant effluent. *Computer Chemical Engineering*, **31**, 1272-1281.

Pepe, F., de Gennaro, B., Aprea, P. & Domenico Caputo, D. (2013). Natural zeolites for heavy metals removal from aqueous solutions: Modelling of the fixed bed Ba^{2+}/Na^{+} ion-exchange process using a mixed phillipsite/chabazite-rich tuff. *Chemical Engineering Journal*, **219**, 37-42.

Peric, J., Trgo, M. & Medvidovic, N.V. (2004). Removal of zinc, copper and lead by natural zeolite – a comparison of adsorption isotherms. *Water Research*, **38**, 1893-1899.

Phongikaroon, S. & Simpson, M.F. (2006). Equilibrium model for ion exchange between multivalent cations and zeolite-A in a molten salt. *American Institute of Chemical Engineering Journal*, **52**, 1736-1743.

Piron, E., Latrille, E. & Rene, F. (1997). Application of artificial neural network for crossflow microfiltration modeling: “black-box” and semi-physical approaches. *Computers and Chemical Engineering*, **21**, 1021-1030.

Prakash, N., Manikandan, S.A., Govindarajan, L. & Vijayagopal, V. (2008). Prediction of biosorption efficiency for the removal of copper (II) using artificial neural networks. *Journal of Hazardous Materials*, **152**, 1268-1275.

Raask, E. (1985). *Minerals impurities in coal combustion: Behaviour, problems and remedial measures*. City of publication: Hemisphere Publishing Corporation, 41.

Rabinowicz, E., Dunn, L.A. & Russell, P.G. (1961). A study of abrasive wear under three body conditions. *Wear*, **4**, 345-355.

Riveros, P.A. (2010). The removal of antimony from copper electrolytes using amino-phosphonic resins: Improving the elution of pentavalent antimony. *Hydrometallurgy*, **105**, 110-114.

Ruthven, D.M. (1984). *Principles of adsorption and adsorption processes*. New York: John Wiley & Sons.

Rutkowski, L. (2004). Generalized regression neural networks in time-varying environment. *IEEE Trans. Neural Networks*, **15** (3), 576-596.

Sadrzadeh, M., Mohammadi, T., Ivakpour, J. & Kasiri, N. (2009). Neural network modelling of Pb^{2+} removal from wastewater using electro dialysis. *Chemical Engineering and Processing: Process Intensification*, **48**, 1371-1381.

Santacesaria, S., Morbidelli, M., Servida, A., Storti, G. & Carrà, S. (1982). Separation of xylenes on Y-zeolites. Note II: breakthrough curves and their interpretation. *Industrial Engineering Chemical Process Design Development*, **21**, 446-451.

Scieszka, S.F. (1996). Method of abrasive wear testing in comminution processes. *Tribotest Journal*, **2**, no 2-3, 257-266.

Shao, R., Zhang, J., Martin, E.B. & Morri, A.J. (1997). Proceedings of the 5th International Conference on Artificial Neural Networks, Cambridge, UK, IEE Conference Publication, no. **440**, 76-81.

Shetty, G.R., Malki, H. & Chellam, S. (2003). Predicting contaminant removal during municipal drinking water nanofiltration using artificial neural networks. *Journal of Membrane Science*, **212**, 99-112.

Shoo, R., Martin, E.B., Zhang, J. & Morris, A.J. (1997). Confidence bounds for neural network representations. *Computers and Chemical Engineering*, **21**, 1173-1178.

Simpson, M.F., Gougar, M.L.D. (2003). Two-site equilibrium model for ion exchange between monovalent cations and zeolite-A in a molten salt. *Industrial and Engineering Chemistry Research*, **42**, 4208-4212.

Sinha, N.C., Sinha, B.K., Roy, T.K. & Krishnan, S.R. (1982). Abrasion characteristics of coals. *Fuel*, **61**, 1285-1286.

Sjoberg, J., Zhang, Q., Ljung, L., Benveniste, A., Delyon, B., Glorennec, P.Y., Hjalmarsson, H. & Juditsky, A. (1995). Non-linear black-box modeling in system identification: A unified overview. *Automatica*, **31**(12), 1691-1724.

Skoog, D.A., Holler, F.J. & Nieman, T.A. (1998). *Principles of instrumental analysis*, 5th ed. Philadelphia, PA: Saunders College of Publishing, 13-14.

Slater, M.I. (1991). *The principles of ion exchange technology*. Oxford: Butterworth-Heinemann.

Sligar, J. (1996). Component wear in vertical spindle mills grinding coal. *International Journal of Mineral Processing*, **44-45**, 569-581.

Snyman, C.P. & Botha, W.J. (1993). Coal in South Africa. *Journal of African Earth Sciences*, **16**, 171-180.

Spero, C. (1990). Assessment and prediction of coal abrasiveness. *Fuel*, **69**, no 9, 1168-1176.

Spero, C., Hargreaves, D.J., Kirkcaldie, R.K. & Flitt, H.J. (1991). Review of test methods for abrasive wear in ore grinding. *Wear*, **146**, 389-408.

Sridhar, D.V., Seagrave, R.C. & Bartlett, E.B. (1996). Process modeling using stacked neural networks. *American Institute of Chemical Engineers Journal*, **42**, 2529-2539.

Stachowiak, G.B. & Stachowiak, G.W. (2001). The effects of particle characteristics on three-body abrasive wear. *Wear*, **249**, 201-207.

Stamboliadis, E. Th. (2004). Energy distribution in comminution, a new approach to the laws of Rittinger, Bond and Kick. *Canadian Metallurgical Quarterly*, **43**, no 2, 249-258.

Stamboliadis, E. Th. (2005). The fracture of brittle materials as an equilibrium of surface and cohesion energy. *Journal of the Mechanical Behavior of Materials*, **16**, no 6, 363-377.

Stamboliadis, E. Th. (2007). The energy distribution theory of comminution specific surface energy, mill efficiency and distribution mode. *Minerals Engineering*, **20**, 140-145.

Swayampakula, K., Boddu, V.M., Nadavala, S.K. & Abburi, K. (2009). Competitive adsorption of Cu (II), Co (II) and Ni (II) from their binary and tertiary aqueous solutions using chitosan-coated perlite beads as biosorbent. *Journal of Hazardous Materials*, **170**, 680-689.

Taty-Costodes, V.C., Fauduet, H., Catherine, C.P. & Delacroix, A. (2003). Removal of Cd (II) and Pb (II) ions, from aqueous solutions, by adsorption onto sawdust of *Pinus sylvestris*. *Journal of Hazardous Materials*, **B105**, 121-142.

Teodosiu, C., Pastravaru, O. & Macoveanu, M. (2000). Neural network models for ultrafiltration and back washing. *Water Research*, **34**, 4371-4380.

Terchick, A.A., Shoenberger, R.W., Perlic, B. & DeRusha, L.F. (1963). Mechanical and related properties of some eastern coals. 145th Nat. Meeting ACS, *Div. Fuel Chemical*, New York, **2**, 95-109.

Thanasiadis, A. & Helmreich, B. (2005). Influence of chemical conditioning on the ion-exchange capacity and on natural silicate minerals. *Journal of Clay Mineral*, **38**, 501-509.

Tibshirani, R. (1996). A comparison of some error estimates for neural network models. *Neural Computation*, **8**, 152-163.

Tichanek, F. (2008). Contribution to determination of coal grindability using Hardgrove method. *Geology Science Engineering*, **1**, 27-32.

Tickner, D. & Maier R.W. (2005). Design consideration for pulverized coal fired boilers combusting Illinois basin coals. Paper presented to Electric Power, April 5-7, Chicago, Illinois, USA.

Tiryaki, B. (2005). Technical note practical assessment of the grindability of coal using its hardness characteristics. *Rock Mechanics and Rock Engineering*, **38**, no 2, 145-151.

Tlotleng, M.T. (2011). Coal characteristics that lead to abrasion during grinding, MSc thesis.

Toma, F.L., Guessasma, S., Klein, D., Montavon, G., Bertrand G. & Coddet, C. (2004). Neural computation to predict TiO₂ photo catalytic efficiency for nitrogen oxides removal. *Journal of Photochemistry and Photobiology A*, **165**, 91-96.

Tomczak, E. (2011). Application of ANN and EA for description of metal ion sorption on chitosan foamed structure-equilibrium and dynamics of packed column. *Computers and Chemical Engineering*, **35**, 226-235.

Toporov, G.V. (1960). Friction and wear in machinery. *Society of Mechanical Engineers*, **12**, 39-59.

Turan, N.G., Mesci, B. & Ozgonenel, O. (2011). The use of artificial neural networks (ANN) for modeling of adsorption of Cu (II) from industrial leachate by pumice. *Chemical Engineering Journal*, **171**, 1091-1097.

Van den Bosch, M.M. (2009). Simulation of ion exchange processes using neuro-fuzzy reasoning. Theses and dissertations. Cape Town, South Africa: Cape Peninsula University of Technology.

Van der Merwe, P.F. (1991). Fundamentals of the elution of gold cyanide from activated carbon, PhD dissertation. Stellenbosch, South Africa: University of Stellenbosch.

Van Deventer, J.S.J. (1984). Kinetic model for the adsorption of metal cyanides onto activated charcoal. PhD dissertation. Stellenbosch, South Africa: University of Stellenbosch.

Van Deventer, J.S.J., Liebenberg, S.P, Lorenzen, L. & Aldrich, C. (1995). Dynamic modelling of competitive elution of activated carbon in columns using neural networks. *Mineral Engineering*, **8**, 1489-1501.

Van Vuuren, M.C.J. (1978). A survey of the Hardgrove grindability indices from colliery product samples. *Fuel Research Institute of South Africa*, **62**, 57-68.

Virta, R.L. (1998). *Zeolites*. US Geological Survey Publication.

Waranusantigul, P., Poketshityook, P., Kruatrachue, M. & Upatham, E.S. (2003). Kinetics of basic dye (methylene blue) biosorption by giant duckweed (*Spirodela polyrrhiza*). *Environmental Pollution Journal*. **3**, (125). 385-392.

Ward, C.R. (2002). Analysis and significance of mineral matter in coal seams. *International Journal of Coal Geology*, **50**, 135-168.

Warren Spring Laboratory, (1962). Grindability test procedure and ball mill size selection. *Mineral Processing Information*, **3**, 1-17.

Watson, G.S. (1964). Smooth regression analysis. *Sankhya, Series A*, **26**, 359-372.

Wells, J.J., Wigley, F., Foster, D.J., Gibb, W.H. & Williamson, J. (2004). The relationship between excluded mineral matter and abrasion index of a coal. *Fuel*, **83**, 3, 359-364.

Wigley, F. & Williamson, J. (2005). Coal mineral transformations – effects on boiler ash behaviour. Report No. COAL R278 DTI/Pub URN 05/659.

Willis, M.J., Massimo, D.I.C, Montgue, G.A., Tham, M.T, & Morris, A.J. (1991). Control theory and applications. *Proc. IEEE*, Part D **138**, (3). 256-266.

Wolpert, D.H. (1992). Stacked generalization. *Neural Networks*, **5**, 241-259.

Yetilmezsay, K. & Demired, S. (2008). Artificial neural network (ANN) approach for modelling of Pb (II) adsorption from aqueous solutions by antep pistachio (*Pistacia Vera L*) shells. *Journal of Hazardous Materials*, **153**, 1288-1300.

Zeng, G.M., Qin, X.S., He, L., Huang, G.H., Lin, H.L. & Lin, Y.P. (2003). A neural network predicting control system for paper mill wastewater treatment. *Engineering Applications of Artificial Intelligence*, **16**, 121-129.

Zhang, J., Martin, E.B., Morris, A.J. & Kiparissides, C. (1997). Inferential estimation of polymer quality using stacked neural networks, computers. *Chemical Engineering*, **21**, S 1025-S1030.

“Neural Networks do not perform miracles. But if used sensibly they can produce some amazing results” (Christo Stergion)

